5-2012

Biochemical Characterization of SAC9, a Putative Phosphoinositide Phosphatase in Arabidopsis thaliana, and Its Role in Cellular Abnormalities

Almut H. Vollmer
Utah State University

BIOCHEMICAL CHARACTERIZATION OF SAC9, A PUTATIVE PHOSPHOINOSITIDE PHOSPHATASE IN ARABIDOPSIS THALIANA, AND ITS ROLE IN CELLULAR ABNORMALITIES

by

Almut H. Vollmer

A dissertation submitted in partial fulfillment
of the requirements for the degree

of

DOCTOR OF PHILOSOPHY

in

Biology

Approved:

_____	_____
Edmund D. Brodie Major Professor	Jon Y. Takemoto Committee Member
_____	_____
Daryll B. DeWald Committee Member	Dennis L. Welker Committee Member
_____	_____
Joan M. Hevel Committee Member	Nabil N. Youssef Committee Member

_____
Mark R. McLellan
Vice President for Research and
Dean of the School of Graduate Studies

UTAH STATE UNIVERSITY
Logan, Utah

2012

ABSTRACT

Biochemical Characterization of SAC9, a Putative Phosphoinositide Phosphatase in *Arabidopsis thaliana*, and Its Role in Cellular Abnormalities

by

Almut H. Vollmer, Doctor of Philosophy

Utah State University, 2012

Major Professor: Edmund D. Brodie, Jr.
Department: Biology

The phospholipid phosphatidylinositol and its phosphorylated derivatives, collectively referred to as phosphoinositides, form the basis for a multifaceted signaling pathway regulating many different cellular processes in eukaryotic cells. Phosphatidylinositol 4,5-bisphosphate, $PI(4,5)P_2$, assumes a central position in this complex pathway. It can serve as a precursor for the generation of second messengers but can also act as a ligand to partner proteins. In order to mediate their physiological effects properly, the location and quantity of $PI(4,5)P_2$ and other phosphoinositides have to be tightly controlled by enzymes.

In general, phospholipid kinases lead to the activation of the pathway, whereas phospholipid phosphatases attenuate or terminate the signaling cascade. The SAC domain-containing protein 9 from *Arabidopsis thaliana* has been identified as a putative phosphoinositide phosphatase, but very little has been published on this particular protein. In my dissertation research, I broadened our knowledge of this protein and the effects seen in *Arabidopsis* plants carrying the mutant allele. I used molecular, genetic, and biochemical

approaches to analyze the function of the putative phosphoinositide phosphatase, SAC9. To understand its physiological role, I investigated the cellular effects of a mutation in the *SAC9* gene at the light microscopy, confocal microscopy, and transmission electron microscopy levels.

My studies show that AtSAC9 is a soluble protein with an apparent molecular mass of 180 kDa and that it most likely is a phosphoinositide phosphatase. Furthermore, I show that the mutation of *SAC9* induced unique cell wall defects that most likely have contributed to the stuntedness of the root. However, the cortical microtubule cytoskeleton was not disturbed in elongating root cells. These data are augmented by applying a novel approach for the mathematical analysis of cortical microtubule orientation.

(154 pages)

PUBLIC ABSTRACT

Biochemical Characterization of SAC9, a Putative Phosphoinositide Phosphatase in *Arabidopsis thaliana*, and Its Role in Cellular Abnormalities

by

Almut H. Vollmer, Doctor of Philosophy

Utah State University, 2012

Major Professor: Edmund D. Brodie, Jr.
Department: Biology

Since the early colonization of land by fungi and plants some 700 million years ago, plants have been continuously faced with changes in their environment. Unlike animals, plants are not free to move about, and can therefore not evade many stress factors. How plants sense and respond to their environment has been of interest not only to scientific research but also in more practical applications such as agriculture.

Signals (such as light or salinity) from the outside of plant cells trigger a flow of information to the inside of the cell. The final target for most of the information is thought to be the nucleus, the structure that contains the cell's hereditary information. Depending on the signal, DNA replication and RNA transcription in the nucleus may lead to the production of molecules which allow the plant to respond in a biologically relevant way. To get signals from the outside of the cell to the nucleus, both animals and plants can use the phosphoinositide (PI) signaling pathway.

In my research, I was interested in how plants use the PI pathway and what happens to plants and their cells when this pathway is disturbed. I focused on the model plant *Arabidopsis thaliana*. This is a small, weedy plant with a short life cycle. It has become a model plant because it can be grown easily in the laboratory and is amenable to genetic manipulation. Its genome is completely sequenced, which makes it easier to define segments of DNA as genes and to add explanatory notes to their possible function.

Central to my research was an enzyme called SAC9 that was speculated to modify one of the main components of the PI pathway. The mechanism(s) by which SAC9 acts in the PI pathway is poorly understood. Plants with a defective copy of the gene that codes for SAC9 show signs of being permanently stressed even though they are not exposed to any stress factor. They are slow growing with small leaves and short roots. In signaling terms, it looks like somebody forgot to turn off the light switch. Understanding the molecular and cytological effects of a dysfunctional SAC9 protein in plant cells is the basis for genetically improving crop species, so they can better withstand stresses from the environment.

My work, which was funded by the National Foundation of Science (NSF), provides insights into the function of the protein SAC9 and its substrate, phosphatidylinositol 4,5-bisphosphate, PI(4,5)P_2. Using different types of microscopes (light microscope, confocal microscope, transmission electron microscope), I discovered that in plants that were defective for the *SAC9* gene, some root cells had unique cell wall abnormalities, which might be the reason for why the roots are shorter. I also found that a network of fibers throughout the cell's cytoplasm, called the cytoskeleton, had some subtle but important changes.

I dedicate this dissertation to my Mother, Roswitha Vollmer-Pfau.

I know how hard it was for you to let me be far away from you all these years.

Without your love and continuous support this work would never have been possible.

Thank you with all my heart.

ACKNOWLEDGMENTS

I wish to thank my former advisor, Daryll DeWald, my current advisor, Edmund Brodie, and my committee members, Joanie Hevel, Jon Takemoto, Dennis Welker, and Nabil Youssef, for their continuous help and interest in my research. In particular, I would like to extend my gratitude to Nabil Youssef for introducing me to the exciting world of electron microscopy. He was instrumental in my coming back to the United States; he helped me to get started and to finish my Ph.D. program.

I am indebted to Mary Williams (American Society of Plant Biologists and University of Glasgow, Scotland, UK) for providing *sac9* seeds, continuous support and kindness throughout the course of the study.

I thank Nancy Chandler and her team at the Electron Microscopy Facility at the University of Utah for creating a welcoming and accommodating working environment. My thanks also go to Chris Rodesch and his team at the Fluorescence Microscopy Core Facility (University of Utah) for helpful advice.

Without the generous gift from Keith Carney (University of Utah) in the form of the custom-generated software in MatLab for Chapter 3, the analysis of angular orientation distributions would not have been possible. I would like to thank Jim Powell for “playing with the data” and providing the von Mises fitting for Chapter 3. I would like to take this opportunity to also show my gratitude to Nazih Youssef for helpful comments he provided on the DFT method, on von Mises probability density functions for circular data, and for being a dear friend.

Statistical consultation by Susan Durham is greatly acknowledged. I thank Richard Mueller for lab space, John Carman for his generous offer to use his growth chamber, Joseph Li for hands-on training in immunological assays, Dale Barnard for valuable comments on enzyme

activity tests, and Michelle Grilley and Kandy Baumgardner for reading many versions of my dissertation and manuscripts.

I have made many friends over the years here and would like to say thank you to all of them. Sunday nights will not be the same without Ellen Klinger, Sarah Supp, Stephanie Cobbold, Ryan O'Donnell, Seth Price, and Settlers of Catan.

This research was funded in part by the National Science Foundation grant MCB-0717904 to Daryll DeWald, the Utah Agricultural Experiment Station (Project # UTA00533), and the Department of Biology at Utah State University.

Almut H. Vollmer

All truths are easy to understand once they are discovered;

the point is to discover them.

Galileo Galilei

Italian astronomer & physicist (1564-1642)

CONTENTS

Page

LIST OF TABLES

LIST OF FIGURES

CHAPTER 1

INTRODUCTION

Phosphoinositides are phosphorylated derivatives of the phospholipid phosphatidylinositol. Although of low abundance, they are found in membranes of all eukaryotic cells, predominantly on the cytosolic surface. As constituents of lipid bilayers, they are structurally important, but they are also strongly involved in signaling where they control growth, differentiation, and responses to the environment by diverse cellular activities, such as Ca^{2+} mobilization, protein and membrane trafficking, cytoskeletal rearrangement, and changes in mobility and cellular adherence characteristics (Berridge 1984; Di Paolo and De Camilli 2006).

Even though phosphoinositides were discovered in the 1930s (Hawthorne et al. 1960), it was not until the early 1980s that their function as regulatory and signaling molecules was recognized (Streb et al. 1983). Since then there has been a major flood of discoveries from newly detected inositol lipids to specific enzymes that regulate this extraordinary system, binding partners and downstream targets. From these and other studies we have a decent understanding of what has become known as the canonical phospholipase C (PLC) signaling pathway in animals, which is now a staple in cellular and molecular textbooks (Alberts et al. 2007). The pathway is triggered by the stimulation of extracellular receptors which activate phospholipase C (PLC). Activated PLC hydrolyzes its target, phosphatidylinositol 4,5-bisphosphate, $PI(4,5)P_2$, and leads to the generation of two second messengers, the soluble inositol 1,4,5-trisphosphate (IP_3) and the lipid-bound diacylglycerol (DAG). Both second messengers can start signaling cascades but in different locations within the cell and with different targets (Berridge 1984).

The detection of $PI(4,5)P_2$ in plants coupled with the discovery of functional PLC homologs led to a widespread believe that plants, like animals, use the same canonical PLC

pathway. This was further solidified by microinjection experiments of caged IP_3 which resulted in the same response as in animals, namely Ca^{2+} release (Blatt et al. 1990). Although we can rightly assume that phospholipid-based signaling is a conserved process among yeast, animals, and plants, various studies have shown that details for each system are different. Thus, the initial optimism over the similarity has yielded to the realization that plant phospholipid signaling has some distinctive modifications. To date, no clear homologs to the primary targets in animal PLC signaling has been identified in the plant genome. Instead, IP_6 and not IP_3 appears to trigger Ca^{2+} release in plants. Similarly, DAG is quickly phosphorylated to phosphatidic acid, which has emerged as a new signaling molecule in plants with its own set of downstream targets (Munnik and Testerink 2009).

Regardless of the differences in the organization of phospholipid signaling in animals and plants, $PI(4,5)P_2$ assumes a central position in both systems. It has become clear that $PI(4,5)P_2$ is not only a precursor for the generation of new signaling molecules, but can also act as a signaling molecule in itself. In animals, $PI(4,5)P_2$ is known to regulate vesicle trafficking, the activity of ion channels, and the state of the actin cytoskeleton (Di Paolo and De Camilli 2006). In plants, $PI(4,5)P_2$ has been implicated in the response to osmotic stress (Meijer et al. 1999; Pical et al. 1999; DeWald et al. 2001; Takahashi et al. 2001; Zonia and Munnik 2004; Williams et al. 2005; Im et al. 2007; van Leeuwen et al. 2007; Konig et al. 2008; Darwish et al. 2009; Mishkind et al. 2009). While higher-plant $PI(4,5)P_2$ is hardly detectable, osmotic stress temporarily increased its levels 4-20-fold (DeWald et al. 2001).

The canonical PLC signaling pathway in animals is terminated through the action of phosphatases that are either specific to IP_3 or $PI(4,5)P_2$. Temporary increases of $PI(4,5)P_2$, such as seen in heat, cold, or salinity-treated plants as mentioned above, are assumed to be decreased to base levels by the action of polyphosphate 5-phosphatases, including bifunctional

SAC domain-containing phosphatases. One gene for such a SAC domain-containing protein is found to be disrupted in the *Arabidopsis thaliana* mutant *sac9*. Mutant analysis showed that PI(4,5)P_2 and IP_3 levels were elevated in the absence of any osmotic stimulation (Williams et al. 2005). *sac9* mutants showed a constitutive stressed phenotype, supporting the role of PI(4,5)P_2 as a universal osmotic stress response. Except for the identification of the affected gene and an initial phenotypic characterization by two independent labs (Williams et al. 2005; Gong et al. 2006), not much is known about SAC9. Yet, this mutant might offer valuable insights into phospholipid signaling in plants and possible cellular downstream effects of stress responses. Phenotypic mutant analysis can shed light on gene function, specifically on a whole system-level. By examining the pathology of the mutant, one can make inferences about the function of the protein of interest in non-mutated, healthy plants. Of particular interest to this study was the fact that *sac9* mutant plants are dwarfed with much shorter roots which accumulate PI(4,5)P_2. Therefore, in Chapter 2, I analyzed the primary root of *sac9* mutants at the light microscopy and ultrastructural level, and report on unique cell wall aberrations and excessive membrane accumulation associated with these abnormal cell walls. In Chapter 3, I investigated the possible involvement of the cytoskeleton as an underlying factor for the unique cell wall aberrations and the overall shorter primary roots of *sac9*. Chapter 4 complements the phenotypic mutant analysis with functional studies of immunoprecipitated SAC9 protein.

REFERENCES

Alberts B, Johnson A, Lewis J, Raff M, Roberts K, Walter P (2007) Molecular Biology of the Cell. 5th edn. Garland Science, New York

Berridge MJ (1984) Inositol trisphosphate and diacylglycerol as second messengers. Biochem J 220 (2):345-360

Blatt MR, Thiel G, Trentham DR (1990) Reversible inactivation of K^+ channels of *Vicia* stomatal guard cells following the photolysis of caged inositol 1,4,5-trisphosphate. Nature 346 (6286):766-769

Darwish E, Testerink C, Khalil M, El-Shihy O, Munnik T (2009) Phospholipid signaling responses in salt-stressed rice leaves. Plant Cell Physiol 50 (5):986-997

DeWald DB, Torabinejad J, Jones CA, Shope JC, Cangelosi AR, Thompson JE, Prestwich GD, Hama H (2001) Rapid accumulation of phosphatidylinositol 4,5-bisphosphate and inositol 1,4,5-trisphosphate correlates with calcium mobilization in salt-stressed Arabidopsis. Plant Physiol 126 (2):759-769

Di Paolo G, De Camilli P (2006) Phosphoinositides in cell regulation and membrane dynamics. Nature 443 (7112):651-657

Gong P, Wu G, Ort DR (2006) Slow dark deactivation of Arabidopsis chloroplast ATP synthase caused by a mutation in a nonplastidic SAC domain protein. Photosynth Res 88 (2):133-142

Hawthorne JN, Kemp P, Ellis RB (1960) Configuration of inositol phosphate in liver phosphatidyl inositol. Nature 185:37-38

Im YJ, Perera IY, Brglez I, Davis AJ, Stevenson-Paulik J, Phillippy BQ, Johannes E, Allen NS, Boss WF (2007) Increasing plasma membrane phosphatidylinositol(4,5)bisphosphate biosynthesis increases phosphoinositide metabolism in *Nicotiana tabacum*. Plant Cell 19 (5):1603-1616

Konig S, Ischebeck T, Lerche J, Stenzel I, Heilmann I (2008) Salt-stress-induced association of phosphatidylinositol 4,5-bisphosphate with clathrin-coated vesicles in plants. Biochem J 415 (3):387-399

Meijer HJ, Divecha N, van den Ende H, Musgrave A, Munnik T (1999) Hyperosmotic stress induces rapid synthesis of phosphatidyl-D-inositol 3,5-bisphosphate in plant cells. Planta 208:294-298

Mishkind M, Vermeer JE, Darwish E, Munnik T (2009) Heat stress activates phospholipase D and triggers PIP accumulation at the plasma membrane and nucleus. Plant J 60 (1):10-21

Munnik T, Testerink C (2009) Plant phospholipid signaling: "in a nutshell". J Lipid Res 50 Suppl:S260-265

Pical C, Westergren T, Dove SK, Larsson C, Sommarin M (1999) Salinity and hyperosmotic stress induce rapid increases in phosphatidylinositol 4,5-bisphosphate, diacylglycerol pyrophosphate, and phosphatidylcholine in *Arabidopsis thaliana* cells. J Biol Chem 274 (53):38232-38240

Streb H, Irvine RF, Berridge MJ, Schulz I (1983) Release of Ca^{2+} from a nonmitochondrial intracellular store in pancreatic acinar cells by inositol-1,4,5-trisphosphate. Nature 306 (5938):67-69

Takahashi S, Katagiri T, Hirayama T, Yamaguchi-Shinozaki K, Shinozaki K (2001) Hyperosmotic stress induces a rapid and transient increase in inositol 1,4,5-trisphosphate independent of abscisic acid in Arabidopsis cell culture. Plant Cell Physiol 42 (2):214-222

van Leeuwen W, Vermeer JE, Gadella TW, Jr., Munnik T (2007) Visualization of phosphatidylinositol 4,5-bisphosphate in the plasma membrane of suspension-cultured tobacco BY-2 cells and whole Arabidopsis seedlings. Plant J 52 (6):1014-1026

Williams ME, Torabinejad J, Cohick E, Parker K, Drake EJ, Thompson JE, Hortter M, DeWald DB (2005) Mutations in the Arabidopsis phosphoinositide phosphatase gene *SAC9* lead to overaccumulation of PtdIns(4,5)P_2 and constitutive expression of the stress-response pathway. Plant Physiol 138 (2):686-700

Zonia L, Munnik T (2004) Osmotically induced cell swelling versus cell shrinking elicits specific changes in phospholipid signals in tobacco pollen tubes. Plant Physiol 134 (2):813-823

CHAPTER 2

UNIQUE CELL WALL ABNORMALITIES IN THE PUTATIVE PHOSPHOINOSITIDE PHOSPHATASE MUTANT *AtSAC9*[*]

ABSTRACT

SAC9 is a putative phosphoinositide phosphatase in *Arabidopsis thaliana* involved in phosphoinositide signaling. *sac9-1* plants have a constitutively stressed phenotype with shorter roots which notably accumulate phosphatidylinositol 4,5-bisphosphate and its hydrolysis product inositol trisphosphate. We investigated the primary roots of *sac9-1* seedlings at the cytological and ultrastructural level to determine the structural basis for this altered growth. Despite the normal appearance of organelles and cytoplasmic elements, our studies reveal extreme abnormalities of cell wall and membrane structures in *sac9-1* primary root cells, regardless of cell type, position within the meristematic area, and plane of section. Cell wall material was deposited locally and in a range of abnormal shapes, sometimes completely fragmenting the cell. Simple protuberances, broad flanges, diffuse patches, elaborate folds, irregular loops and other complex three-dimensional structures were found to extend randomly from the pre-existing cell wall. Abundant vesicles and excessive membrane material were associated with these irregular wall structures. We argue that a perturbed phosphoinositide metabolism most likely induced these observed abnormalities and hypothesize that a disorganized cytoskeleton and excessive membrane trafficking mediate the cell wall defects.

---

* Vollmer AH, Youssef NN, DeWald DB (2011) Unique cell wall abnormalities in the putative phosphoinositide phosphatase mutant *AtSAC9*. Planta 234 (5):993-1005

ABBREVIATIONS

IP_3	Inositol trisphosphate
LM	Light Microscopy
PtdIns(4,5)P_2	Phosphatidylinositol 4,5-bisphosphate
SAC domain	Suppressor of Actin domain
TEM	Transmission Electron Microscopy
WT	Wild Type
½ MS	Half-Strength Murashige and Skoog Medium

INTRODUCTION

Phosphoinositides are important lipid signaling molecules in animals, plants, and yeast. In animals and yeast they were found to respond to growth factors, hormones and neurotransmitters. They translate the extracellular stimulus into intracellular signaling cascades and thereby control fundamental cellular processes such as cell proliferation and motility, exo- and endocytosis, and reorganization of the cytoskeleton (Berridge 2009). Phosphatidylinositol 4,5-bisphosphate (PtdIns(4,5)P_2) assumes a central role in this canonical receptor-mediated signaling pathway as precursor to two second messengers, the cytosolic inositol trisphosphate (IP_3) and the membrane-bound diacylglycerol. Recent studies made it clear, however, that PtdIns(4,5)P_2 is a signaling molecule in itself and has been implicated, among others, in the regulation of membrane and vesicle trafficking and control of the cytoskeleton under stressed and non-stressed conditions (Jost et al. 1998; Abe et al. 2008; Di Paolo and De Camilli 2006).

Plants share many of the same components of the phosphoinositide signaling system, although some striking differences exist (Munnik and Testerink 2009). It was demonstrated that

phosphoinositides in plants were also central to signaling events regulating membrane and vesicle trafficking, the actin cytoskeleton, tip growth of pollen and root hairs, and stress and hormonal responses (reviewed in Munnik 2010). Recently, phosphoinositides have also been linked to cell morphogenesis, and, of particular interest to this study, secondary cell wall synthesis (Zhong et al. 2004; 2005).

Phosphoinositide signaling is dynamic as evidenced by quantitative and qualitative changes in the phosphoinositide species profile brought about by the concerted action of kinases, phosphatases and phospholipases. For example, a dramatic increase in PtdIns(4,5)P_2 was detected only minutes after exposing plants to heat, salt, and polyamines (Mishkind et al. 2009; Pical et al. 1999; DeWald et al. 2001; Takahashi et al. 2001; Zonia and Munnik 2004; Echevarria-Machado et al. 2005). In order to mediate physiological responses correctly to these various stimuli, PtdIns(4,5)P_2 and other phosphoinositide species have to be under tight spatio-temporal control. Therefore, elevated levels of PtdIns(4,5)P_2 have to be down-regulated to basal levels after stimulation. This is done in part by type II inositol polyphosphate 5-phosphatases and SAC domain phosphatases (Majerus et al. 1999; Mitchell et al. 2002; Whisstock et al. 2002; Hughes et al. 2000).

The suppressor of actin (SAC) domain is a highly conserved region of about 400 amino acids first found in yeast Sac1p, where it suppresses defects in certain actin mutants (Novick et al. 1989; Hughes 2001). A genome wide search in *Arabidopsis thaliana* identified a gene family (*AtSAC1-AtSAC9*) with high sequence similarity to the yeast protein Sac1p (Zhong and Ye 2003). Only three of the nine family members have been characterized so far (Despres et al. 2003; Williams et al. 2005; Zhong et al. 2005; Thole et al. 2008). *AtSAC1/FRA7* encodes a phosphoinositide phosphatase with substrate specificity towards phosphatidylinositol 3,5-bisphosphate (Zhong et al. 2005). Mutation of *AtSAC1/FRA7* causes defects in the cell wall and

the actin cytoskeleton, accompanied by an overall dwarfed phenotype. AtSAC7/RHD4 hydrolyzes preferentially phosphatidylinositol 4-phosphate and was proposed to organize the polarized secretion in root hair tip growth. Root hair-defective *rhd4* mutant plants had shorter root hairs with random bulges along their length, a disturbed actin cytoskeleton, and accumulated phosphatidylinositol 4-phosphate *in vivo* (Thole et al. 2008). AtSAC9 has been characterized as a putative phosphoinositide phosphatase distinct from other SAC domain-containing proteins and thought to be involved in stress signaling in *A. thaliana* (Williams et al. 2005). *sac9-1* plants have a constitutively stressed phenotype even when grown under non-stress conditions and most notably accumulate PtdIns(4,5)P_2 and IP_3. Interestingly, this changed phosphoinositide profile was only detected in extracts of roots and not in shoots. *sac9-1* plants are dwarfed with smaller hyponastic leaves and decreased root mass with shorter primary and fewer lateral roots.

In our study we investigated the primary roots of *sac9-1* seedlings at the cytological and ultrastructural level to address the cellular basis for this particular phenotype. *A. thaliana* roots are a paragon of simplicity in regard to development and structure. A small set of initial cells within the closed root meristem generates the root body in a predictable fashion and gives rise to four sets of continuous cell files: the root cap or columella, the epidermis and lateral root cap, the cortex and endodermis, and the stele or vascular cylinder. These cell files are arranged in symmetric radial layers which can be easily recognized in transverse sections (Dolan et al. 1993). The relatively simple cell and tissue organization of *A. thaliana* roots and the small variance in cell position and number facilitates characterization of structural abnormalities that are caused by a mutation rather than representing natural variability and plasticity.

Here we report on aberrant cell wall formation in cells of the primary root meristem in seedlings carrying the mutant allele *sac9-1* that might explain the stunted phenotype. Cell wall

material was deposited locally and in a range of abnormal shapes, sometimes completely fragmenting the cell. Excessive membrane material was associated with these irregular wall structures. We argue that a perturbed phosphoinositide metabolism most likely induced these observed abnormalities and hypothesize that a disorganized cytoskeleton and excessive membrane trafficking mediate the cell wall defects.

MATERIAL AND METHODS

Plant material and growth conditions

Arabidopsis thaliana wild-type (WT) seeds (*A. thaliana*, ecotype Col-0, CS1092) and *A. thaliana* seeds carrying the mutant allele *sac9-1* (kindly provided by Dr. Mary Williams formerly of Harvey Mudd College, Claremont, CA) were used in this study. For simplicity, the mutant seedline is referred to as *sac9* without further allele specification. Seeds were surface-sterilized for 5 minutes in 5x diluted Clorox with 0.05% Tween-20, followed by 5 rinses with sterile distilled water. Seeds were sown on a layer of Phytagel-solidified medium (½ MS, half-strength Murashige and Skoog medium, Research Products International Corp, IL, M10200), supplemented with 0.05% MES (Sigma, M2933) and solidified with 0.6% Phytagel (Sigma, P8169), pH 5.8, without sucrose supplement. Petri dishes were sealed with Parafilm and stratified for 3-4 days at 4°C to synchronize germination, after which they were positioned vertically in racks in a growth chamber with day and night temperature at 22/20°C ± 1°C and 14 hour lighting at ~200 µmol $m^{-2}s^{-2}$. Alternatively, seeds were surface-sterilized and cold-treated as above but germinated on sterile filter paper. Two to three days post germination, seedlings were carefully transferred to 2x2 inch pots containing wetted potting soil mix (Miracle Gro) and grown under a 14 hour day/10 hour night cycle and ambient temperature.

Primary root length measurements

Six-day-old seedlings with primary roots of equal length (7 mm ± 1 mm) were transferred to freshly prepared Phytagel-solidified ½ MS medium in square Petri dishes. WT and *sac9* seedlings were grown side by side on a plate and a total of 48 WT and 48 *sac9* seedlings on 16 independent Petri dishes were used. Root growth was monitored for 14 days by tracing roots with a permanent marker on the surface of the dish every other day. Root traces were scanned and digital images were converted to root length measurements using the RootLM program under MatLab (Qi et al. 2007). Statistical analysis (ANOVA) for significant differences in root length at day 20 was performed in SAS.

Light and transmission electron microscopy

Ten-day-old *A. thaliana* seedlings grown on Phytagel-solidified ½ MS plates were fixed in situ following a modified protocol by Sack and Kiss (1989). Briefly, the seedlings were carefully flooded in the dish with primary fixative (1% paraformaldehyde, 2% glutaraldehyde, in 50 mM sodium cacodylate buffer with 5 mM CaCl2, pH 7.2) for 15 minutes at room temperature. Primary root tips were then cut off and transferred immediately to vials with fresh primary fixative for an overnight incubation period at 4°C. Samples were rinsed in cacodylate buffer three times for 10 minutes and postfixed with 4% osmium tetroxide for 1 hour at room temperature followed by three 10-minute rinses in distilled water. Samples were dehydrated in an ascending series of acetone baths and stepwise infiltrated with Transmit epoxy resin, grade medium (TAAB Laboratories Equipment Ltd, UK), over 2 days. Flat-embedded root tips were cured at 70°C for 16 hours. For light microscopy, thick sections (1.5-2 µm) were dry-cut on a glass knife using an RMC MTX ultramicrotome (Boeckeler Instruments, Tucson, AZ), stained with epoxy tissue stain (EM Sciences, 14950) and viewed on an Olympus BH2 light microscope.

Images were captured with a PaxCam^{2+} digital microscope camera (MIS Inc., IL). For transmission electron microscopy, thin sections (100-130 nm) were cut on a diamond knife, collected on nickel grids, and double-stained with 2% aqueous uranyl acetate and lead citrate. Sections were examined either on a Hitachi 7100 transmission electron microscope at 75 kV or a Philips Tecnai 12 transmission electron microscope at 80 kV at the Electron Microscopy Facility at the University of Utah, Salt Lake City, UT. Scanned negatives were digitally processed with Photoshop. Over 1200 images obtained from 8 WT and 8 *sac9* primary root tips randomly chosen from more than 40 different seedlings were analyzed in the course of the study.

RESULTS

sac9 primary roots are stunted

Primary roots of plate-grown (no sucrose supplement) *sac9* seedlings elongated at a slower rate and were significantly shorter (Fig. 2-1). After 3 weeks (day 20 of the growth experiment), they were found to be only half as long as WT primary roots. A similar ratio was seen with *sac9* seedlings grown on plates supplemented with 1% sucrose (data not shown). Mature *sac9* plants grown in potting mix also showed a drastic reduction in root length and overall mass (Fig. 2-2a).

sac9 primary roots have regular tissue organization

Transverse sections cut through the meristematic region (100-150 μm distal to the root cap) revealed that both, *sac9* and WT seedlings had the same radial tissue organization of the primary root which is characterized by concentric layers of remnants of the lateral root cap, epidermis, cortex, endodermis and pericycle surrounding the vascular tissue (Fig. 2-2d, e).

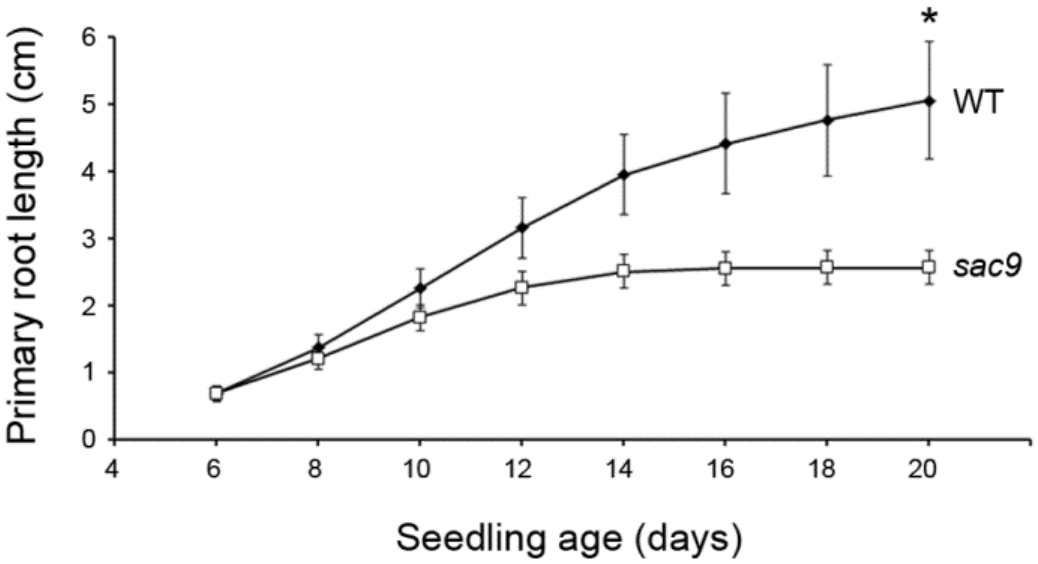

Fig. 2-1 Growth kinetics of WT and *sac9* primary roots. 6-day-old *A. thaliana* wild-type and *sac9* seedlings with approximately equal primary root length were transferred to fresh Phytagel-solidified ½ MS plates (no sucrose supplement) and primary root elongation was traced every other day for 2 weeks. Note that WT primary roots elongated much faster and were significantly longer at the end of the experiment. Asterisk marks statistical significance at day 20 (α=0.05, $p<0.0001$, n=96). Root measurements are given as mean ± SD

The epidermis consisted of a variable number of cells, yet the kidney-shaped cortex cells and the endodermis cells almost invariably formed a ring of 8 cells. Xylem and phloem elements were not yet differentiated within the stele. At the light microscopy level, none of the cells of *sac9* were noticeably different in size, shape, or alignment. Median longitudinal sections also did not differ in gross cytological morphology (Fig. 2-2b, c). Cell fate seemed to be maintained as evidenced by the fact that all cell files could be traced to a small set of initial cells which gave rise to functionally related but developmentally different cells in a lineage. Most cell files exhibited an orderly pattern of anticlinal divisions (perpendicular to the growth axis) with the occasional *sac9* root showing a slightly disturbed pattern in the epidermis and cortex cell lines of the meristematic region with some irregularly enlarged apoplastic spaces (data not shown).

Thus we conclude that despite the obvious differences in root growth and root mass appearance of *sac9* and WT seedlings, cytological analysis of the meristematic region at the light microscopic level was not sufficient to reveal any major differences between *sac9* and WT.

sac9 root cells have normal appearing organelles and are metabolically active

Since we could not find any obvious differences at the light microscopy (LM) level, we turned to transmission electron microscopy (TEM) to better understand root development in *sac9* seedlings. The same root tissues that were embedded in TAAB resin and used for LM were analyzed by TEM. At low magnification (1000x), cell organization was the same as seen with LM. Investigation of the fine structure of primary root cells of *sac9* demonstrated that organelles and cytoplasmic elements were normal. Both WT and *sac9* nuclei were mostly spherical to spheroidal (Figs. 2-3a-c, 2-4f, 2-5d). The majority of *sac9* interphase nuclei showed one prominent nucleolus and evenly dispersed chromatin suggestive of high transcriptional activity. The nuclear envelope appeared as a uniformly spaced distinct boundary layer between nucleoplasm and cytoplasm. Shorter and longer strands of rough endoplasmic reticulum (ER) ramified throughout the cytoplasm which was densely populated by free ribosomes, active Golgi stacks with numerous vesicles, mitochondria with regular morphology and simply structured proplastids, sometimes with dark plastoglobuli (Figs. 2-4, 5). These results indicate the preponderance of metabolically very active meristematic cells in *sac9* primary roots with morphologically indistinguishable subcellular organelles when compared to WT.

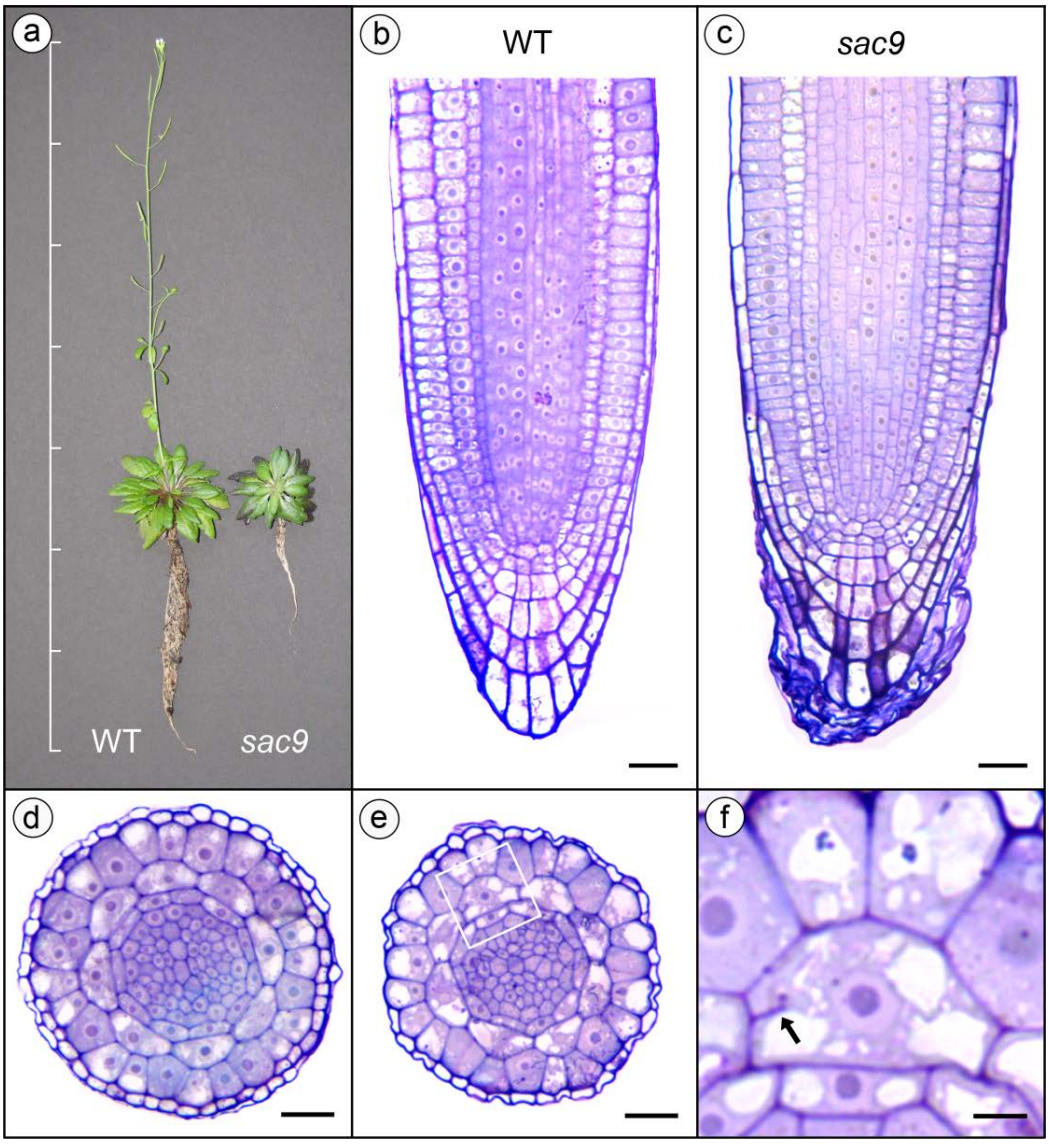

Fig. 2-2 Phenotype and tissue organization of WT and *sac9* primary roots. **a** Picture of 14-week-old *A. thaliana* WT and *sac9* plants demonstrating the dwarfed phenotype of *sac9*. Seeds were germinated on filter paper and 3-day-old seedlings were transferred to soilless potting mix and photographed on a weekly basis for 14 weeks. Note deeply purple older leaves, considerably less root mass and delayed bolting of the mutant. Bar increments, 5 cm; **b-f** Light micrographs of primary root tips from 10-day-old WT and *sac9* seedlings grown on Phytagel-solidified ½ MS plates. Seedlings were chemically fixed, embedded in resin, and 2 µm sections were cut and stained. **b, c** Longitudinal median sections of primary roots of WT (**b**) and *sac9* (**c**) seedlings, illustrating the closed organization of the root apical meristem with continuous cell files arising from initial cells. Sloughed off root cap cells are visible in (**c**). Bar, 20 µm; **d-f** Transverse sections of primary roots of WT (**d**) and *sac9* (**e, f**) seedlings approximately 150 µm behind the root apex, showing characteristic radial tissue organization with concentric layers of (from the outside in) lateral root cap, epidermis, cortex, endodermis, and the central cylinder with biarch protophloem poles; f Enlargement of insert presented in (**e**). Arrow points to a *sac9* cortex cell with an abnormal cell wall protuberance. Bar, 5 µm

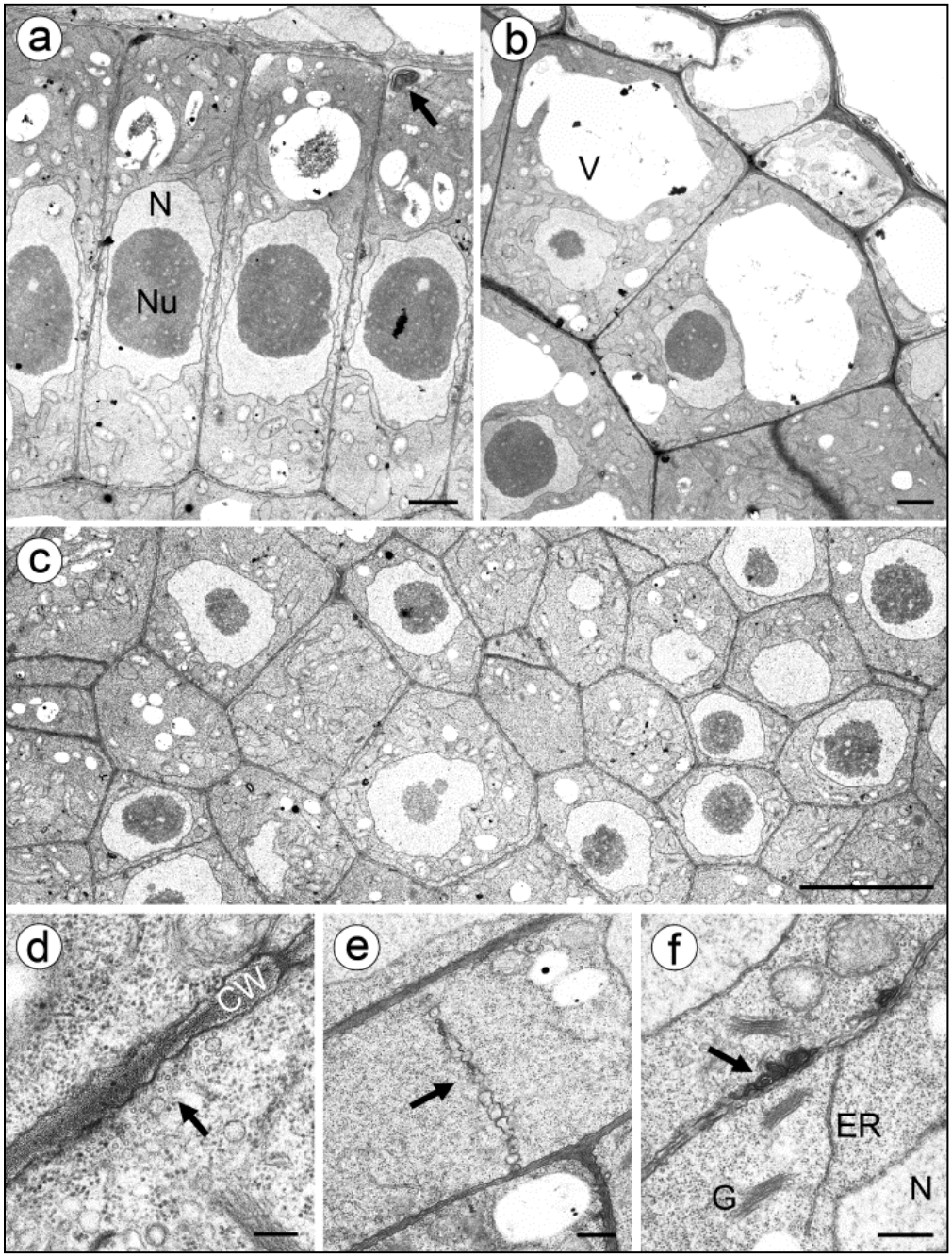

Fig. 2-3 WT root cells with normal appearing cell walls. Transmission electron micrographs of meristematic WT root cells show regular cell walls in every cell type. Epidermal cells in transverse (**a**) and longitudinal median (**b**) section. Arrow in (**a**) points to a membrane whorl in one of the epidermis cells. Bar, 2 µm; **c** Cells from the central cylinder in transverse section. Note the normal appearance of the cell walls. Bar, 5 µm; **d-f** Consecutive stages of new cell wall formation during somatic cytokinesis as demonstrated by the preprophase band (**d**, arrow), nascent cell plate (**e**, arrow), and newly formed cell wall between two prominent nuclei (**f**). Membranes are associated with the new cell wall (**f**, arrow). Bar, 500 nm. CW cell wall, ER endoplasmic reticulum, G Golgi stack, M mitochondrion, N nucleus, Nu nucleolus, V vacuole

Some *sac9* root cells have abnormal cell wall protuberances

Examination of the cell wall revealed a different scenario. In *sac9* roots, we found cells in almost every plane of section that had abnormalities, regardless of cell type and position within the meristematic region. These abnormalities included unusual spur-like protuberances of varying length and shape arising from the existing cell wall and intruding into the cytoplasm (Fig. 2-4a-d), pinching of cytoplasm resulting in fragmentation of cells (Figs. 2-4d-f, 2-5a), highly abnormal accumulation of cell wall material tight to membranes (Figs. 2-4d, 2-5b-e, 2-6, 2-7), and undulating internal cell walls (Fig. 2-7). The nature of the protuberances could be identified at higher magnification as cell wall comparable. They had the same electron dense staining pattern with striations as normal appearing cell walls of *sac9* and control cell walls in WT. Furthermore, the cell wall material of the protuberances was contained by a continuation of the plasma membrane as seen in Figure 2-4a-c. The protuberances varied in size from undetectable at lower magnification to very conspicuous at higher magnification. The smallest protuberance measured less than 100 nm, whereas larger ones were found in the range of several µm. Some extended from one side of the cell to the other (Fig. 2-4d, e). The majority of the protuberances, however, were very small (< 1 µm). This explains why we were not able to observe them at the light microscopy level until we gathered information at higher levels of magnification, with the exception of very large protuberances (Fig. 2-2f). Some protuberances appeared to end in the middle of the cytoplasm in a bulbous (Fig. 2-4b) or branched structure (Fig. 2-4c) with amorphous looking cell wall areas. Flattened membrane vesicles could be seen embedded in the cell wall matrix of some protuberances (Fig. 2-4b). Other protuberances seemed to continue to expand centripetally by addition of multiple membrane vesicles to the growing end (Fig. 2-5b, c), similar to vesicles frequently associated with the nascent cell plate in freshly divided cells.

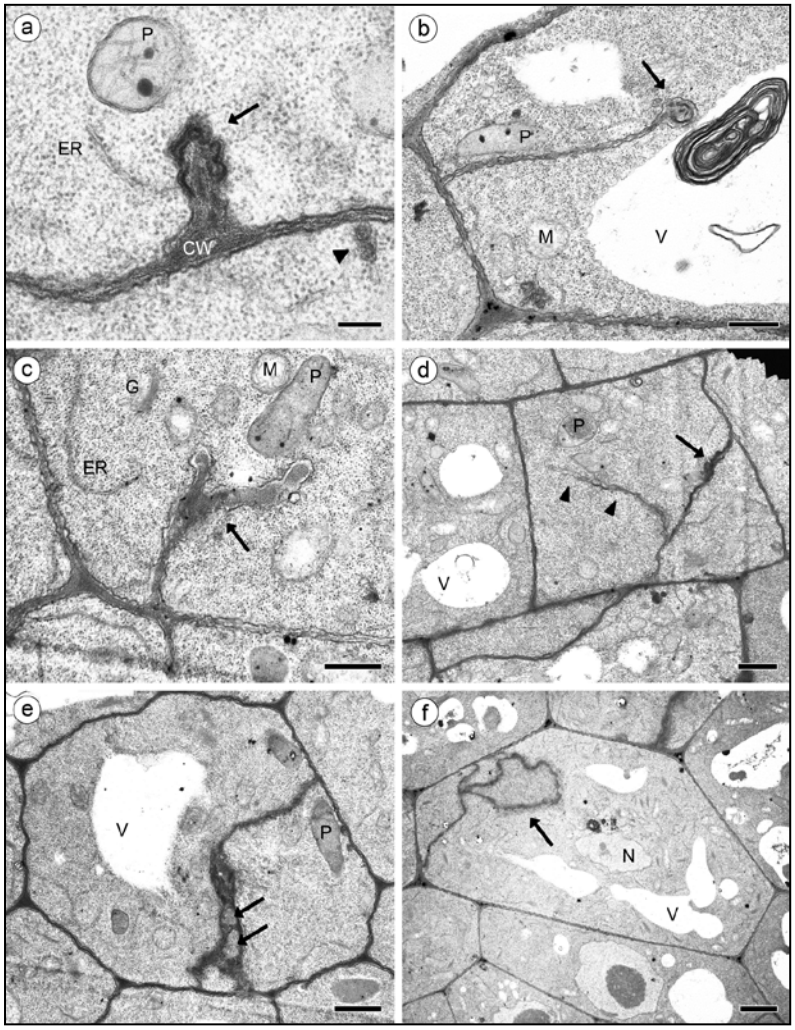

Fig. 2-4 Abnormal cell wall ingrowths in *sac9* root cells. Transmission electron micrographs of meristematic *sac9* root cells show irregular cell wall protuberances of varying size and shape. **a** Transverse section of an endodermis cell with a small cell wall stub protruding into the cytoplasm. Note the wavy layers of membranes at the tip of the protuberance (arrow). The arrowhead points to a developing shaved cell wall protuberance in the neighboring cell that, in this plane of section, is not connected to the wall. Bar 200 nm; **b** Transverse section of an endodermis cell with a long uniform cell wall protuberance ending in an enlarged bulbous structure (arrow). Note the flattened and curved vesicles embedded in the cell wall material of the bulb. A large membrane whorl can be seen within the vacuole in close proximity to the bulbous structure. Bar 500 nm; **c** Transverse section of a cell from the stele with a small branched cell wall protuberance. Note the uneven thickness of the cell wall material particularly at the branched area (arrow). Bar 1 µm; **d** Longitudinal median section of an endodermis cell with a large branched cell wall protuberance (arrowheads). Note also the membrane accumulation at the internal wall (arrow). Bar 1 µm; **e** Transverse section of a cell from the stele fragmented by uneven internal walls. The arrows point to pockets of cytoplasm which appear pinched off by the branched walls. Bar 1 µm; **f** Transverse section of a cortex cell showing an irregularly looped internal cell wall structure (arrow). Bar, 5 µm. CW cell wall, ER endoplasmic reticulum, G Golgi stack, M mitochondrion, P proplastid, N nucleus, V vacuole

However, it is interesting to note that none of the cells with protuberances were enlarged or were multi-nucleated, the typical morphological characteristics of cytokinesis mutants (Jaber et al. 2010). It looked as if the protuberances occurred randomly as a misdirected layering of cell wall material on the inner surface of the existing primary cell wall. In contrast to *sac9* root cells, we did not observe any irregular wall protuberances in WT root cells (Fig. 2-3).

sac9 wall protuberances are associated with excessive membrane material

At the ultrastructural level, we noticed excessive membrane material in either direct contact or close to the wall forming the protuberances (Figs. 2-5, 2-6). Membranous vesicles and more complex membrane inclusions in tight or loose concentric layers similar to myelinated figures appeared to be associated with the aberrant wall formation. These whorl-like structure were not limited to the cytoplasm, but were also found in vacuoles (Fig. 2-4b).

Membrane inclusions were also observed in the cytoplasm and vacuoles of WT root cells (Fig. 2-3a, arrow) and adjacent to newly formed cell walls after somatic cytokinesis (Fig. 2-3f, arrow). This most likely indicated a normal degenerative process of phagocytized cytoplasmic material and/or recycling of excessive membrane material. However, the extreme accumulation of these membranous inclusions in some *sac9* root cells, as exemplified by Figure 2-6, was obvious and might point to either higher membrane turnover or trafficking or a combination of both.

sac9 wall protuberances are randomly distributed and can be extensive

In order to investigate the spatial distribution of these protuberances, we analyzed transverse, longitudinal and even oblique sections through the meristematic region of *sac9* primary roots. Protuberances of different sizes and shapes were found at random in all different planes of section (Figs. 2-2f, 2-4a-c, 2-5, 2-7 for transverse sections; Figs. 2-4d, 2-6 for

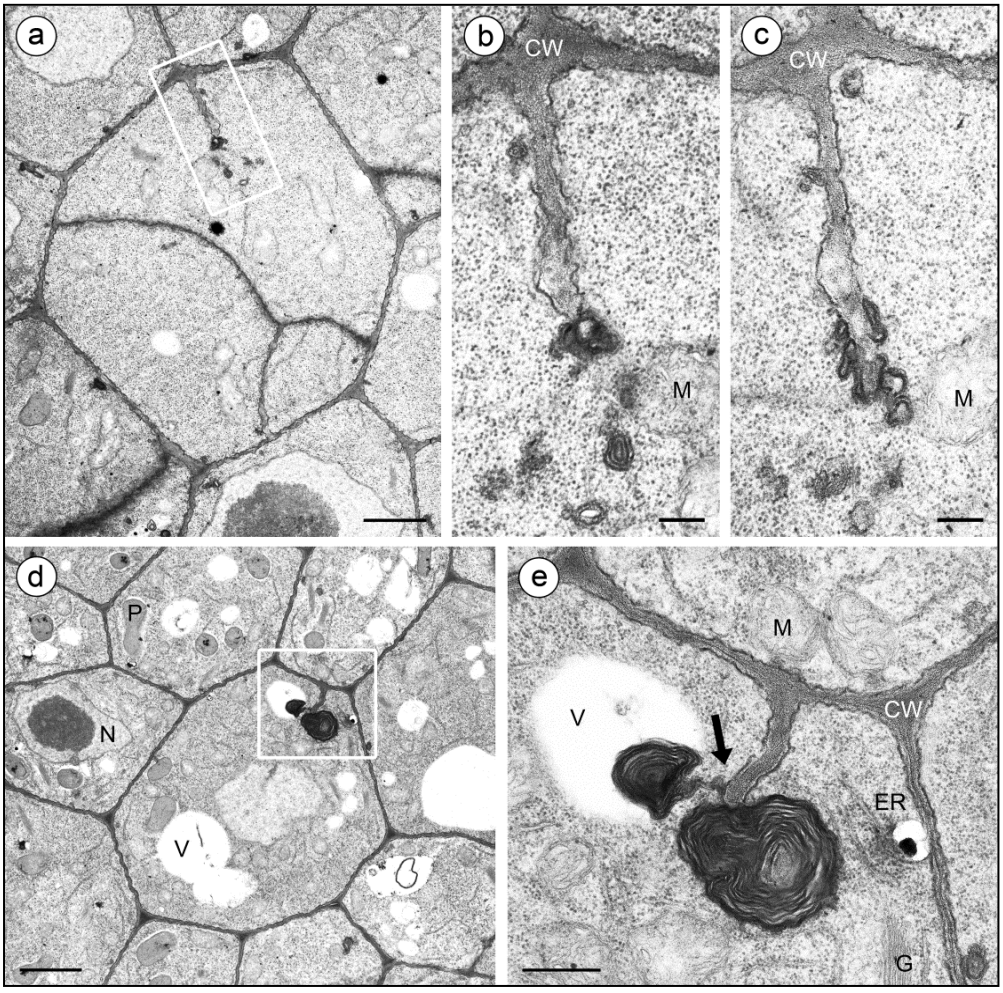

Fig. 2-5 Centripetal cell wall ingrowth in *sac9* primary root cells and association of excessive membrane material with cell wall ingrowth. **a** Transmission electron micrograph of a cell from the central cylinder illustrating the centripetal elongation of a cell wall protuberance. Note that the cell is also fragmented by a branched internal wall. Bar, 1 µm; **b** Enlargement of insert shown in (**a**). Note the vesicles containing concentric layers of membranes and other electron dense material in close proximity to the tip of the protuberance. Bar, 200 nm; **c** The same protuberance as presented in (**b**) but from a succeeding section. Note that some of the vesicles seen in (**b**) have fused to the tip of the protuberance and are still recognizable as partially flattened membrane inclusions. It becomes evident that the protuberance arose as a continuation from the pre-existing cell wall and grew towards the center of the cell by fusion of vesicles to the elongating end. Note the uneven thickness of the aberrant cell wall suggesting undirected growth. Bar, 200 nm; **d** Transmission electron micrograph from a similar region as in (**a**) but from a different *sac9* seedling showing two densely stained inclusions closely associated with the curved cell wall protuberance. Bar, 2 µm; **e** Enlargement of insert presented in (**d**). Note the direct connection from the plasma membrane surrounding the aberrant cell wall ingrowth to the smaller of the two membrane whorls (arrow). It appears that the smaller membrane whorl is partially engulfed into the vacuole. Also note the tight concentric membrane layers of both membrane whorls. Bar, 500 nm; CW cell wall; ER endoplasmic reticulum; G Golgi stack; M mitochondrion; N nucleus; P proplastid; V vacuole

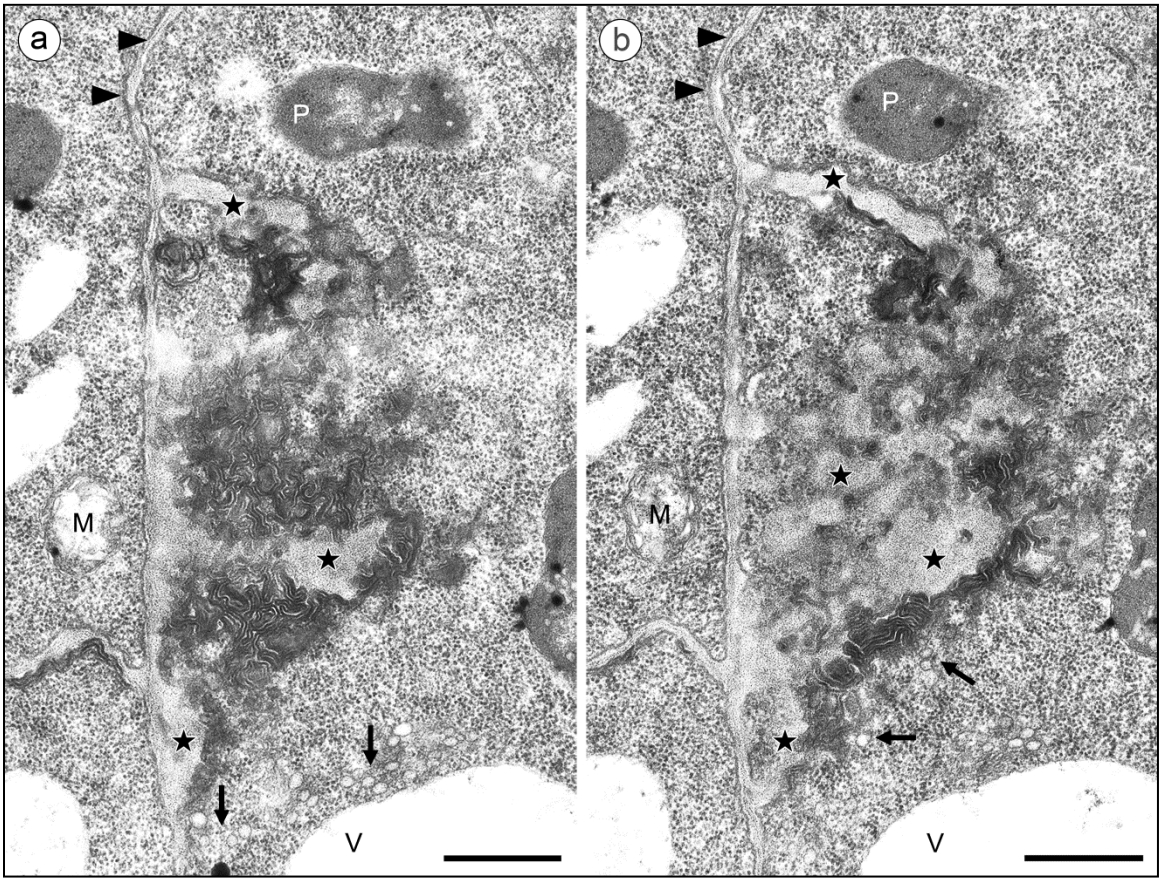

Fig. 2-6 An extreme example of excessive membrane material associated with the aberrant deposition of irregular cell wall material in *sac9* seedlings. **a, b** Transmission electron micrographs of two consecutive longitudinal median sections through the central cylinder of the primary root close to the apex revealing densely winding, parallel membranes in direct contact with cell wall material. Stars point to randomly deposited and diffuse-appearing cell wall material, whereas arrowheads indicate a normal-looking cell wall area with even thickness. Note the massive accumulation of vesicles presumably containing cell wall precursors in close proximity to the irregular cell wall deposition (arrows). Bar, 500 nm. M mitochondrion; P proplastid; V vacuole

longitudinal sections; oblique sections not shown). These results suggest that protuberances could arise independently of the regular plane of anticlinal and periclinal cell divisions.

Serial sections were cut to examine the architecture of the protuberances in more detail. A presentation of five serial sections illustrates the elaborate and peculiar appearance of the cell wall aberration seen in a *sac9* epidermal cell of the root meristem (Fig. 2-7a-e).

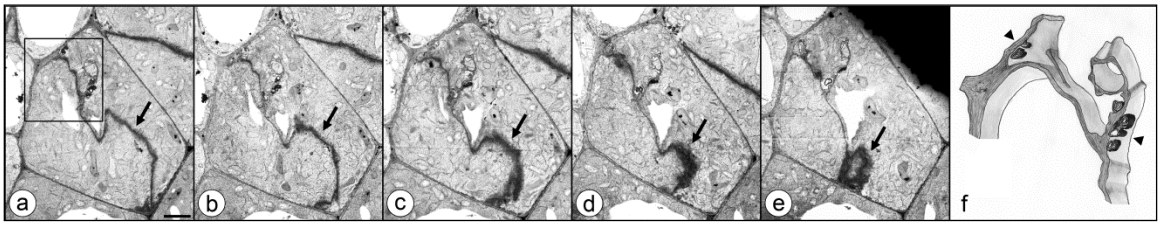

Fig. 2-7 Serial sections of a cell wall ingrowth in an epidermal *sac9* root cell and corresponding 3D rendering. **a-e** Transmission electron micrographs of five transverse serial sections through the meristematic region of the primary root of *sac9* showing a large cell wall protuberance forming a cylinder-like structure (boxed area in a). Note the extremely shifting internal cell wall (arrows). Bar, 2 µm. **f** Three-dimensional rendering of the cylinder-like cell wall aberration based on the previous and other serial sections of the same cell. Excessive membranes in the form of electron dense concentric whorls are closely associated with the aberrant cell wall (arrowheads)

From these and other consecutive serial sections it became clear that the abnormal wall was undulating and shifting extremely throughout the cytoplasm in these sections (Fig. 2-7a-e, arrows). The abnormal cell wall branched off to one side and formed a complete circle which did not appear to change its position much; i.e. the circle in a two-dimensional section (Fig. 2-7a, boxed area) turned out to be a cylinder-like structure deeply penetrating the cytoplasm in a three-dimensional interpretation from serial sections (Fig. 2-7f). Membrane vesicles and whorls could be seen in close proximity to the cylinder, either adding more cell wall material to the structure or being recycled as excessive membrane material (Fig. 2-7f, arrowheads).

These results indicate that the previously described cell wall protuberances were most likely part of a much larger three-dimensional cell wall aberration which appeared highly irregular in nature. To account for the varying architecture, we shall refer to these protuberances subsequently as cell wall ingrowths.

DISCUSSION

AtSAC9 mutants are highly interesting because of their multifaceted phenotype, which might be a direct or indirect consequence of perturbed signal transduction pathways centering around elevated endogenous levels of PtdIns(4,5)P_2 in *sac9* roots. Williams et al. (2005) and Gong et al. (2006) both documented shorter primary roots and fewer lateral roots in *sac9* seedlings. To determine the structural basis for this altered growth, we examined the tissue organization as well as fine and ultrastructure of cells from *sac9* primary root meristems. Although we found that the tissue organization and the cellular organelles appeared normal, we did observe unusual cell wall and membrane structures within many *sac9* cells of the root meristem. The cell wall ingrowths ranged from simple protuberances to broad flanges, diffuse patches, elaborate folds, irregular loops and other complex three-dimensional structures. Serial sections showed that they were associated with abundant vesicles and excessive membrane inclusions.

Is *sac9* a cytokinesis mutant?

Cell wall ingrowths related to various stages of somatic cytokinesis have been found in other *A. thaliana* mutants and have been described as cell wall stubs by several authors. Lukowitz et al. (1996) reported enlarged, multinucleated and polyploid cells in *knolle* embryos with wall defects in the form of incomplete cell walls with gaps in the middle and T-shaped cross walls attached to the parental cell wall. Assaad et al. (1996) described comparable cell wall defects in *keule* embryos. Similar abnormalities were induced by incubating different plant seedlings with drugs, such as caffeine in bean (Röper and Röper 1977), or treating with herbicides, such as dichlobenil in onion (Vaughn et al. 1996). Both treatments disrupted cell plate formation and led to extensions of the parental wall, referred to as centripetal wall

formation by Röper and Röper (1977). Abnormal embryos with variably enlarged cells, incomplete cell walls and multiple nuclei were also seen in *A. thaliana* mutants in which HINKEL, a kinesin-related protein, was not functional (Strompen et al. 2002). The authors speculated that the HINKEL protein was involved in the coordination of cell plate formation with phragmoplast microtubule depolymerization, which is necessary for lateral expansion of the phragmoplast (Jurgens 2005). Other typical cytokinesis defects were visible to varying degrees in *pleiade* seedlings (Muller et al. 2002), *cyt1* embryos (Nickle and Meinke 1998), and *kor1-1* embryos (Zuo et al. 2000). *cyt1* and *kor1-1* are notable, as they both seem to be involved in the regulation of cell wall synthesis in addition to cytokinesis.

The phenotypic features of *sac9* root cells, however, particularly the already described cell wall ingrowths, are not indicative of cytokinesis defects, as no enlarged or bi- or multinucleated cells were observed. In our study, cell wall defects were only found in cells with a single nucleus which was predominantly in interphase. In many cytokinesis mutants, the reported cell wall stubs were situated in the equatorial division plane attached to the parental wall at opposite ends, sometimes leaving a gap in the middle, suggesting that cell plate formation, expansion, or maturation, had failed at some point (Assaad et al. 1996; Jaber et al. 2010; Lukowitz et al. 1996). In contrast, cell wall ingrowths in *sac9* cells arose at random sites from the pre-existing wall growing towards the center of the cell, but not restricted to the position of a future cell plate. In addition, if cytokinesis had been affected in *sac9* embryos, seedling lethality might be expected. Many cytokinesis mutants do not survive the embryo stage (Assaad et al. 1996; Jaber et al. 2010; Liu et al. 1995; Lukowitz et al. 1996; Strompen et al. 2002) or are merely conditional mutants (Eleftheriou et al. 2005). However, *sac9* seeds germinated and seedlings successfully established, ruling out a primary defect in cytokinesis. This is also supported by the observation that *sac9* cells without wall defects showed the typical Golgi-

derived belt of fusing vesicles forming the nascent cell plate, which at the end of cytokinesis had matured into the plasma membranes and primary walls between daughter cells (data not shown). It is worth emphasizing that *sac9* cells with wall protuberances were found in the meristematic area of the root but nonetheless never seen in the stage leading to or exiting mitosis. This might be interpreted as a failure of mitosis to take place in these particular cells.

Are *sac9* root cells with wall ingrowths modified transfer cells?

It could be argued that the architecture of some type of cell wall ingrowths in *sac9* cells (i.e., simple protuberances and flanges) bears resemblance to localized wall deposition in transfer cells. Transfer cells are anatomically and functionally specialized plant cells which facilitate membrane-mediated transfer of various solutes (Gunning et al. 1968; Gunning and Pate 1969). To achieve this, they develop extensive wall ingrowths with concomitant amplification of the plasma membrane surface for solute transport (Offler et al. 2003).

Although the resemblance to transfer cells is only speculative, these specialized cells might provide insights into the formation of localized wall deposition in *sac9* root cells. Cell wall ingrowth in transfer cells can be broadly categorized as either reticulate- or flange-like (Talbot et al. 2002). Transfer cells of the reticulate type have papillate projections of cell wall material that in later stages fuse to form a complex labyrinth-like network. Flange wall ingrowth is characterized by rib-shaped projections.

Transmission electron microscopy and field emission scanning microscopy demonstrated that both types are not only morphologically very different, but they also seem to have different ontogenies (Talbot et al. 2002). The earliest signs of reticulate ingrowth were localized appositions of randomly oriented cellulose microfibrils over a new layer of parallel

cellulose microfibrils. In contrast, flange ingrowths emerged over bundles of parallel cellulose microfibers over otherwise randomly arranged cellulose microfibers (Talbot et al. 2007).
Cell wall ingrowth in *sac9* cells ranged from simple papilla-like projections to flanges but also encompassed clearly more complex structures which were very distinct from any cell wall ingrowth found in transfer cells. Varying staining patterns within some *sac9* cell wall ingrowths also point to a unique deposition pattern of cell wall material. The cell walls of smaller, simple projections often appear regular whereas larger or convoluted ingrowths are less lamellated, more amorphous and of uneven thickness. Careful comparison between normal cell wall protuberances in transfer cells and abnormal cell wall ingrowths in *sac9* root cells makes it clear that the aberrations found in *sac9* root cells are morphologically unique. Furthermore, there is a clear structure-function-relationship in transfer cells, where function directly dictates structure. An analogous function of short distance solute transfer in *sac9* cells with wall ingrowths seems physiologically not plausible.

A possible role of the cytoskeleton in the formation of localized cell walls in *sac9*

The cytoskeleton is a major contributor in the formation of cell walls. Actin filaments are known to organize the cellular architecture, to orchestrate endo- and exocytosis, and vesicle trafficking. In particular, the latter is essential for the delivery of vesicles containing cell wall precursors and cell wall synthesizing and modifying enzymes to the plasma membrane, although microtubules are also involved in this process, specifically at the cell plate (Jurgens 2005).

It is more likely that the *sac9* mutation is based on a defective actin rather than a defective microtubule cytoskeleton. The link between the actin cytoskeleton and phospholipid signaling has long been established in animals and lower eukaryotes (reviewed in Takenawa and Itoh 2001). Evidence is emerging that some phospholipids regulate actin organization and

dynamics in a comparable fashion in plants by binding and modulating the activity (and most likely the intercellular location) of actin-binding proteins (ABPs). More than 70 classes of ABPs are known in eukaryotes (Staiger and Blanchoin 2006) and they affect all aspects of the actin cytoskeleton. ABPs control the ratio of G- to F-actin and hence the pool of available subunits and state of polymerization and depolymerization. They influence filament length and breakage, and they nucleate new filaments and crosslink existing filaments in higher order structures such as bundles (reviewed in McCurdy et al. 2001).

Some plant ABPs have also been shown to bind to PtdIns(4,5)P_2, including profilin (Drøbak et al. 1994), ADF/cofilin (Gungabissoon et al. 1998) and capping protein, CP (Huang et al. 2003). Therefore, it seems plausible that the elevated levels of PtdIns(4,5)P_2 in *sac9* seedlings could serve as additional anchor points for binding of ABPs and localizing them to the plasma membrane. Thus, these ABPs seem attractive mediators of phospholipid-based changes in the actin cytoskeleton and, ultimately, the cell wall.

At the current knowledge however, it would be premature to speculate about the phenotypic consequences of such possible binding in *sac9* cells since many ABPs are also regulated by pH, Ca^{2+} concentrations, phosphorylation, and the presence of other ABPs (Wasteneys and Galway 2003; Hussey et al. 2006).

Do other *A. thaliana* mutants with defects in SAC domain-containing proteins and/or elevated levels of PtdIns(4,5)P_2 have cell wall aberrations?

Another line of evidence that the *SAC9* gene is potentially implicated in the indirect regulation of the actin cytoskeleton comes from detailed morphological characterization of SAC domain-containing mutants (Zhong et al. 2005) and mutants with a disturbed phospholipid metabolism (Zhong et al. 2004). There are several reports of a temporary increase of

PtdIns(4,5)P_2 elicited by environmental stresses (Pical et al. 1999; DeWald et al. 2001; Zonia and Munnik 2004; Mishkind et al. 2009), hormones (Krinke et al. 2007) and polyamines (Echevarria-Machado et al. 2005), but none of these investigations included morphological data.

To our knowledge, there is only one *A. thaliana* mutant described with endogenous elevated levels of PtdIns(4,5)P_2 and IP_3 that is also cytologically characterized (Zhong et al. 2004). *fra3* inflorescence stems showed a two-fold increase in endogenous concentration of PtdIns(4,5)P_2 and IP_3, and a moderate but significant increase of PtdIns(4,5)P_2 in seedlings. The *FRA3* gene encodes a type II inositol polyphosphate 5-phosphatase with high substrate affinity for PtdIns(4,5)P_2. Morphological analysis revealed abnormalities in the thickness of fiber cell walls and concurrent abnormal actin bundling in the same cell type while the microtubule cytoskeleton was not affected. Based on the mutant phenotype and functional assays of recombinant FRA3 protein, the authors concluded that the perturbed phosphoinositide metabolism, in particular the elevated levels of PtdIns(4,5)P_2, likely caused the actin abnormalities and thus led to a decrease in cell wall thickness of fiber cells. It is worth pointing out that the FRA3 protein does not contain a SAC domain.

AtSAC1 shares the SAC domain and other sequence similarity with SAC9 (Zhong and Ye 2003). Results from morphological studies of *sac1* mutants resembled those obtained from *fra3* mutants. Both showed reduced cell wall thickness and altered F-actin organization, mostly in fiber, but also in non-fiber cells of elongating stems. This explains why they were both discovered in the same screen for defective fiber mutants (Zhong et al. 2004). Again, a correlation between the actin cytoskeleton and cell wall synthesis was inferred. However, endogenous levels of PIs were not measured. This would be particularly informative in the light of biochemical data indicating *in vitro* substrate activity of the AtSAC1 phosphatase only against PtdIns(3,5)P_2.

CONCLUSION

In conclusion, this study links elevated PtdIns(4,5)P_2 levels in the putative phosphoinositide phosphatase mutant *sac9* with aberrant formation of wall ingrowths in a number of cells of the primary root. We provide evidence that cell walls could develop independently of cytokinesis by haphazard but localized deposition of cell wall material on pre-existing cell walls without the typical formation of a cell plate. Because of the lack of direction and the spontaneous generation of these cell walls, normal cell division does not take place, and the cell becomes fragmented with concomitant growth retardation. We hypothesize that the formation and winding of these abnormal cell walls is a result of undirected development, probably due to a lack or disorganization of the cytoskeletal elements orchestrated by a perturbed phosphoinositide metabolism.

The observed cell wall ingrowths in *sac9* mutants provide a unique example of localized wall deposition, which has been extensively studied in tracheary elements and transfer cells. Although much progress has been made in the organization and composition of these highly specialized cells, the underlying molecular mechanism(s) that regulate the formation of localized wall deposition remain(s) elusive. Understanding how PtdIns(4,5)P_2 affects the cytoskeleton in *sac9* seedlings might shed further light on the process of localized wall formation in *A. thaliana*.

REFERENCES

Abe N, Inoue T, Galvez T, Klein L, Meyer T (2008) Dissecting the role of PtdIns(4,5)P_2 in endocytosis and recycling of the transferrin receptor. J Cell Sci 121 (Pt 9):1488-1494

Assaad FF, Mayer U, Wanner G, Jurgens G (1996) The *KEULE* gene is involved in cytokinesis in *Arabidopsis*. Mol Gen Genet 253 (3):267-277

Berridge MJ (2009) Inositol trisphosphate and calcium signalling mechanisms. Biochim Biophys Acta 1793 (6):933-940

Despres B, Bouissonnie F, Wu HJ, Gomord V, Guilleminot J, Grellet F, Berger F, Delseny M, Devic M (2003) Three *SAC1*-like genes show overlapping patterns of expression in *Arabidopsis* but are remarkably silent during embryo development. Plant J 34 (3):293-306

DeWald DB, Torabinejad J, Jones CA, Shope JC, Cangelosi AR, Thompson JE, Prestwich GD, Hama H (2001) Rapid accumulation of phosphatidylinositol 4,5-bisphosphate and inositol 1,4,5-trisphosphate correlates with calcium mobilization in salt-stressed Arabidopsis. Plant Physiol 126 (2):759-769

Di Paolo G, De Camilli P (2006) Phosphoinositides in cell regulation and membrane dynamics. Nature 443 (7112):651-657

Dolan L, Janmaat K, Willemsen V, Linstead P, Poethig S, Roberts K, Scheres B (1993) Cellular organization of the *Arabidopsis thaliana* root. Development 119 (1):71-84

Drøbak BK, Watkins PAC, Valenta R, Dove SK, Lloyd CW, Staiger CJ (1994) Inhibition of plant plasma membrane phosphoinositide phospholipase C by the actin-binding protein, profilin. Plant J 6 (3):389-400

Echevarria-Machado I, Ramos-Diaz A, Brito-Argaez L, Racagni-Di Palma G, Loyola-Vargas VM, Hernandez-Sotomayor SM (2005) Polyamines modify the components of phospholipids-based signal transduction pathway in *Coffea arabica* L. cells. Plant Physiol Biochem 43 (9):874-881

Eleftheriou EP, Baskin TI, Hepler PK (2005) Aberrant cell plate formation in the *Arabidopsis thaliana microtubule organization 1* mutant. Plant Cell Physiol 46 (4):671-675

Gong P, Wu G, Ort DR (2006) Slow dark deactivation of Arabidopsis chloroplast ATP synthase caused by a mutation in a nonplastidic SAC domain protein. Photosynth Res 88 (2):133-142

Gungabissoon RA, Jiang C-J, Drøbak BK, Maciver SK, Hussey PJ (1998) Interaction of maize actin-depolymerising factor with actin and phosphoinositides and its inhibition of plant phospholipase C. Plant J 16 (6):689-696

Gunning BE, Pate JS, Briarty LG (1968) Specialized "transfer cells" in minor veins of leaves and their possible significance in phloem translocation. J Cell Biol 37 (3):C7-12

Gunning BES, Pate JS (1969) “Transfer cells” Plant cells with wall ingrowths, specialized in relation to short distance transport of solutes—Their occurrence, structure, and development. Protoplasma 68 (1):107-133

Huang S, Blanchoin L, Kovar DR, Staiger CJ (2003) *Arabidopsis* capping protein (AtCP) is a heterodimer that regulates assembly at the barbed ends of actin filaments. J Biol Chem 278 (45):44832-44842

Hughes WE (2001) The Sac phosphatase domain. Curr Biol 11 (7):R249

Hughes WE, Cooke FT, Parker PJ (2000) Sac phosphatase domain proteins. Biochem J 350 Pt 2:337-352

Hussey PJ, Ketelaar T, Deeks MJ (2006) Control of the actin cytoskeleton in plant cell growth. Annu Rev Plant Biol 57:109-125

Jaber E, Thiele K, Kindzierski V, Loderer C, Rybak K, Jurgens G, Mayer U, Sollner R, Wanner G, Assaad FF (2010) A putative TRAPPII tethering factor is required for cell plate assembly during cytokinesis in *Arabidopsis*. New Phytol 187 (3):751-763

Jost M, Simpson F, Kavran JM, Lemmon MA, Schmid SL (1998) Phosphatidylinositol-4,5-bisphosphate is required for endocytic coated vesicle formation. Curr Biol 8 (25):1399-1402

Jurgens G (2005) Cytokinesis in higher plants. Annu Rev Plant Biol 56:281-299

Krinke O, Ruelland E, Valentova O, Vergnolle C, Renou JP, Taconnat L, Flemr M, Burketova L, Zachowski A (2007) Phosphatidylinositol 4-kinase activation is an early response to salicylic acid in Arabidopsis suspension cells. Plant Physiol 144 (3):1347-1359

Liu CM, Johnson S, Wang TL (1995) *cyd*, a mutant of pea that alters embryo morphology is defective in cytokinesis. Vol 16. Wiley Subscription Services, Inc., A Wiley Company. Hoboken, NJ. DOI:10.1002/dvg.1020160405

Lukowitz W, Mayer U, Jurgens G (1996) Cytokinesis in the Arabidopsis embryo involves the syntaxin-related KNOLLE gene product. Cell 84 (1):61-71

Majerus PW, Kisseleva MV, Norris FA (1999) The role of phosphatases in inositol signaling reactions. J Biol Chem 274 (16):10669-10672

McCurdy DW, Kovar DR, Staiger CJ (2001) Actin and actin-binding proteins in higher plants. Protoplasma 215 (1-4):89-104

Mishkind M, Vermeer JE, Darwish E, Munnik T (2009) Heat stress activates phospholipase D and triggers PIP_2 accumulation at the plasma membrane and nucleus. Plant J 60 (1):10-21

Mitchell CA, Gurung R, Kong AM, Dyson JM, Tan A, Ooms LM (2002) Inositol polyphosphate 5-phosphatases: lipid phosphatases with flair. IUBMB Life 53 (1):25-36

Muller S, Fuchs E, Ovecka M, Wysocka-Diller J, Benfey PN, Hauser MT (2002) Two new loci, *PLEIADE* and *HYADE*, implicate organ-specific regulation of cytokinesis in Arabidopsis. Plant Physiol 130 (1):312-324

Munnik T (2010) Lipid signaling in plants. Plant cell monographs. Vol 16. Springer. Heidelberg, Germany

Munnik T, Testerink C (2009) Plant phospholipid signaling: "in a nutshell". J Lipid Res 50 Suppl:S260-265

Nickle TC, Meinke DW (1998) A cytokinesis-defective mutant of Arabidopsis (*cyt1*) characterized by embryonic lethality, incomplete cell walls, and excessive callose accumulation. Plant J 15 (3):321-332

Novick P, Osmond BC, Botstein D (1989) Suppressors of yeast actin mutations. Genetics 121 (4):659-674

Offler CE, McCurdy DW, Patrick JW, Talbot MJ (2003) Transfer cells: cells specialized for a special purpose. Annu Rev Plant Biol 54:431-454

Pical C, Westergren T, Dove SK, Larsson C, Sommarin M (1999) Salinity and hyperosmotic stress induce rapid increases in phosphatidylinositol 4,5-bisphosphate, diacylglycerol pyrophosphate, and phosphatidylcholine in *Arabidopsis thaliana* cells. J Biol Chem 274 (53):38232-38240

Qi X, Qi J, Wu Y (2007) RootLM: a simple color image analysis program for length measurements of primary roots in *Arabidopsis*. Plant Root 1:10-16

Röper W, Röper S (1977) Centripetal wall formation in roots of *Vicia faba* after caffeine treatment. Protoplasma 93 (1):89-100

Sack FD, Kiss JZ (1989) Rootcap structure in wild type and in a starchless mutant of Arabidopsis. Am J Bot 76 (3):454-464

Staiger CJ, Blanchoin L (2006) Actin dynamics: old friends with new stories. Curr Opin Plant Biol 9 (6):554-562

Strompen G, El Kasmi F, Richter S, Lukowitz W, Assaad FF, Jurgens G, Mayer U (2002) The Arabidopsis *HINKEL* gene encodes a kinesin-related protein involved in cytokinesis and is expressed in a cell cycle-dependent manner. Curr Biol 12 (2):153-158

Takahashi S, Katagiri T, Hirayama T, Yamaguchi-Shinozaki K, Shinozaki K (2001) Hyperosmotic stress induces a rapid and transient increase in inositol 1,4,5-trisphosphate independent of abscisic acid in Arabidopsis cell culture. Plant Cell Physiol 42 (2):214-222

Takenawa T, Itoh T (2001) Phosphoinositides, key molecules for regulation of actin cytoskeletal organization and membrane traffic from the plasma membrane. B B A 1533 (3):190-206

Talbot MJ, Offler CE, McCurdy DW (2002) Transfer cell wall architecture: a contribution towards understanding localized wall deposition. Protoplasma 219 (3-4):197-209

Talbot MJ, Wasteneys GO, Offler CE, McCurdy DW (2007) Cellulose synthesis is required for deposition of reticulate wall ingrowths in transfer cells. Plant Cell Physiol 48 (1):147-158

Thole JM, Vermeer JE, Zhang Y, Gadella TW, Jr., Nielsen E (2008) *ROOT HAIR DEFECTIVE4* encodes a phosphatidylinositol-4-phosphate phosphatase required for proper root hair development in *Arabidopsis thaliana*. Plant Cell 20 (2):381-395

Vaughn KC, Hoffman JC, Hahn MG, Staehelin LA (1996) The herbicide dichlobenil disrupts cell plate formation: immunogold characterization. Protoplasma 194 (3):117-132

Wasteneys GO, Galway ME (2003) Remodeling the cytoskeleton for growth and form: an overview with some new views. Annu Rev Plant Biol 54:691-722

Whisstock JC, Wiradjaja F, Waters JE, Gurung R (2002) The structure and function of catalytic domains within inositol polyphosphate 5-phosphatases. IUBMB Life 53 (1):15-23

Williams ME, Torabinejad J, Cohick E, Parker K, Drake EJ, Thompson JE, Hortter M, DeWald DB (2005) Mutations in the Arabidopsis phosphoinositide phosphatase gene *SAC9* lead to overaccumulation of PtdIns(4,5)P_2 and constitutive expression of the stress-response pathway. Plant Physiol 138 (2):686-700

Zhong R, Burk DH, Morrison WH, 3rd, Ye ZH (2004) *FRAGILE FIBER3*, an Arabidopsis gene encoding a type II inositol polyphosphate 5-phosphatase, is required for secondary wall synthesis and actin organization in fiber cells. Plant Cell 16 (12):3242-3259

Zhong R, Burk DH, Nairn CJ, Wood-Jones A, Morrison WH, 3rd, Ye ZH (2005) Mutation of SAC1, an Arabidopsis SAC domain phosphoinositide phosphatase, causes alterations in cell morphogenesis, cell wall synthesis, and actin organization. Plant Cell 17 (5):1449-1466

Zhong R, Ye ZH (2003) The SAC domain-containing protein gene family in Arabidopsis. Plant Physiol 132 (2):544-555

Zonia L, Munnik T (2004) Osmotically induced cell swelling versus cell shrinking elicits specific changes in phospholipid signals in tobacco pollen tubes. Plant Physiol 134 (2):813-823

Zuo J, Niu QW, Nishizawa N, Wu Y, Kost B, Chua NH (2000) KORRIGAN, an Arabidopsis endo-1,4-beta-glucanase, localizes to the cell plate by polarized targeting and is essential for cytokinesis. Plant Cell 12 (7):1137-1152

CHAPTER 3

ANALYSIS OF THE CORTICAL MICROTUBULE CYTOSKELETON IN THE DEVELOPING ROOT OF THE PUTATIVE PHOSPHOINOSITIDE PHOSPHATASE MUTANT *AtSAC9*

ABSTRACT

The cortical microtubule (MT) cytoskeleton was investigated in the stunted root of the putative phosphoinositide phosphatase mutant *sac9-1* in *Arabidopsis thaliana* by means of immunofluorescence and transmission electron microscopy (TEM). On the TEM level, there were no apparent morphological differences of cortical MTs in *sac9-1* root cells. Their spatial association with the plasma membrane also appeared undisturbed. The global distribution of cortical MTs was then observed with confocal microscopy of immunostained roots. To gain a better insight of microtubule orientation, I applied the filtered two-dimensional discrete Fourier transform (DFT) method (Marquez 2006). By using the modified Marquez's DFT method, I showed that cortical MT arrays in *sac9-1* root cells of the elongation zone were similar to wild type, but the orientation changed faster from perpendicular to oblique in respect to the growth axis in the differentiation zone. I also demonstrate the suitability and effectiveness of this method. Additionally, I discuss the advantages of the optimized DFT technique in accurately characterizing angular orientations of cortical MTs, and conclude that it is a valid additional technique to traditional and rather time-consuming methods. I speculate that factors other than cortical MT orientation might play a more dominant role in affecting the normal elongation of root cells in the *sac9-1* mutant.

ABBREVIATIONS

DFT	Discrete Fourier Transform
MT(s)	Microtubule(s)
PBS	Phosphate-Buffered Saline
PEMT	Phosphate-EGTA-$MgCl_2$-Triton X-100 buffer
SAC	Suppressor of Actin 1 (Sac1) homology domain
SAC9	SAC domain-containing protein 9
TEM	Transmission Electron Microscopy
WT	Wild Type
½ MS	Half-strength Murashige and Skoog medium

INTRODUCTION

Microtubules (MTs) are slender, hollow structures, made up of a staggered lateral assembly of 13 protofilaments, each composed of the same alternating subunits (α- and β-tubulin). The relative uniform appearance of MTs at the confocal and the electron microscopy level deceives their range of functions. Far from being static implants, they are part of the plant cytoskeleton, and are involved in basic processes such as cell division (Eleftheriou et al. 2005; Jurgens 2005; Kawamura et al. 2006) and cell morphogenesis (Bibikova et al. 1999; Roberts et al. 2004; Wasteneys and Fujita 2006; Paradez et al. 2006; Wightman and Turner 2008; Crowell et al. 2009). They further contribute to the positioning of the nucleus (Holzinger and Lutz-Meindl 2003) and chloroplasts (Holzinger et al. 2007; 2008).

MTs are dynamic structures that change in accordance with the progression through the cell cycle (Vantard et al. 2000; Azimzadeh et al. 2001), as well as along the growth axis of the

root (Hogetsu and Oshima 1986; Baluska et al. 1992; Sugimoto et al. 2000). Before a plant cell enters mitosis, MTs form a transient, narrow but densely packed band (preprophase band) encircling the cell at its periphery in the equatorial plane. In a yet unknown process, these MTs mark the plane of the future cell plate. In metaphase, MTs build the mitotic spindle perpendicular to the equatorial plane that leads to the separation of the chromosomes into the daughter cells. During late cytokinesis, MTs along with actin filaments and other associated proteins form the phragmoplast and guide the delivery of vesicles containing cell wall precursors to the nascent cell plate (reviewed in Jurgens 2005). Cortical MTs in rapidly dividing, isodiametric cells of the apical meristem are randomly arranged during interphase, whereas they are positioned in parallel bundles at right angles to the growth axis in elongating cells (like a thread on a spool), and obliquely in older cells that have ceased to enlarge (Laskowski 1990; Sugimoto et al. 2000; Granger and Cyr 2001).

Over the last four decades, the conspicuous co-alignment of MTs with cellulose microfibrils in elongating cells has spawned an ongoing debate about the nature of this relationship and potential implications for MTs in cell morphogenesis (Ledbetter and Porter 1963; Heath 1974; Giddings and Staehelin 1991; Fisher and Cyr 1998; Baskin 2001; Wasteneys 2004; Paradez et al. 2006; Emons et al. 2007; Lloyd and Chan 2008; Baskin et al. 1999; Burk and Ye 2002). Cellulose microfibrils are the major load-bearing components of cell walls. By affecting the orientation of these crystalline polymers, the polarity of the growth axis is established by conferring a mechanical bias for extension in length rather than width. This anisotropic growth is a requirement for normal tissue development in the root and shoot of all plants. In an outstanding set of experiments Paradez et al. (2006) used the reporter constructs YFP:CESA6 (yellow fluorescent protein fused to cellulose synthase component 6) and CFP:TUA1 (citrine fluorescent protein fused to α-tubulin 1) and elegantly demonstrated that the cellulose

microfibril synthesizing complex (CESA) was indeed functionally related to the organization of cortical MTs in elongating cells of *Arabidopsis* hypocotyls. Imaging of living samples showed that YFP:CESA6 followed on trajectories, even on discordant ones, determined by the position of CFP:TUA1. Concurrent changes in the orientation of MTs and the arrangement of YFP:CESA6 were recorded for normal development as well as for blue-light stimulated reorientation of the cortical MT arrays. Partial disruption of the MT array by depolymerization with the herbicide oryzalin lead to correlated changes in the YFP:CESA6 localization. This study was the first explicit *in vivo* evidence to support the hypothesis put forward by Heath (1974) that MTs directly guide CESA complexes (molecular rail hypothesis). It also discredited the alternative (bumper-rail or constraint hypothesis), advanced by Giddings and Staehelin (1991), which proposed that MTs indirectly guided the CESA complexes by channeling and constraining them between MTs. The additional surprising observation by Paradez et al. (2006) that, in spite of the absence of MTs (i.e., in cells with completely disrupted MTs), the CESA complexes still can move in parallel, oblique trajectories, albeit only for some time, may explain the discord over the co-alignment hypothesis in general (Sugimoto et al. 2003; Wasteneys 2004; Himmelspach et al. 2003).

Chapter 2 reported unique cell wall aberrations in *A. thaliana sac9-1* root cells that possibly contributed to the development of shorter primary roots. Abnormalities were observed in some cells in the meristem and ranged from simple stubs to forked and undulating protuberances originating from the cell wall. These abnormalities were not related to specific cytokinesis defects. SAC9 is a unique member of the suppressor of actin (SAC) domain-containing protein family in *Arabidopsis* (Zhong et al. 2003). Although the SAC domain in AtSAC9 lacks motif seven, the catalytic core is conserved (Zhong et al. 2003), and therefore is presumed to confer phosphatase activity towards phosphoinositides (Williams et al. 2005). AtSAC9 has not been biochemically confirmed as a phosphoinositide phosphatase. However, its involvement in

phospholipid signaling is strongly hypothesized by the observation of endogenously elevated levels of inositol 1,4,5-trisphosphate, IP_3, and phosphatidylinositol 4,5-bisphosphate, $PI(4,5)P_2$, in roots of *sac9-1* mutants (Williams et al. 2005).

sac9-1 roots are much shorter than wild-type roots (Chapter 2), and given the importance of cortical MTs in elongating cells by dictating the location of the cellulose synthase complex and thus cell shape, I visualized the global MT organization of *sac9-1* roots by immunolocalization and the ultrastructure of individual MTs by transmission electron microscopy. I applied a modified Discrete Fourier Transform (DFT) to characterize angular orientation distributions of cortical MTs from confocal images of root epidermal cells along a developmental gradient, and demonstrate the suitability and effectiveness of this method. In this study, I show that the cortical MT arrays in *sac9-1* root cells of the elongation zone were wild-type-like but changed faster than WT from perpendicular to oblique in respect to the growth axis in the differentiation zone. TEM images indicated a wild-type-like ultrastructure of cortical MTs in *sac9-1* root cells with a normal spatial association to the plasma membrane. I conclude that the DFT method is a valid addition to traditional and rather time-consuming methods of angular measurements of elongated objects, and that factors other than cortical MT orientation might play a more dominant role in affecting the normal elongation of root cells in the *sac9-1* mutant.

MATERIAL AND METHODS

Plant material and growth conditions

The *A. thaliana* genotypes used in this study were WT (Col-0) and *sac9-1*, a putative phosphoinositide phosphatase mutant (kindly provided by Dr. Mary Williams, formerly of Harvey Mudd College, Claremont, CA). In this report, the mutant genotype is referred to simply

as *sac9* without further allele specification. Seeds were surface-sterilized by soaking for 5 min in 20% commercial bleach containing 0.05% Tween-20 followed by five rinses with sterile distilled water. Seeds were directly plated on glass microscope slides (25 x 75 x 1 mm, precleaned and frosted) coated with growth medium just below the slide frosted area. The coating medium, one-mm-thick, consisted of ½ Murashige and Skoog medium (MS, Sigma, M5524), pH 5.7, supplemented with 1% sucrose and solidified with 0.6% bacto-agar (Difco Laboratories). Glass slides with plated seeds on ½ MS medium were kept in a sealed Petri dish for a stratification period of 3-6 days at 4°C in the dark, and then transferred to a growth chamber and maintained in a vertical position at 22/20°C ± 1°C (day/night) under a 14 h light/10 h dark cycle (~200 µmol $m^{-2}s^{-1}$).

Root growth measurements

Roots of live 8-10-day-old seedlings were visualized in bright field on an inverted Olympus FV1000-XY microscope with a dry 10x lens. Images with a size of 1024x1024 px were recorded and analyzed with PaxCam^{2+} software (MIS Inc., Villa Park, IL). Root diameter was measured in the differentiation zone where trichomes were well visible. The combined length of the meristematic region (zone I) and the elongation zone (zones II and III) was measured along the growth axis starting from the quiescent center to the onset of root hairs. When this length exceeded one field of view, as was the case for some wild-type roots, images of two overlapping field of views were stitched together prior to measuring. Results from 15-20 primary roots per genotype were scored and tested for differences by analysis of variance using SAS 9.2 (SAS Institute Inc, Cary, NC). Measurements were made from two independent growth experiments.

Immunofluorescence

Six- and 7-day-old seedlings were used in this study. Microtubules were visualized using the combined techniques of Sugimoto et al. (2000) and Collings and Wasteneys (2005) with few modifications. All incubation steps were carried out at room temperature unless otherwise stated. This was especially important for the fixation step since microtubules are cold-labile. Whole seedlings were fixed in situ for 40 min in PEMT buffer (50 mM Pipes, 2 mM EGTA, 2 mM $MgSO_4$, 0.1% Triton X-100, pH 7.2) containing 4% formaldehyde and 1% glutaraldehyde, followed by three 10 min washes with PEMT buffer. Samples were extracted by incubating in PEMT buffer with Triton X-100 adjusted to 1% for 1 h, followed by three 10 min rinses with PEMT buffer. Cell walls were digested by a twenty-minute treatment with 0.05% Pectolyase Y-23 (Duchefa Biochemie, P8004, Haarlem, The Netherlands) in PEMT buffer with 0.4 M mannitol. The enzyme was removed by three 10 min washes with PEMT buffer. Samples were then treated with ice-cold (-20°C) methanol for 10 min to permeabilize membranes; this necessitated a subsequent 10 min rehydration step with PBS, pH 7.4 (Sigma, P3813). Samples were flooded with sodium borohydride (1 mg/ml in PBS, 20 min) to remove unreduced aldehydes from the fixation step. After three 10 min washes with PBS and 30 min blocking with incubation buffer (PBS, 1% BSA, 50 mM glycine), seedlings were incubated overnight with monoclonal mouse anti-β-tubulin-antibodies (Sigma, T5201) at a concentration of 1:1000 in incubation buffer. Goat $F(ab)_2$ fragments conjugated to Alexa Fluor 488 were used to recognize the mouse IgG and IgM (Molecular Probes, A-11017). Secondary antibodies were applied at 1:500 in PBS for 3 h. The labeled seedlings were then rinsed three times for 10 min each with PBS between and after antibody treatments. Excess liquid was removed from the surface of the growth medium and shoots were cut off and carefully removed. The remaining roots on the slide were mounted in Fluoromount G with DAPI (EMS, 17984-24) and covered with a 24 x 50 mm coverslip (No. 1).

Slides were kept at 4°C in the dark until examination with confocal microscopes at the Fluorescence Microscopy Facility, University of Utah, Salt Lake City, UT.

Microscopy and image acquisition

Confocal images were acquired on an inverted FV1000-XY Olympus IX81 microscope with a motorized stage. For tissue orientation, a dry 10x lens was used. Microtubules were imaged with a 60x (NA 1.42) oil immersion lens with a 2x digital zoom. The stains were excited with a 405/488 nm laser and the emission spectra were filtered between 425-475 nm for DAPI and 500-600 nm for Alexa Fluor 488. Images were acquired in sequential scan mode with Kahlman filtering applied over two frames. Z-stacks consisting of 1 µm steps were captured at a scan speed of 10 µs/px and with a resolution of 138 nm/px. Scan size was 1024x1024 pixels. Optical sections were projected with maximum intensity. The number of optical sections combined this way was determined empirically to maximize the signal-to-noise ratio. Images were taken along the main axis of the root at four stages: the meristematic area of the root tip (I), the rapidly growing region of elongating cells (II), the slowly growing region of elongating cells (III), and the early differentiation zone (IV).

Analysis of cortical MT orientation

The angular orientation distribution of cortical MTs in root cells was determined from confocal images with the filtered Discrete Fourier Transform (DFT) method described by Marquez 2006. The custom-written software running under MatLab (The MathWorks Inc, Natick, MA) was generously provided by Keith Carney (University of Utah, Salt Lake City, UT). RGB confocal images were changed to 8-bit black and white TIFF images in Photoshop (Adobe Systems Inc., San Jose, CA). Ten 11 x 11 µm squares (=79 x 79 px) were cropped from each image and used as subsamples. The square size was determined by the minimum cell size in the

meristematic region of the root. I am aware of the limitation that the samples I selected were not random, as the squares had to be placed intentionally inside the cell to minimize errors that may stem from interfering cell wall structures. To further minimize errors, the location of the squares was normalized by adjusting their orientation relative to the cell long axis. Five wild-type and *sac9* roots were analyzed this way resulting in 50 polar plots per zone and genotype, totaling 200 polar plots each.

Transmission electron microscopy

The reader is referred to Chapter 2 for a detailed protocol. Briefly, 10-day-old seedlings were fixed with 1% paraformaldehyde, 2% glutaraldehyde in 50 mM sodium cacodylate buffer with 5 mM $CaCl_2$, pH 7.2 followed by osmification. Cut off root tips were dehydrated in increasing concentrations of acetone and stepwise infiltrated with Transmit epoxy resin (TAAB Laboratories Equipment Ltd, UK). Flat embedded samples were cured, trimmed and then sectioned on an RMC MTX ultramicrotome (Boeckeler Instruments, Tucson, AZ). Gold sections were double-stained and examined on a Philips Tecnai 12 transmission electron microscope at the Electron Microscopy Facility, University of Utah, Salt Lake City, UT.

RESULTS

***sac9* primary roots have shorter tip regions than WT but are not swollen**

Measurements of the combined length of the zones of cell division and elongation indicated that *sac9* primary root tips of six-to-seven-day-old seedlings were significantly shorter compared to WT (-35%, $P<0.0001$ by Student's t-test). However, *sac9* roots showed no sign of swelling at any point along the growth axis. Not surprisingly, *sac9* root diameters were slightly smaller than WT (-13%, $P<0.0001$ by Student's t-test, Table 3-1).

Table 3-1 Growth parameters of *A. thaliana* WT and *sac9* primary roots

Genotype	Root tip length [µm]	Root diameter [µm]
WT	1223 ± 163 (13.3%)	140 ± 8 (5.9%)
sac9	802 ± 170 (21.2%)	122 ± 8 (6.8%)
p-value	<0.0001	<0.0001

Root tip length was defined as the combined length of zone I-III, starting from the quiescent center to the onset of root hair formation. Root diameter was taken in the mature region of the root where root hairs were clearly visible. Data represent means ± SD from 15-20 seedlings per genotype with two biological replicates of which only one is shown here. Although there were some differences between the two replicates, inferential testing provided similar P-values. The Coefficient variant is given in parentheses. P-values were calculated from Student's t-test (α=0.05)

The ultrastructure of cortical MTs appears unaffected in *sac9* root cells

To investigate if the structure of cortical microtubules or their association with the plasma membrane in non-dividing cells were affected in *sac9*, I analyzed WT and *sac9* root cells at the TEM. After glutaraldehyde/formaldehyde-osmium-fixation, cortical MTs appeared well-preserved (Fig. 3-1). In both genotypes, cortical MTs were visible as dark circles enclosing an electron-opaque center when sectioned transversely. These 25-nm-structures were found either in long single rows (Fig. 3-3d, black arrow) underlying the plasma membrane, or in short patches arranged in two to three rows and were uniform in shape (Fig. 3-3a-b). In shaving sections through the tangential cell walls, MTs appeared as those typically seen in sagital profiles (Fig. 3-3d, f). The parallel array of individual cortical MTs was mostly perpendicular to the cell axis, confirming the assessment of immunolabeled images of elongating root cells at the confocal level. Taken together, these results indicate that cortical MTs were structurally normal in *sac9* root cells, and their association with the cell wall and underlying plasma membrane was not impaired.

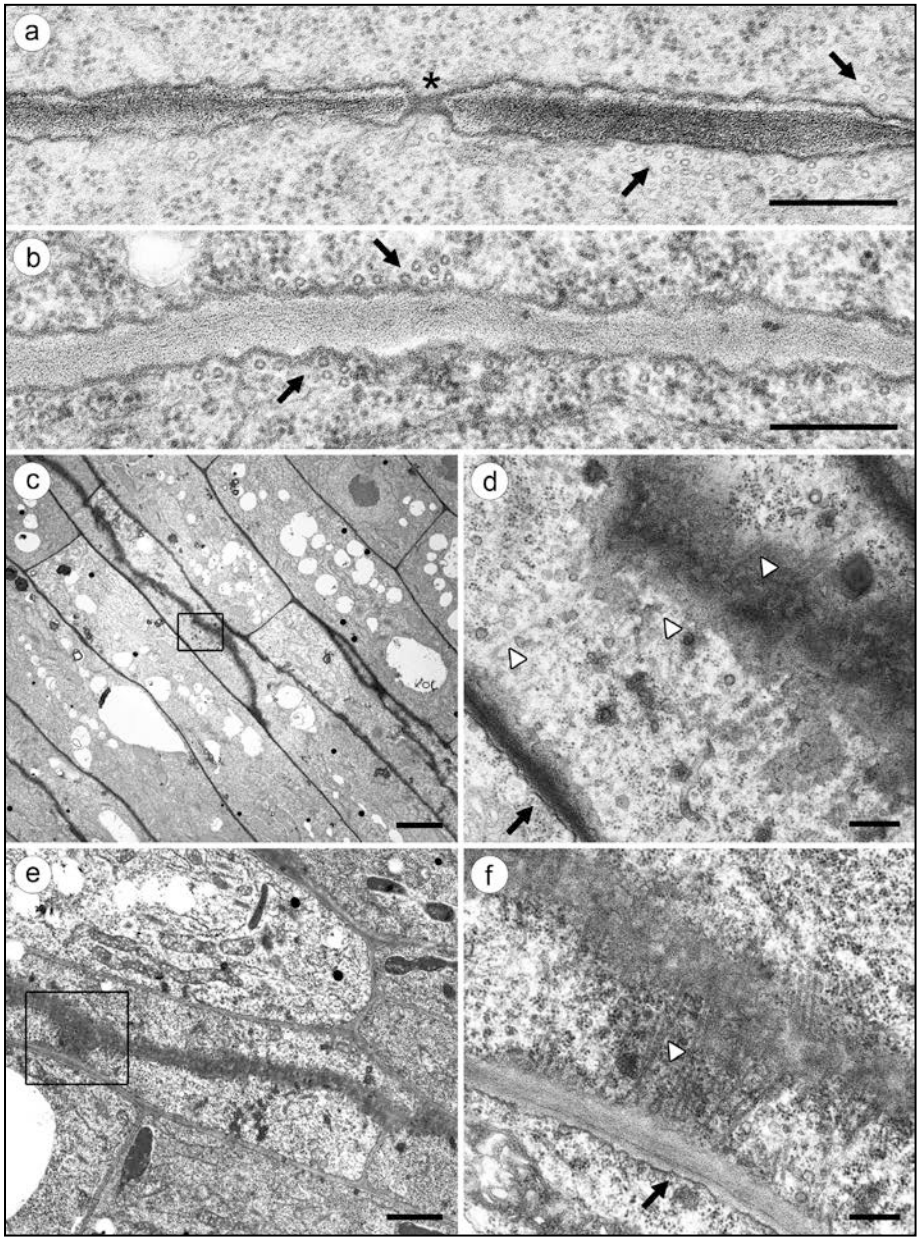

Fig. 3-1 Cortical MTs in the elongation zone of WT and *sac9* root cells as visualized by transmission electron microscopy (TEM). Transverse sections of (**a**) WT and (**b**) *sac9* root cells show MTs as hollow tubes in close proximity to and at both sides of the cell wall (arrows). Asterisk in (**a**) points out the site of a plasmodesma. Bar 200 nm. In longitudinal sections (**c-f**), these hollow tubes can be seen as two parallel dark lines bridging a brighter center reminiscent of rail road tracks (white arrowheads). **c** Longitudinal section through the central cylinder of WT. Bar 5 µm. **d** Enlarged insert from (**c**), black arrow points to a row of single MTs in cross section in the adjacent cell. Bar 500 nm. It becomes evident that MTs in longitudinal view are only rarely encountered in glancing sections through the cell wall (diffusely dark area). **e** Longitudinal section through the central cylinder of *sac9*. Bar 2 µm. **f** Enlarged insert from (**e**). The spacing and alignment of MTs appears wild-type-like. As with (**d**), MTs can be seen in the adjacent cell in cross section (black arrow). Bar 500 nm

Meristematic and rapidly growing *sac9* root epidermal cells have normal cortical MT arrays but the distribution differs in the root hair zone: qualitative assessment by IF

Transmission electron microscopy is an irreplaceable tool for the detailed structural investigation of subcellar components. However, its advantage of high resolution images can also be its disadvantage if the focus of interest is the investigation of a more global distribution of subcellular components. In this case, confocal microscopy is better suited.

To test the hypothesis that the distribution of cortical MTs is potentially the underlying cause for the reduced length of the root tip in *sac9* mutants, I immunostained whole root mounts for β-tubulin. Figure 3-2b-i shows maximum intensity projections of confocal images and illustrates the cortical MT distribution patterns at four distinctive stages (zones I-IV) of the developing root in WT (Fig. 3-2b-e) and *sac9* (Fig. 3-2f-i). Zone I includes the cells of the meristem, zone II and III comprise the region of rapid (II) and slow (III) cell elongation, respectively, and zone IV encompasses differentiated cells as marked by the onset of root hair formation (Fig. 3-2a). In WT, cortical MTs were seen in the tangential walls of non-dividing epidermal cells in characteristic arrays that correlated with the developmental status along the root axis. In cells from the meristem (that were not occluded from view by the overlying cells of the root cap), the cortical MTs were observed as short and randomly distributed (Fig. 3-2b). Once the disk-shaped to isodiametric cells started to elongate, first rapidly (Zone II), and then more slowly (Zone III), bundles of larger and parallel MTs with a net orientation perpendicular to the growth axis were visible (Fig. 3-2c,d). The parallel nature of these MT bundles was maintained in zone III but the orientation was no longer perpendicular to the growth axis. Although Fig. 3-2d gives the impression of a uniform deviation from 90°, this was not always the case. The orientation was sometimes different within the same cell and between adjacent cells (data not shown). With the differentiation of epidermal cells into root hairs, the angle of cortical

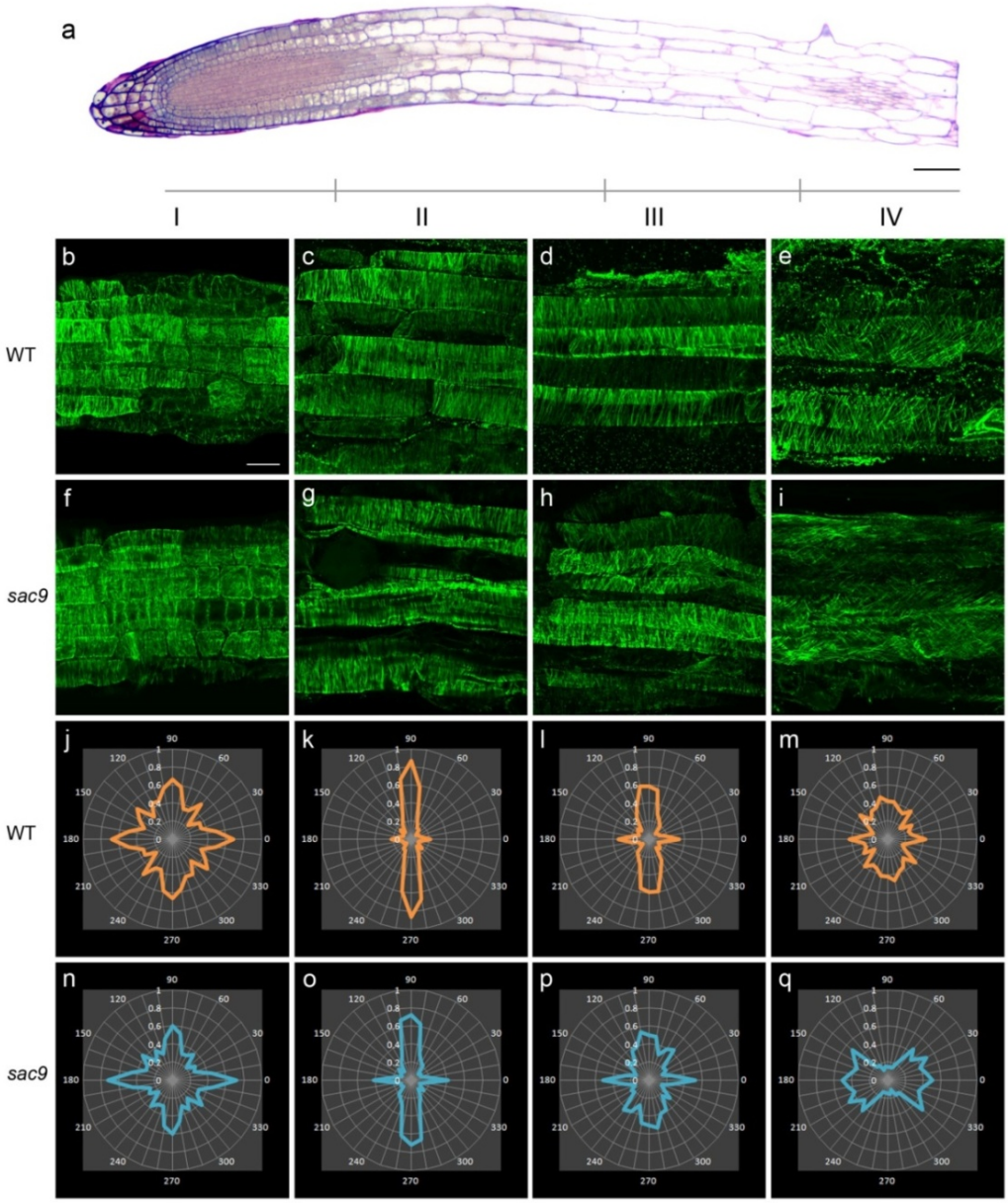

Fig. 3-2 Cortical MT orientation in developing WT and *sac9* roots. **a** Resin-embedded longitudinal section through the primary root tip of WT depicting four developmental zones (zone I: meristem, zone II: proximal elongation with rapidly elongating cells, zone III: distal elongation with slowly elongating cells, zone IV: differentiation with the onset of root hair formation). The absolute length of each zone can vary. Bar 50 µm. **b-i** Representative confocal images of immunostained cortical MTs in the consecutive developmental zones of WT (**b-e**) and *sac9* (**f-I**). Bar 20 µm. Confocal images with immunostained MTs were Fourier transformed and the relative strength (from 0-1) of the concentration of the periodic structures (here MTs) was plotted against the mean angular orientation distributions of cortical MTs along the developmental gradient in WT (**j-m**) and in *sac9* (**n-q**). The plots are averages from ten subsamples per image from five individual primary roots per genotype. More detailed information is presented in the following text

MT bundles in respect to the 90°-axis became even more oblique, and occasionally, were almost parallel to the cell axis (Fig. 3-2e and unpublished data). Not only did the angular distribution of cortical MTs change with the progression through the different growth zones, but also MT bundle density appeared to correlate with the same zones. In WT, they were densely packed in the zone of rapid cell elongation, but seemed to lose their compactness as cells reached their maximum length (Fig. 3-2e). The orientation of cortical MTs in *sac9* root cells as judged by confocal microscopy images of immunolabeled β-tubulin appeared qualitatively similar to that found in WT (Fig. 3-2f-i), although it looked as if some differences in the acuteness of the angle existed in the later growth zones.

Quantitative assessment of angular orientation distributions of cortical MTs by DFT

To characterize the angular orientation distribution of cortical MTs, I applied a fully automated and optimized two-dimensional Discrete Fourier Transform (DFT) technique on subsamples from each confocal image as discussed in Marquez (2006). The DFT uncovers periodic information in an image, and any feature in an image can be decomposed into a set of amplitudes corresponding to horizontal and vertical frequencies, where the magnitudes of these amplitude sets correspond to the particular size of the feature in the image. The location of peaks in the DFT can then be related to the orientation of the corresponding feature. The applied DFT is filtered to define elongated features, and thus can be effectively used on images depicting MTs. The data seen in Figure 3-2j-q represent polar plots of DFTs, where the relative strength (0-1) of a periodic structure (here MTs) was plotted against the angle (0-360°) of this particular structure. The plots are averages from ten subsamples per image from five individual primary roots per genotype. They quantitatively reflect the qualitative assessment of cortical MT orientation as seen in Figure 3-2b-i. The star-shaped polar plot for WT zone I (Fig. 3-2j) proved

the random orientation of cortical MTs as fibers were detected at any given angle. The polar plot for zone II (Fig. 3-2k), however, strongly indicated a high concentration of MTs with a shift in orientation towards 90°, like a needle on a compass points to north, with a value of 0.9 for its relative strength. The 'needle' tended to get broader, and its relative strength of 0.6 was smaller in zone III, implying more fibers deviating from 90° (± 10°). In zone IV, the relative strength of MT concentration that was oriented towards 90° was much smaller, with a value of 0.45 for its relative strength, with deviation exceeding 50°. A high concentration of some MTs was oriented towards 0°, translating in occasional fibers almost parallel to the cell axis. The polar plots based on data collected from zone I and II from *sac9* primary roots were nearly identical with those from WT (Fig. 3-2j-q), in other words, there was no difference in the angular orientation distributions for cortical MTs in the meristematic and the proximal elongation zone between the two genotypes. The difference, however, started to show in zone III of *sac9* roots with a higher degree of oblique fibers that deviated from 90° up to ± 40°. The angular orientation distribution was somewhat reminiscent of that in WT zone II. In zone IV, a drastic difference could be seen in the most mature cells of *sac9* roots, where a high concentration of the fiber orientation was localized around 0° and 180° angles, and fibers were almost never seen transversely oriented to the cell axis. All generated polar plots are collectively presented in Figure 3-3 to demonstrate the different degrees of variability in the angular orientation distributions depending on subsample and individual root; information that was lost after averaging as seen in Figure 3-2j-q. It is interesting to note that the variability is higher among the ten subsamples than between the five independent roots. Taken together, the qualitative and quantitative analysis of cortical MTs indicated a wild-type-like distribution in the meristematic and early elongation zone of *sac9* primary roots. The distribution of cortical MTs in differentiated *sac9* root cells, however, was on average markedly different from WT.

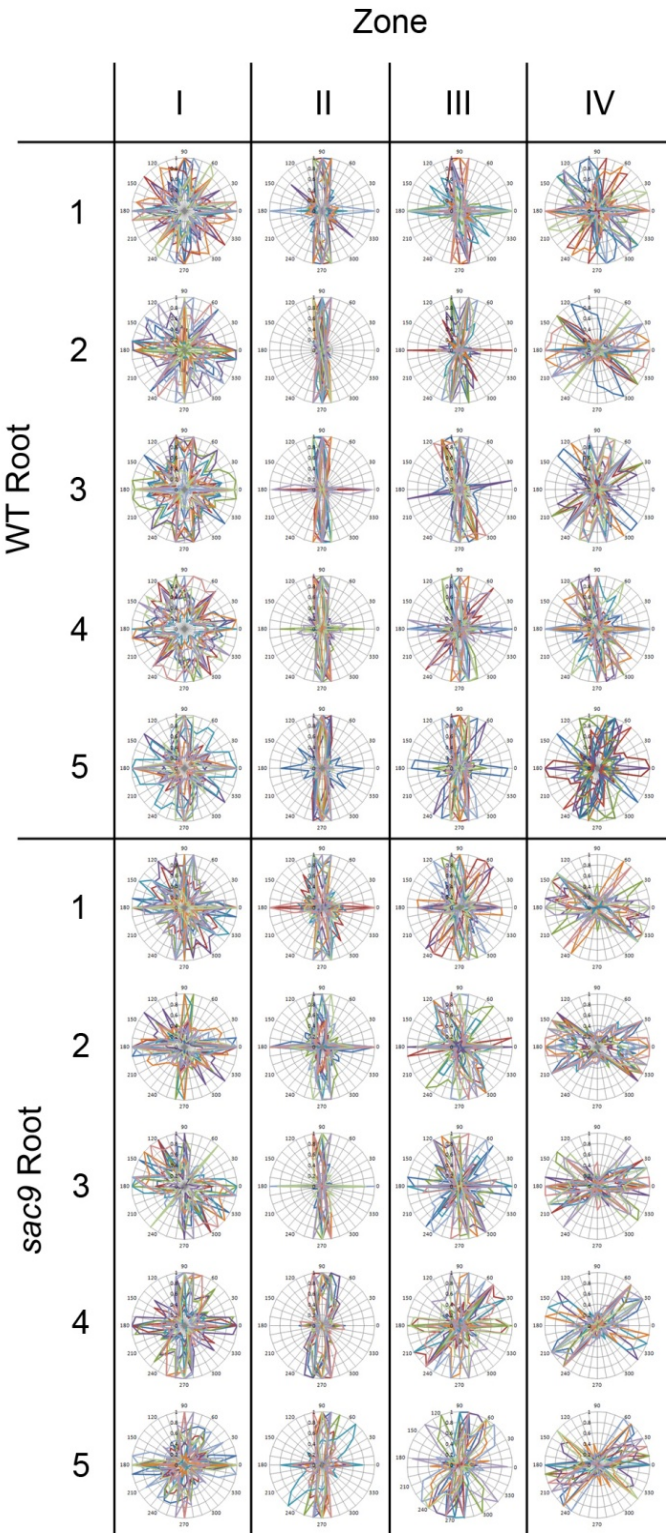

Fig. 3-3 Polar plots of angular orientation distributions of MTs according to growth zone from five WT and *sac9* primary roots. Each circular plot contains the results from all ten subsamples per image (see Material and Methods)

Von Mises fitting of angular orientation distributions of cortical MTs

To further evaluate the data obtained for angular orientation distributions of cortical MTs and to assess the suitability of the DFT method for this particular application, models were fitted to the values obtained from the DFT using non-linear maximum likelihood assuming a circular von Mises distribution (Fig. 3-4).

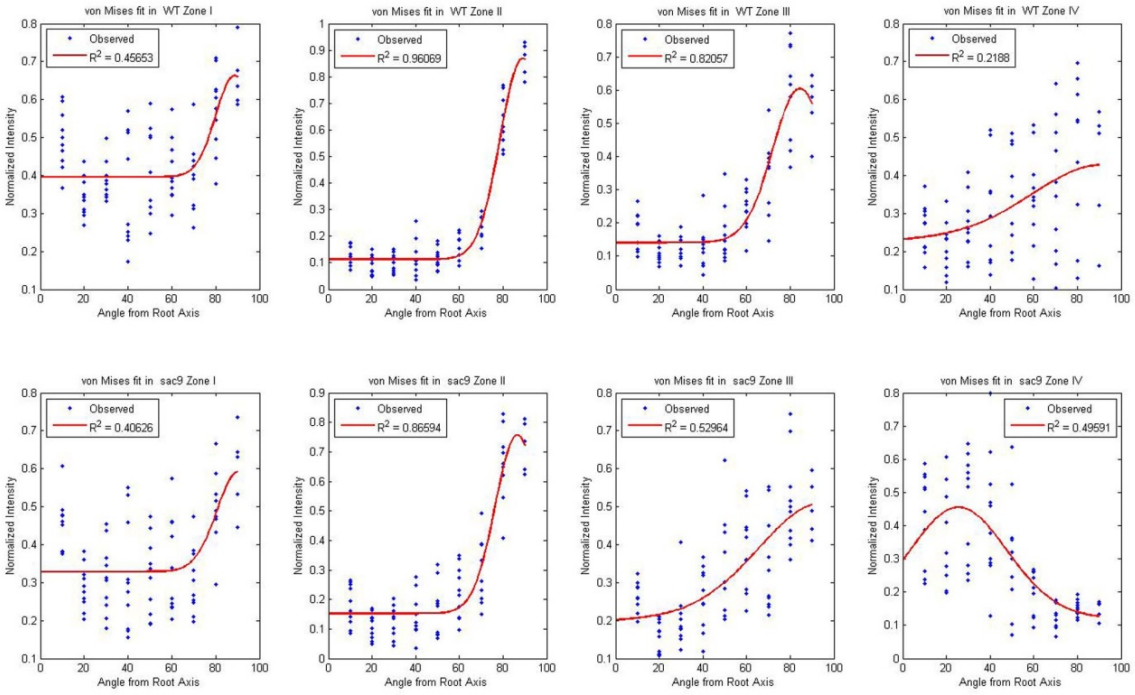

Fig. 3-4 von Mises fitting probability density function for the angular orientation θ for cortical MTs in four zones from developing WT and *sac9* roots. Data used for modeling included only DFT measurements for the vertically reflected angles from 10-170° (blue diamonds). The vertical axis presents the normalized intensity (probability density function) and the horizontal axis presents the angular orientation θ. The red line is a von Mises fitting. R^2 represents the coefficient of determination that describes the fluctuation of normalized intensity as a function of θ. Charts are courtesy of Dr. James Powell (Utah State University, Logan, UT)

The following probability density function was used for the orientation angle θ:

$$f(\theta)=\text{background} + N \exp [\kappa \cos(\theta-\mu)]$$

where,

θ	angle of the cortical MT
background	certain background intensity at all angles
N	a normalization constant
K	the concentration of the data around its mean
μ	the mean angle of the cortical MT.

The fitted curves (Fig. 3-4) indicate that the probability density function peaks around 90° for all zones except zone IV for *sac9*, which peaks around 26°. The strength of the probability density decreases as we move from zone II to zone IV, as seen by the Kappa values (Table 3-2). This is in excellent agreement with the observation of Figure 3-2j-q. These curves seem to overall support the contention that the angular orientation distributions of cortical MTs in *sac9* root cells started to differ from WT in zone III and displayed a drastic change in zone IV. The models appear to fit particularly well for zone II for WT and *sac9*, as indicated by the least standard deviation between fitted models and observations and expressed by the high values of the coefficient of determination, R^2. To gain more understanding of the mathematical models, the parameters that were used in fitting of von Mises curves are presented in Table 3-2.

Table 3-2 Parameters used for fitting von Mises curves for the angular orientation distributions of cortical MTs from developing WT and *sac9* roots

Zone	N	κ (kappa)	μ (mu)	σ (sigma)	background
WT_zone I	0.101	44.107	88.659	0.098	0.396
WT_zone II	0.339	31.635	88.981	0.053	0.113
WT_zone III	0.252	21.477	84.398	0.081	0.141
WT_zone IV	0.305	3.118	91.196	0.130	0.224
sac9_zone I	0.116	32.848	90.493	0.110	0.329
sac9_zone II	0.267	32.500	86.577	0.085	0.153
sac9_zone III	0.412	3.879	94.384	0.101	0.197
sac9_zone IV	0.334	6.611	25.506	0.124	0.119

Zones I-IV refer to (in order of development): I-meristem, II-proximal elongation, III-distal elongation, IV-differentiation. N is a normalization constant. It is capturing what fraction of the data is rising above the background level of intensity as well as distinguishing from a uniform distribution across angles. Kappa is the concentration of the data around its mean with a higher value translating into tighter distributions (= smaller variance). Mu corresponds to the mean angle of the cortical MTs. Sigma is the average standard deviation between the fitted model and observations. Background reflects both background and illuminance in the images as well as the fraction of the data described by a uniform distribution. Courtesy of Dr. James Powell

DISCUSSION

The main goal of this study was to address the underlying factors governing the shortened root tip, here defined as the combined length of meristem and cell elongation zone, in *sac9* mutants. In pharmacological studies, seedlings treated with MT-stabilizing and destabilizing drugs, as well as many tubulin and MT-associated mutants, often display reduced elongation, radial swelling of the root and/or disturbed arrays of cortical MTs (Baskin et al. 1994; Bao et al. 2001; Burk and Ye 2002; Sugimoto et al. 2003; Bannigan et al. 2006; Kawamura et al. 2006; Chu et al. 2007). Therefore, I speculated that the stuntedness of *sac9* roots may have resulted from abnormal or disorganized cortical microtubules.

The shortened root tips in the *sac9* mutant were not caused by a disturbed cortical MT array

Since my electron microscopy studies revealed that cortical MTs were structurally normal in non-dividing *sac9* root cells (Fig. 3-1), immunolocalization experiments were conducted to evaluate the spatial arrangement and distribution patterns of cortical MTs. The results from immunolocalization experiments showed a random distribution of cortical MTs in the meristematic area for both WT, and *sac9* root cells (Fig. 3-2b,f, j, n). Contrary to my assumptions, cortical MT arrays were also not disturbed in the elongation zone of *sac9* root cells, as confocal images showed a wild-type net transverse orientation of MTs. Thus I conclude that cortical MT orientation did not affect elongation in *sac9* roots.

Discrete Fourier Transform as an additional method to calculate angular MT orientation distributions

As a follow-up step, I decided to use a mathematical approach (Discrete Fourier Transform and von Mises probability fitting) to see if visual results were sufficient to come to my conclusion that the MTs in both genotypes were similar and that MTs were not involved in the stuntedness of *sac9* roots.

In the past, analysis of MT orientation ranged from basic, qualitative-descriptive (Hogetsu and Oshima 1986), to the use of a broad classification system, where MTs were grouped into 30° sectors (Laskowski 1990). For a more detailed analysis, angles of individual MTs or MT bundles were measured manually with respect to the long axis to the cell (Burk and Ye 2002). For large numbers of samples, this approach is very tedious and time-consuming. More advanced image analysis codes can decrease sampling time, but are dependent on thresholding and other image processing steps to enable computational pattern recognition. The data thus obtained are commonly presented in frequency distribution histograms. The filtered DFT

technique as optimized by Marquez (2006), on the other hand, can be used on raw images, provided they are in the form of black-and-white 8-bit TIFF files with square side dimensions. The resultant data are typically shown as polar plots with the relative intensity of a periodic structure plotted against the particular direction (angle) of this structure.

The main advantage in applying the filtered DFT technique to confocal images of cortical MTs lies in the automated measurement of angular orientation distributions, which translates into great time-efficiencies. Measurements can be done in seconds, and since they are automated and follow basic computer algorithms, are bias-free.

The second compelling advantage of this method is its reliability and the ease of interpretation of the presented data in form of polar plots. For tightly parallel objects, the polar plot shows the orientation distribution in a particular angle like a needle on a compass. This is thus intuitive to comprehend and allows for rapid comparison of MT orientation between different developmental zones and genotypes.

Results from my Discrete Fourier Transform and the fitting of von Mises probabilities showed that there was no difference in distribution patterns of cortical MTs between WT and *sac9* in the meristem and in the elongation zone. Therefore I conclude that the orientation of cortical MTs did not contribute to the stuntedness of the root in *sac9*. In differentiated *sac9* root cells, though, there was an clear difference in the orientation of microtubules. This was not obvious from qualitative description of confocal images and proved the strength of the quantitative assessment by DFT and von Mises probability fitting. It appeared that microtubules had changed their position from transverse to oblique much faster than wild type in the zone of differentiation (zone IV, Fig. 3-2m, q).

Possible physiological effects of altered MT orientation in mature *sac9* root cells

It was shown that once root cells slowed to grow longitudinally and showed signs of differentiation (root hair formation), cortical MTs arrays assumed an oblique position in respect to the growth axis (Sugimoto et al. 2000). This transition was visible in the *sac9* mutants as well. However, it appeared to happen earlier than in developmentally comparable regions from WT. Two possibilities arise: either the different zones in *sac9* roots are a physically shorter (i.e. with fewer or smaller cells per zone or a combination of both), or if one assumes a correlation between relative cell age and cortical MT array, cells from the same zone might be physiologically older in *sac9* mutants than WT; an interesting hypothesis in the light of the overall retarded growth in *sac9* plants.

The fact that the polar plots from Figure 3-2o and p (*sac9*, zone II and III) are almost congruent with Figure 3-2l and m (WT, zone III and IV) leads to the question if a similar angular distribution of cortical MTs as seen in Figure 3-2q (*sac9*, zone IV) might also be found in more distal cells of the differentiation zone in wild-type roots. Unfortunately, this cannot be answered with the technique used here as it was reported that cortical MTs were not reliably labeled in cells beyond the elongation zone after mild enzymatic digestion and cold methanol treatment (Sugimoto et al. 2000). Although immunolabeling in this study was successful for all reported zones, I can confirm that epidermal cells from the distal differentiation zone were only irregularly labeled and therefore had to be excluded from any statistical analysis.

Possible mechanical effects of altered MT orientation in mature *sac9* root cells

The relevance of the finding that cortical MTs in early differentiated cells of the *sac9* root were markedly different from wild type is not apparent. Although we now know that the parallel-transverse bands of MTs serve as direct guidance for the movement of the CESA

complex and thus indirectly for the structured deposition of cellulose microfibrils, the current literature does not provide any insights into the biological function(s) of the change to oblique angles in cells that have ceased to grow longitudinally. Experiments in the field of material science show that the orientation distribution of fibers in a short-fiber reinforced composite is fundamentally affecting the mechanical properties of the composite (Fu and Lauke 1996). Corresponding functions in the field of biology are not hard to find (Thomopoulos et al. 2006). From experiments on the stress needed to produce a given strain in one delignified sisal fiber, Spark et al. (1958) found that an almost parallel orientation of cellulose fibers (10°) required much more force (6x) than a more oblique orientation of cellulose (42°). With the additional assumption that there was some cellulose microfibril deposition even in cells that had ceased to grow, Laskowski (1990) interpreted these findings as a possibility for increasing the strength to withstand tensile stresses, such as bending, in epidermal cells. However, roots are exposed to different forces in relation to the soil-environment compared to the air-environment for shoots, and air-driven bending does not occur in most roots. It is reasonable to assume though, that bending forces experienced by the shoot are relayed to the root, and by mechanical reinforcement of the non-growing part of the root and thus providing anchorage, the shoot is better protected from toppling over in the event of severe air movement. In this light, it would be interesting to measure tensile stresses required for breakage of the shoot, such as they were applied in screens for the *fragile fiber* mutants (Zhong et al. 2004).

Unique cell wall abnormalities likely as an indirect cause for root stuntedness

Since cells in the differentiation zone had ceased to elongate, I postulated that the reported differences in the orientation of cortical MTs in mature *sac9* root cells (zone IV) were not the cause for the observed stuntedness in *sac9* roots. Now I ask the question, what might be

responsible for the stuntedness? I propose that the abnormalities associated with the cell wall in some meristematic cells as reported in Chapter 2 are indirectly responsible for the stuntedness. It is possible that cellular or subcellular disturbances in MT orientation were not detected with the method I used because the DFT is based on averaging large amounts of data. The unique cell wall aberrations were very small, on average less than one micrometer, and thus are not readily visible with techniques that are limited by the resolution of the light microscope, such as confocal microscopy. Due to fact that only a small number of cells showed abnormalities coupled with the small size of the aberrations themselves, makes it likely that information was lost in the averaging process and therefore was not reflected in the results. In addition, cortical MTs in epidermal cells in the meristem were difficult to visualize with confocal microscopy, as the strong fluorescent signal originating from root cap cells with transverse bands of cortical MTs directly overlying the epidermal cells sometimes obscured the weaker fluorescent signal from these shorter and randomly distributed MTs. That these aberrations were seen in ultrastructural investigations of *sac9* root cells emphasizes the importance of transmission electron microscopy for mutant analysis.

It should also be noted, as mentioned earlier in Chapter 2, that meristematic cells with cell wall abnormalities probably did not divide. Interestingly, it looked like these cells could elongate. Since the total number of dividing cells was reduced, this may explain the stuntedness.

CONCLUSION

Here I showed that the distribution of cortical MTs in elongating *sac9* root cells was not disturbed, and therefore was not the reason for the shortened root tips. As evident from the current literature, MTs are not static structures in the cytoplasm simply providing a scaffold for other molecules. Therefore, the defect in *sac9* root cells might still be MT-related, but not

resolved with images providing only snapshots of a fast-changing process. Also, resolution was limited by the light microscopy level. Alternatively, the spatial and temporal network of actin fibers as the other dominant cytoskeletal component might be a good candidate for the underlying mechanisms leading to cell wall aberrations and a shortening of the root in *sac9* mutants. As of now, it seems reasonable to assume that the unique cell wall abnormalities in *sac9* root cells are indirectly responsible for the shortened roots.

The difference in the orientation of cortical MTs in differentiated *sac9* cells might indicate differences in physiological or physical properties of the main root axis and stem. However, this needs to be further tested.

For the first time, I successfully applied a recently optimized technique (DFT) to quantitatively assess the angular orientation distributions of cortical MTs and found it a very fast method enabling large data collections. I deem this method particularly suited to accurately characterize the orientation patterns for cortical MTs in cells of the elongation and early differentiation zone.

REFERENCES

Azimzadeh J, Traas J, Pastuglia M (2001) Molecular aspects of microtubule dynamics in plants. Curr Opin Plant Biol 4 (6):513-519

Baluska F, Parker JS, Barlow PW (1992) Specific patterns of cortical and endoplasmic microtubules associated with cell growth and tissue differentiation in roots of maize (Zea mays L.). J Cell Sci 103 (1):191-200

Bannigan A, Wiedemeier AM, Williamson RE, Overall RL, Baskin TI (2006) Cortical microtubule arrays lose uniform alignment between cells and are oryzalin resistant in the Arabidopsis mutant, *radially swollen 6*. Plant Cell Physiol 47 (7):949-958

Bao Y, Kost B, Chua NH (2001) Reduced expression of alpha-tubulin genes in *Arabidopsis thaliana* specifically affects root growth and morphology, root hair development and root gravitropism. Plant J 28 (2):145-157

Baskin TI (2001) On the alignment of cellulose microfibrils by cortical microtubules: a review and a model. Protoplasma 215 (1-4):150-171

Baskin TI, Meekes HT, Liang BM, Sharp RE (1999) Regulation of growth anisotropy in well-watered and water-stressed maize roots. II. Role of cortical microtubules and cellulose microfibrils. Plant Physiol 119 (2):681-692

Baskin TI, Wilson JE, Cork A, Williamson RE (1994) Morphology and microtubule organization in Arabidopsis roots exposed to oryzalin or taxol. Plant Cell Physiol 35 (6):935-942

Bibikova TN, Blancaflor EB, Gilroy S (1999) Microtubules regulate tip growth and orientation in root hairs of *Arabidopsis thaliana*. Plant J 17 (6):657-665

Burk DH, Ye ZH (2002) Alteration of oriented deposition of cellulose microfibrils by mutation of a katanin-like microtubule-severing protein. Plant Cell 14 (9):2145-2160

Chu Z, Chen H, Zhang Y, Zhang Z, Zheng N, Yin B, Yan H, Zhu L, Zhao X, Yuan M, Zhang X, Xie Q (2007) Knockout of the *AtCESA2* gene affects microtubule orientation and causes abnormal cell expansion in Arabidopsis. Plant Physiol 143 (1):213-224

Collings DA, Wasteneys GO (2005) Actin microfilament and microtubule distribution patterns in the expanding root of *Arabidopsis thaliana*. Can J Bot 83 (6):579-590

Crowell EF, Bischoff V, Desprez T, Rolland A, Stierhof YD, Schumacher K, Gonneau M, Hofte H, Vernhettes S (2009) Pausing of Golgi bodies on microtubules regulates secretion of cellulose synthase complexes in *Arabidopsis*. Plant Cell 21 (4):1141-1154

Eleftheriou EP, Baskin TI, Hepler PK (2005) Aberrant cell plate formation in the *Arabidopsis thaliana microtubule organization 1* mutant. Plant Cell Physiol 46 (4):671-675

Emons AM, Hofte H, Mulder BM (2007) Microtubules and cellulose microfibrils: how intimate is their relationship? Trends Plant Sci 12 (7):279-281

Fisher DD, Cyr RJ (1998) Extending the microtubule/microfibril paradigm. Cellulose synthesis is required for normal cortical microtubule alignment in elongating cells. Plant Physiol 116 (3):1043-1051

Fu S-Y, Lauke B (1996) Effects of fiber length and fiber orientation distributions on the tensile strength of short-fiber-reinforced polymers. Compos Sci Technol 56 (10):1179-1190

Giddings TH, Staehelin LA (1991) Microtubule-mediated control of microfibril deposition: a re-examination of the hypothesis. In: Lloyd CW (ed) The cytoskeletal basis of plant growth and form. Academic Press, San Diego, pp 85-100

Granger CL, Cyr RJ (2001) Spatiotemporal relationships between growth and microtubule orientation as revealed in living root cells of *Arabidopsis thaliana* transformed with green-fluorescent-protein gene construct *GFP-MBD*. Protoplasma 216 (3-4):201-214

Heath IB (1974) A unified hypothesis for the role of membrane bound enzyme complexes and microtubules in plant cell wall synthesis. J Theor Biol 48 (2):445-449

Himmelspach R, Williamson RE, Wasteneys GO (2003) Cellulose microfibril alignment recovers from DCB-induced disruption despite microtubule disorganization. Plant J 36 (4):565-575

Hogetsu T, Oshima Y (1986) Immunofluorescence microscopy of microtubule arrangement in root cells of *Pisum sativum* L. var. Alaska. Plant Cell Physiol 27 (6):939-945

Holzinger A, Kwok EY, Hanson MR (2008) Effects of *arc3*, *arc5* and *arc6* mutations on plastid morphology and stromule formation in green and nongreen tissues of *Arabidopsis thaliana*. Photochem Photobiol 84 (6):1324-1335

Holzinger A, Lutz-Meindl U (2003) Evidence for kinesin- and dynein-like protein function in circular nuclear migration in the green alga *Pleurenterium tumidum*: digital time lapse analysis of inhibitor effects. J Phycol 39 (1):106-114

Holzinger A, Wasteneys GO, Lutz C (2007) Investigating cytoskeletal function in chloroplast protrusion formation in the arctic-alpine plant *Oxyria digyna*. Plant Biol (Stuttg) 9 (3):400-410

Jurgens G (2005) Cytokinesis in higher plants. Annu Rev Plant Biol 56:281-299

Kawamura E, Himmelspach R, Rashbrooke MC, Whittington AT, Gale KR, Collings DA, Wasteneys GO (2006) MICROTUBULE ORGANIZATION 1 regulates structure and function of microtubule arrays during mitosis and cytokinesis in the Arabidopsis root. Plant Physiol 140 (1):102-114

Laskowski MJ (1990) Microtubule orientation in pea stem cells: a change in orientation follows the initiation of growth rate decline. Planta 181 (1):44-52

Ledbetter MC, Porter KR (1963) A "microtubule" in plant cell fine structure. J Cell Biol 19 (1):239-250

Lloyd C, Chan J (2008) The parallel lives of microtubules and cellulose microfibrils. Curr Opin Plant Biol 11 (6):641-646

Marquez JP (2006) Fourier analysis and automated measurement of cell and fiber angular orientation distributions. Int J Solids Struct 43 (21):6413-6423

Paradez A, Wright A, Ehrhardt DW (2006) Microtubule cortical array organization and plant cell morphogenesis. Curr Opin Plant Biol 9 (6):571-578

Roberts AW, Frost AO, Roberts EM, Haigler CH (2004) Roles of microtubules and cellulose microfibril assembly in the localization of secondary-cell-wall deposition in developing tracheary elements. Protoplasma 224 (3-4):217-229

Spark LC, Darnbrough G, Preston RD (1958) Structure and mechanical properties of vegetable fibers: II. A micro-extensiometer for the automatic recording of load-extension curves for single fibrous cells. J Text I 49 (7):T309-T316

Sugimoto K, Himmelspach R, Williamson RE, Wasteneys GO (2003) Mutation or drug-dependent microtubule disruption causes radial swelling without altering parallel cellulose microfibril deposition in Arabidopsis root cells. Plant Cell 15 (6):1414-1429

Sugimoto K, Williamson RE, Wasteneys GO (2000) New techniques enable comparative analysis of microtubule orientation, wall texture, and growth rate in intact roots of Arabidopsis. Plant Physiol 124 (4):1493-1506

Thomopoulos S, Marquez JP, Weinberger B, Birman V, Genin GM (2006) Collagen fiber orientation at the tendon to bone insertion and its influence on stress concentrations. J Biomech 39 (10):1842-1851

Vantard M, Cowling R, Delichere C (2000) Cell cycle regulation of the microtubular cytoskeleton. Plant Mol Biol 43 (5-6):691-703

Wasteneys GO (2004) Progress in understanding the role of microtubules in plant cells. Curr Opin Plant Biol 7 (6):651-660

Wasteneys GO, Fujita M (2006) Establishing and maintaining axial growth: wall mechanical properties and the cytoskeleton. J Plant Res 119 (1):5-10

Wightman R, Turner SR (2008) The roles of the cytoskeleton during cellulose deposition at the secondary cell wall. Plant J 54 (5):794-805

Williams ME, Torabinejad J, Cohick E, Parker K, Drake EJ, Thompson JE, Hortter M, DeWald DB (2005) Mutations in the Arabidopsis phosphoinositide phosphatase gene *SAC9* lead to overaccumulation of PtdIns(4,5)P_2 and constitutive expression of the stress-response pathway. Plant Physiol 138 (2):686-700

Zhong R, Burk DH, Morrison WH, 3rd, Ye ZH (2004) *FRAGILE FIBER3*, an Arabidopsis gene encoding a type II inositol polyphosphate 5-phosphatase, is required for secondary wall synthesis and actin organization in fiber cells. Plant Cell 16 (12):3242-3259

Zhong R, Morrison WH, 3rd, Freshour GD, Hahn MG, Ye ZH (2003) Expression of a mutant form of cellulose synthase AtCesA7 causes dominant negative effect on cellulose biosynthesis. Plant Physiol 132 (2):786-795

CHAPTER 4

MOLECULAR AND BIOCHEMICAL CHARACTERIZATION OF SAC9 IN *ARABIDOPSIS THALIANA*

ABSTRACT

The *SAC9* gene in *Arabidopsis thaliana* is predicted to encode a protein with phosphoinositide phosphatase activity based on mutant analysis and the presence of a SAC domain (suppressor of actin1 homology domain). I tested this hypothesis. Anti-peptide-antibodies against sequences from the *SAC9* gene were generated and used to immunoprecipitate SAC9 from wild-type extracts. Functional assays for phosphatase activity were performed with PI(4,5)P_2 as the substrate. In a parallel approach, SAC9 protein was obtained as a fusion protein expressed in yeast, followed by purification with affinity chromatography. Western blots with anti-SAC9-antibodies indicated that SAC9 is a soluble protein with an apparent molecular mass of 180 kDa and that the protein exists possibly in a splice variant with an apparent molecular mass of 140 kDa. Malachite Green Assays suggested that immunoprecipitated SAC9 most likely has phosphatase activity towards PI(4,5)P_2. However, more studies are warranted to confirm or refute this conclusion.

ABBREVIATIONS

AB(s)	Antibody(ies)
AGI	*Arabidopsis thaliana* Gene Index
aa	Amino acid
bp	Base pair
BSA	Bovine Serum Albumin
dH_20	Distilled water

EDTA	Ethylenediaminetetraacedic Acid
ELISA	Enzyme-Linked Immunosorbent Assay
IgA, G, M	Immunoglobulin A, G, M
IMAC	Immobilized Metal Affinity Chromatography
IP	Immunoprecipitation
IP_3	Inositol 1,4,5-trisphosphate
HRP	Horse Radish Peroxidase
kDa	Kilo Dalton
LB	Luria-Bertani medium
PI	Phosphatidylinositol
PI(3)P	Phosphatidylinositol 3-phosphate
PI(4)P	Phosphatidylinositol 4-phosphate
$PI(3,5)P_2$	Phosphatidylinositol 3,5-bisphosphate
$PI(4,5)P_2$	Phosphatidylinositol 4,5-bisphosphate
$PI(3,4,5)P_3$	Phosphatidylinositol 3,4,5-trisphosphate
PBS	Phosphate-Buffered Saline
Ptase	Phosphatase
PVDF	Polyvinyl Difluoride
RT	Room Temperature
SAC	Suppressor of Actin1 (Sac1) homology domain
SAC9	SAC domain-containing protein 9
SC-U	Synthetic minimal medium without Uracil
SDS-PAGE	Sodium Dodecyl Sulfate Polyacrylamide Gel Electrophoresis
TAIR	The *Arabidopsis* Information Resource

TBS-T	Tris-Buffered Saline with Tween-20
WT	Wild Type
½ MS	Half-strength Murashige and Skoog medium
6xHis	Polyhistidine tag

INTRODUCTION

Phosphatidylinositol and its phosphorylated derivatives are components of all eukaryotic membranes. They function in various cellular processes, such as vesicle trafficking, cytoskeletal rearrangements, ion channel activity, and signal transduction (Odorizzi et al. 2000; Takenawa and Itoh 2001; Di Paolo and De Camilli 2006; Berridge 2009). They bring about these changes by either physically providing a scaffold for protein binding, or by presenting substrates for the generation of other signaling molecules. Key to this versatility is a tightly controlled distribution of phospholipids in time and space by a plethora of phospholipid-modifying enzymes, such as phospholipases, lipid kinases, and lipid phosphatases.

Several classes of phospholipases hydrolyze phospholipids into fatty acids and other substances. As an example, phospholipase C plays a central role in signal transduction in yeast and animals by releasing two new second messengers, diacylglycerol and inositol trisphosphate, the later one being a powerful activator of protein kinase pathways (Berridge 1984). It was shown that the action of phospholipase D leads to the generation of phosphatidic acid, a potent signaling molecule emerging in plants (Munnik and Nielsen 2011; Testerink and Munnik 2011).

Kinases on the other hand catalyze the transfer of phosphate groups from high energy donor molecules, such as ATP, to the 3-, 4-, or 5-hydroxyl position of the inositol head group of phosphatidylinositol (PI), thereby generating seven known PI derivatives. Phosphatases act in opposition to kinases; they enzymatically remove a phosphate group from the substrate by

hydrolyzing phosphoric acid monoesters. The concerted action of kinases and phosphatases builds the regulatory framework of phospholipid metabolism. Whereas phospholipid kinases have attracted much attention over the last decades, phospholipid phosphatases were poorly studied until the discovery of a novel group of phospholipid-specific phosphatases called SAC domain (for suppressor of actin1 homology domain) phosphatases (McPherson et al. 1996; Srinivasan et al. 1997; Stolz et al. 1998a; Stolz et al. 1998b; Guo et al. 1999; Hughes et al. 2000a; Hughes et al. 2000b; Nemoto et al. 2000; Minagawa et al. 2001; Despres et al. 2003; Zhong and Ye 2003; Williams et al. 2005; Zhong et al. 2005; Manford et al. 2010). The SAC domain is a region of homology between the amino terminus of synaptojanin, a mammalian inositol 5-phosphatase involved in synaptic recycling (McPherson et al. 1996), and Sac1p, a yeast protein genetically implicated in phospholipid metabolism and actin organization (Novick et al. 1989). Phosphatase activity was found to be associated with the SAC domain of yeast Sac1p, rat Sac1,rat Sac3, human synaptojanin and human Sac2 (Guo et al. 1999; Nemoto et al. 2000; Minagawa et al. 2001; Yuan et al. 2007). The SAC domain encompasses seven highly conserved motifs over a 400 amino acid-long region, including the conserved catalytic $CX_5R(T/S)$ site within the sixth motif responsible for the hydrolytic release of phosphate groups from several positions on the inositol head group (Hughes 2001). SAC domain-containing proteins fall into two sub-families. Class I includes phosphoinositide phosphatases with only the SAC domain, such as the founding member Sac1p. Members of class II have an additional 5-phosphatase domain and are thus more like the bi-functional synaptojanin (Hughes et al. 2000a). Several proteins have been indentified in both classes as summarized in Table 4-1.

Table 4-1 SAC domain-containing proteins from mammals, yeast, and plants

Organism	Protein	Function / Class	Substrate	Domain(s)	Reference(s)
Human (*Homo sapiens*)	synaptojanin	Ptase / II	PI(4,5)P_2, IP_3	SAC, 5-Ptase	McPherson et al. 1996; Guo et al. 1999
Human (*H. sapiens*)	hSac2	Ptase / I	PI(4,5)P_2, PI(3,4,5)P_3	SAC	Minagawa et al. 2001
Rat (*Rattus norvegicus*)	rSac1	Ptase / I	PI(3), PI(4), PI(3,5)P_2	SAC	Nemoto et al. 2000
Rat (*R. norvegicus*)	rSac3	Ptase / I	PI(3), PI(4), PI(3,5)P_2	SAC	Yuan et al. 2007
Yeast (*Saccharomyces cerevisiae*)	Sac1p	Ptase / I	PI(3), PI(4), PI(3,5)P_2	SAC	Guo et al. 1999; Hughes et al. 2000b; Foti et al. 2001; Manford et al. 2010
Yeast (*S. cerevisiae*)	Inp51p/Sjl1p Inp52p/Sjl2p Inp53p/Sjl3p	Ptase / II	PI(3), PI(4), PI(3,5)P_2, PI(4,5)P_2	SAC, 5-Ptase	Srinivasan et al. 1997; Stolz et al. 1998a; Stolz et al. 1998b; Guo et al. 1999; Stefan et al. 2002;
Yeast (*S. cerevisiae*)	Fig4p	Ptase / I	PI(3,5)P_2	SAC	Erdman et al. 1998; Rudge et al. 2004
Plant (*Oryza sativa*)	AAK92639	Putative Ptase	None tested	SAC, 5-Ptase	Zhong and Ye 2003
Plant (*O. sativa*)	BAB19411	Putative Ptase	None tested	SAC, WW	Zhong and Ye 2003; Williams et al. 2005
Plant (*Arabidopsis thaliana*)	AtSAC1a AtSAC1b AtSAC1c	Putative Ptase	None tested but PI(4) suggested	SAC	Despres et al. 2003
Plant (*A. thaliana*)	AtSAC1	Ptase / I	PI(3,5)P_2	SAC	Zhong et al. 2005
Plant (*A. thaliana*)	AtSAC7/ RHD4	Ptase / I	PI(4)P	SAC	Thole et al. 2008
Plant (*A. thaliana*)	AtSAC9	Putative Ptase	None tested but PI(4,5)P_2 suggested	SAC, WW	Williams et al. 2005; Gong et al. 2006

A genome wide search of *Arabidopsis thaliana* with the SAC domain sequence of Sac1P resulted in the identification of a protein gene family with nine members (*AtSAC1-AtSAC9*, Table 4-2; Zhong and Ye 2003).

Table 4-2 SAC domain-containing protein gene family members in *Arabidopsis*. Adopted from Zhong and Ye (2003) with additional information obtained from TAIR

Gene family name	Predicted protein length (amino acids)	Predicted molecular weight (kDa)	Chromosomal location	AGI (TAIR) accession (cDNA)	GenBank accession (cDNA)
AtSAC1	912	103	I	At1g22620	AY227244
AtSAC2	808	92	III	At3g14205	AY227245
AtSAC3	818	93	III	At3g43220	AY227246
AtSAC4	831	94	V	At5g20840	AY227247
AtSAC5	785	90	I	At1g17340	AY227248
AtSAC6	593	68	V	At5g66020	AY227249
AtSAC7	597	68	III	At3g51460	AY227250
AtSAC8	588	66	III	At3g51830	AY227251
AtSAC9	1630	182	III	At3g59770	AY227252

All nine family members share the SAC domain as a characterizing feature without any other recognizable phosphatase domains. Therefore, they are all members of class I SAC domain-containing proteins. Based on sequence similarity and intron-exon structures, hydropathy profiles and phylogenetic relationships, these nine members were grouped into three distinct subgroups. Subgroup (I) has five members (AtSAC1-AtSAC5) of medium length (785-913 residues) with 13 exons. Subgroup (II) has only three members (AtSAC6-AtSAC8) - all short proteins (588-597 residues) synthesized from 16 exons. They also contain two putative C-terminal transmembrane helixes. AtSAC8 is predicted to have an additional prenylation site at

the C-terminus. All members of subgroup (II) therefore seem to be membrane-integrated or at least membrane-associated. Subgroup (III) has only one member, AtSAC9. AtSAC9 is set apart from members of subgroup (I) and (II) by its length (1630 residues), intron-exon structure, and the fact that it has an additional protein domain (WW domain) instead of motif seven in the SAC domain. The catalytic site in motif six is conserved, although the second cysteine is changed to a serine. However, this was hypothesized not to affect catalytic activity, as only the first cysteine in the $CX_5R(T/S)$ site was required for activity (Williams et al. 2005). Phylogenetic analysis also showed a clear separation of AtSAC9 from members of the other two subgroups.

Both Williams et al. (2005) and Gong et al. (2006) identified and characterized mutants in the *AtSAC9* gene. These mutants constitutively express a systemic stressed phenotype in the absence of any stress factors. The phenotype was speculated to be caused by altered cellular signaling resulting from elevated levels of $PI(4,5)P_2$ and IP_3 in the *sac9* mutants. Both molecules are considered important in various signal transduction pathways in yeast, animals, and also in plants. Other described phenotypes of the mutant included overexpression of stress-induced genes, accumulation of reactive oxygen species and anthocyanin in the leaves, constitutively closed guard cells, shorter primary roots, fewer lateral roots, and overall retarded growth. Gong et al. (2006) expanded this list of phenotypes when they studied *cfs* (coupling factor slow recovery) mutants and saw that the ATP synthase was dysfunctional in *cfs* leaves. It turned out that the *cfs* mutation was situated on the same locus as *SAC9* but that a different allele was affected. Following Williams' nomenclature, they denoted the *cfs* allele as *sac9-4*.

Williams et al. (2005) showed that *sac9* roots accumulate $PI(4,5)P_2$ and - to a lesser extent - its hydrolysis product IP_3. This and the fact that the N-terminal region of SAC9 defines it as a member of the SAC domain-containing gene family, prompted Williams et al. (2005) to speculate that *SAC9* encodes a putative phosphoinositide phosphatase. Others went further by

inattentively pronouncing SAC9 to be a 5-phosphoinositide phosphatase (Munnik and Testerink 2009), even though this still awaits biochemical evidence.

Although many phosphoinositide phosphatases have activity against a broad number of substrates *in vitro*, their *in vivo* activities may be quite different due to restricted access to substrates based on their subcellular localization (Hughes et al. 2000a). The endogenously elevated levels of PI(4,5)P_2 in SAC9-deficient roots suggest that this lipid is the major *in vivo* substrate.

In this chapter, I provide data for the *in vitro* function of SAC9 based on recombinant expression of His-tagged SAC9 from yeast and the purification of the fusion protein by immobilized metal affinity chromatography. Since mass spectrophotometry indicated that the protein purified by GenScript was not the target protein, I used an alternative approach. I obtained anti-peptide-antibodies against sequences specific to SAC9, immunoprecipitated and purified SAC9 protein with these antibodies; I then tested the resultant protein for phosphatase activity towards PI(4,5)P_2 as detected by inorganic phosphate release with the Malachite Green Assay.

MATERIAL AND METHODS

Cell culture

Saccharomyces cerevisiae strain INV*Sc*1 carrying the galactose-inducible plasmid pYES-DEST52+SAC9 was propagated at 30°C with shaking (130 rpm) in liquid synthetic minimal medium without uracil (SC-U, 0.85 g/l yeast nitrogen base without amino acids and $(NH_4)_2S0_4$, 2.5 g/l $(NH_4)_2SO_4$, 0.3 g/l drop-out mix, US Biological #D9535; all w/v, pH 6-6.3) and in the presence of 2% (w/v) glucose as a carbon source. SAC9 expression was induced by changing the medium to SC-U containing 2% (w/v) galactose.

Recombinant expression of SAC9

Transformed yeast colonies harboring the Gateway™ destination and inducible expression vector pYES-DEST52 (Invitrogen #12286-019) with the cDNA of the full length AtSAC9 were generously provided by Dr. Mary Williams (formerly of Harvey Mudd College, Claremont, CA). The cDNA had been inserted by the Williams' lab between the two recombination sites (*att*R1 and *att*R2) through a lambda phage site-specific recombination event, thereby inactivating the *ccd*B gene (the *ccdB* gene encodes a lethal toxin which kills *E. coli* carrying the plasmid without insert). The cDNA was in frame with a C-terminal V5 epitope and polyhistidine (6xHis) tag for detection and purification. A plasmid map of pYES-DEST52+SAC9 is presented in Figure 4-1.

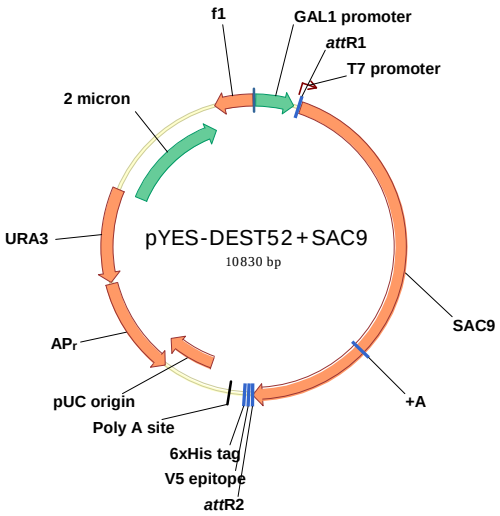

Fig. 4-1 Plasmid map of pYES-DEST52 with the complete cDNA for SAC9. The plasmid contained the following elements: yeast *GAL1* promoter for high-level, galactose-inducible protein expression *in S. cerevisiae*; two recombination sites, *att*R1 and *att*R2, downstream of the *GAL1* promoter for recombinational cloning of the gene of interest – here *AtSAC9*; the V5 epitope and 6xHis tag for detection and purification; 2 micron for episomal maintenance and high copy replication; *URA3* auxotrophic marker for selection of yeast transformants; the pUC origin for high copy replication and maintenance of the plasmid in *E. coli*; APr, the ampicillin (*bla*) resistance gene for selection of transformants in *E. coli*; the T7 promoter to regulate expression in *E. coli*; the f1 intergenic region for production of single-strand DNA in F plasmid-containing *E. coli*. +A denotes the site of a point mutation in this vector as confirmed by DNA sequencing

Time course of SAC9 induction, SDS-PAGE, and Western blotting

A time course of protein induction was performed as follows: A single colony was picked from plate-grown INV*Sc*1 carrying pYES-DEST52+SAC9 and used to inoculate 15 ml of SC-U medium supplemented with 2% (w/v) glucose and grown overnight. The optical density of the overnight culture was determined and used to calculate the amount of starter culture needed to reach a final absorption 0.4 at 600 nm in a volume of 50 ml. Calculated amounts of overnight culture were taken, centrifuged at 4°C, and resuspended in either 50 ml induction medium or regular growth medium (control). Cultures were grown for 48 h in a shaker. At certain time intervals (t = 0, 4, 8, 12, 24, 48 h), 5 ml aliquots were aseptically removed. Cells were centrifuged and washed in sterile water, and the collected pellet was stored at -20°C until further usage. Thawed cells were resuspended in Y-PER® Yeast Protein Extraction Reagent (Thermo Fisher Scientific, Pierce Protein Products #78991) containing 1X Halt™ Protease Inhibitor Cocktail without EDTA (Thermo Fisher Scientific, Pierce Protein Products #78410), and detergent-lysed according to manufacturer's suggestions. The homogenous mixture was gently agitated for 20 min at room temperature (RT), and soluble proteins were separated from cell debris by centrifugation. The total protein concentration of the cleared lysate was estimated with the BCA method (Thermo Fisher Scientific, Pierce Protein Products #23225). Twenty µg of the cleared lysate were mixed with 6x SDS loading buffer and denatured by boiling for 5 min at 95°C. Samples were analyzed by 10% SDS-PAGE (100 V, 20 mA, ~ 3.5 h), and proteins were subsequently electro-transferred (30 V, overnight at 4°C) to a polyvinyl difluoride (PVDF) membrane (Thermo Fisher Scientific, Pierce Protein Products #88518) in Tris-Glycine buffer (BioRad #161-0771) containing 20% methanol. After transfer, membranes were blotted in blocking buffer (TBS-T with 7% dry milk powder w/v; 150 mM NaCl, 10 mM Tris-base, 0.1% Tween, pH 7.2) for 2 h at RT. The membranes were incubated overnight at 4°C with mouse anti-

V5-antibody (Invitrogen, #R96025) diluted 1:5,000 in 0.2X blocking buffer or mouse anti-His(C-term)-antibody (Invitrogen, #R93025). The membranes were rinsed three times with TBS-T for 5 min each, then incubated with secondary antibody (horse anti-mouse IgG, HRP-linked, 2 mg/ml stock, diluted 1:10,000 in TBS-T; Cell Signaling Technology, #7076) for 1 h at RT followed by another set of three washes with TBS-T. Enzyme activity was detected by chemiluminescence (Thermo Fisher Scientific, Pierce Protein Products #32106). Membranes were exposed to CL-XPosure™ Film (Thermo Scientific, Pierce Protein Products #34091) for various time periods and developed.

Purification of recombinant SAC9 by IMAC (Immobilized Metal Affinity Chromatography)

Cleared soluble protein lysate extracted from induced cells after a 24 h growth period was purified by nickel-agarose chromatography (Thermo Fisher Scientific, Pierce Protein Products #78994). The lysate was loaded directly on the equilibrated pre-packed columns containing Ni^{2+}-chelated iminodiacetic acid that had been covalently immobilized to 4% beaded agarose. Cell lysate was allowed to flow through the gel bed gravimetrically. The flow through fraction was collected for later analysis of binding efficiency. After several wash steps with two different wash buffers (Wash Buffer 1 contained sodium phosphate buffer, 10 mM imidazole, pH 7.4, and 0.5X concentration of proprietary Y-PER Reagent additives; Wash Buffer 2 contained 50 mM Tris, 300 mM NaCl, 25 mM imidazole, 10% glycerol, pH 6.8), the purified 6xHis-tagged protein was eluted with an imidazole buffer (Elution Buffer contained 50 mM Tris, 300 mM NaCl, 200 mM imidazole, 10% glycerol, pH 6.8). All collected fractions were analyzed by SDS-PAGE and Western blotting as described above, and by SDS-PAGE and silver staining with the Silver Stain Plus Kit® according to the manufacturer's protocol (Bio-Rad, #161-0449).

Verification of the construct sequence, pYES-DEST52+SAC9

To make sure that the 6xHis tag was present in the plasmid, a Western blot was performed on crude protein extracts from induced yeast cells carrying pYES-DEST52+SAC9 as described earlier, and probed with the C-terminal anti-6xHis-antibody instead of the anti-V5-antibody.

A second approach of construct and insert verification was undertaken by sequencing through the complete insert + 500 bp upstream and 500 bp downstream to the insert. This included several steps:

1. DNA extraction from yeast cells harboring the construct pYES-DEST52 with the full length *SAC9* gene,
2. transformation of yeast plasmid into competent *Escherichia coli* by electroporation,
3. propagation of the plasmid in *E. coli*,
4. plasmid isolation from *E. coli*,
5. restriction digest of plasmid to confirm insert presence in the *E. coli* clone,
6. large scale propagation of *E. coli* with plasmid carrying the insert,
7. large scale plasmid isolation from *E. coli*,
8. DNA concentration estimates,
9. design and synthesis of 23 primers for sequencing of ~500 bp long overlapping fragments for 1-3X coverage through the promoter region of the plasmid, the full length cDNA insert, and the C-terminal V5 epitope and 6xHis tag,
10. sequencing reactions and,
11. assembly of contigs and alignment with AtSAC9 cDNA.

Construct repair

The repair of the construct was generously performed by Dr. Dennis Welker (Utah State University, Logan, UT). It included excising the area around the mutation by restriction digest and cloning a repaired version of that exact region by site-directed mutagenesis. An LB plate with ampicillin as a selection marker was provided and contained several *E. coli* clones with the fixed construct (marked as SAC9_76A-F). All *E. coli* clones were subcultured in fresh LB medium supplemented with 50 mM ampicillin, and glycerol stocks were made.

Verification of the repaired construct, pYES-DEST52+SAC9-76F

E. coli plasmids were isolated with the Plasmid Mini Kit® according to manufacturers' instructions (Qiagen, #12123), and sequencing cocktails were prepared with plasmid DNA from clone SAC9_76F. Sequencing was performed at the DNA Sequencing Facility, University of Utah, Salt Lake City, UT. Contigs were assembled in Vector NTI (Invitrogen), and a consensus sequence of all aligned contigs was compared to the cDNA of AtSAC9 (GenBank accession number AAP49842.1).

Plasmid transformation into yeast

Transformation of *S. cerevisiae* strain INV*Sc*1 was performed with the S.c. Easy Comp Transformation Kit® (Invitrogen, #K5050-10) following manufacturer's suggestions. Transformations included 1) INV*Sc*1 with pYES-DEST52 + SAC9-76F, 2) INV*Sc*1 with pYES-DEST52 only, and 3) only INV*Sc*1 as a negative control, as only yeast cells that have incorporated either 1) or 2) would grow on selective plates due to the uracil auxotrophy gene *URA3* on the plasmid.

Verification of the insert from new transformants

Yeast DNA was extracted with the Yeast DNA Extraction Kit® according to manufacturer's suggestions (Thermo Fisher Scientific, Pierce Protein Products #78870), DNA concentrations were estimated, and nested PCRs were performed to amplify first a 700 bp, and then a 500 bp region around the site of the mutation. These PCR fragments were used for sequence analysis at the Sequencing Facility at the University of Utah, Salt Lake City, UT.

Generation of anti-SAC9-antibodies

Production of antigens

The protein sequence of AtSAC9 was analyzed with Antigen Profiler™ (Thermo Fisher Scientific), and three candidate peptides that optimized synthesis, solubility and antigenicity were identified. After consultation with Dr. Joseph Li (Utah State University, Logan, UT) and Open Biosystems (Open Biosystems, Thermo Fisher Scientific), two peptides were chosen for synthesis and subsequent antibody production (Table 4-3). The decision for selection was based on unique features of the protein (WW motif for SAC9:515-533 and longer carboxy-terminus for SAC9:940-961).

Table 4-3 Selected antigen peptides for the production of anti-SAC9-antibodies

	Name	Peptide sequence	Position	Length (aa)
Peptide 1	SAC9:515-533	EKRADAVTGKSYYIDHNTK	515	19
Peptide 2	SAC9:940-961	EYRGSDTVPDGSVPQNKRPKD	940	21

Production of antibodies

Open Biosystems synthesized the selected peptides and conjugated them to a carrier protein (KLH, keyhole limpet hemocyanin). Certified specific pathogen-free (SPF) New Zealand

white rabbits were injected subcutaneously with the immunogen mixed with Freund's adjuvant according to the company's 90-day protocol. Four rabbits were immunized with either conjugated-peptide immunogen in one primary immunization followed by three booster shots. Serum was collected two weeks after each booster shot by Open Biosystems.

Quality control of crude and purified sera by modified ELISA (immunodot blot)

Crude sera collected from all four animals two weeks after the final immunization shot were tested for affinity towards the synthetic peptides. The minimum concentration of peptide and antibody required for a chemiluminescent signal was determined in a modified ELISA procedure. Frozen aliquots of reconstituted synthetic peptide (5 mg/ml in sterile 1x PBS) were thawed and diluted to a final concentration of 1 mg/ml in PBS. A two-fold dilution series was prepared in PBS, covering a concentration range from 1-500 μg of peptide. A 9x12 cm sheet of nitrocellulose membrane with 0.45 μm pore size (BioRad, #162-0117) was soaked in dH_2O for 5 min, followed by a change to PBS, and then air-dried. One microliter of each peptide dilution was spotted on five millimeter wide strips, allowed to air-dry before placing in the incubation chamber (Hoefer Scientific Instruments), and blocked with 5% BSA (Calbiochem® #126575, EMD Chemicals) in PBS for 1.5 h at RT. Strips were then incubated with serially diluted crude sera over night at 4°C. The next morning, strips were washed three times in PBS for 5-10 min and incubated with the secondary antibody (anti-rabbit-IgG, HRP-linked, 2 mg/ml stock diluted 1:1,000 in PBS, #7074, Cell Signaling Technology) for 2 h at RT, after which they were washed again three times with PBS for 5-10 min. The substrate for the enzyme was provided (Millipore Visualizer™ Spray and Glow™ ECL Western Blotting Detection System, #17-373), and the resultant reaction was visualized by chemiluminescence and recorded on x-ray film.

Affinity purification of anti-SAC9-antibodies

Affinity purification of pooled crude antisera from two animals per immunogen was performed by Open Biosystems. It included an ammonium sulfate precipitation pre-step to isolate IgGs from the crude sera which contained predominantly IgG with IgA and IgM as well. Affinity of the now purified anti-SAC9-antibodies towards the synthetic peptides was tested in immunodot blots as described above for the crude sera.

Specificity testing of purified antisera towards SAC9 isolated from *A. thaliana*

Growth conditions

A. thaliana WT plants were either grown in soil for up to 2 months under long-day conditions (14 h day/10 h night) and ambient temperature, or seedlings were grown on Phytagel-solidified ½ MS plates for up to 3 weeks under long-day conditions and 22/20°C (day/night) in a growth chamber.

Harvest, lysis, and extraction of total protein content

The protein extraction protocol used here was adapted from Harris et al. (1999). Plant material was harvested and pulverized to a powder with a pre-chilled mortar and pestle under liquid nitrogen. For soil-grown plant material, whole plants were removed from growing medium, cleaned and blotted dry. Plate-grown seedlings did not need any cleaning and could therefore be used directly after weighing. Pulverized plant material was quickly transferred to a centrifuge tube and suspended in grinding buffer (50 mM HEPES, pH 7.5, 5 mM DTT, and 0.1X Protease Inhibitor Cocktail Set VI, Calbiochem #539133, EMD Chemicals) in a 1:2 ratio (plant material/buffer) and vortexed for 30 sec. The Protease Inhibitor Cocktail contained six protease inhibitors with broad specificity for the inhibition of aspartic, cysteine, serine, and metalloproteinases, as well as aminopeptidases. The final concentration of inhibitors used was

as follows: 2 mM AEBSF, HCl (serine protease), 200 µM betastatin (aminopeptidase B and leucine peptidase), 20 µM E-64 (cysteine protease), 20 µM leupeptin hemisulfate (cysteine protease and trypsin-like protease), 5 mM 1,10-phenanthroline (metalloprotease), 20 µM pepstatin (aspartic protease). The homogenate was centrifuged at 12,000 x g for 10 min at 4°C. The supernatant was filtered through two layers of cheesecloth before being centrifuged again at 17,000 x g for 10 min at 4°C. The supernatant was carefully collected and 1-ml-aliquots were kept on ice and subsequently immunoprecipitated with anti-SAC9-antibodies, or stored at -20°C until further analysis.

Western blotting

Protein content of plant extracts was estimated with the BCA assay. Soluble proteins were mixed with 6x SDS loading buffer and denatured by boiling for 5 min at 95°C. Variable amounts were loaded onto polyacrylamide gels and separated by 10%, 4-15% or 4-20% SDS-PAGE and electro-transferred to a PVDF membrane as described earlier. The membrane was blocked by standard procedures and probed for the target protein with either or both anti-SAC9-antibodies (3 mg/ml stock diluted 1:500 in PBS). Membranes were incubated with HRP-conjugated secondary antibodies (horse anti-rabbit IgG, HRP-linked, 2 mg/ml stock diluted 1:1,000 in PBS, #7074, Cell Signaling Technology). The signal was detected by chemiluminescence.

Immunoprecipitation of SAC9 from plant cell lysates

Immunoprecipitation of SAC9 from plant cell lysate was performed with the Immunoprecipitation Kit – Dynabeads® Protein A (or Protein G, Invitrogen, #100-06D or -07D) as follows. Sedimented Dynabeads were brought back into suspension by slowly rotating the beads for 5 min. A quantity of Dynabeads (50 µl) was transferred to a test tube and separated on the

magnet until the supernatant was clear. The supernatant was removed and 3-300 µg anti-SAC9-antibodies, diluted in 200 µl AB-Binding and Washing Buffer, was added and incubated with rotation for 10 min at room temperature (RT). The Dynabeads-AB-complex was gently washed with 200 µl AB-Binding and Washing Buffer. After magnetic separation and removal of the supernatant, typically 1 ml of cell lysate was added and gently pipetted to resuspend the Dynabeads-AB-complex, and incubated for 10 min at RT while rotating. The supernatant was removed by magnetic separation, and the Dynabeads-AB-antigen-complex was washed three times using 200 µl Washing Buffer for each step. The beads were resuspended in 100 µl Washing Buffer and transferred to a clean tube to avoid eluting proteins that adhered non-specifically to the wall of the tube. The antigen was eluted either under denaturing conditions, which included the addition of 20 µl Elution Buffer (0.1 M glycine, pH 3) and 10 µl 6x SDS loading buffer, and heating for 5 min at 95°C followed by a final magnetic separation. The supernatant containing the eluted antigen was removed and analyzed by SDS-PAGE and Western blotting. The non-denaturing elution was accomplished by shearing forces generated through rotation while incubating in 20 µl Elution buffer for 2 min. The eluted antigen was magnetically separated and transferred to a clean tube. In order to use the eluted antigen in functional assays, the native conformation of the eluted antigen was restored by adjusting the pH of the elute with 0.5 M Tris, pH 7.5.

Functional assay of immunoprecipitated SAC9 with the Malachite Green Assay for inorganic phosphate release

The activity test and quantification of the reaction product was adopted from Maehama et al. (2000) and Taylor and Dixon (2004). The substrate phosphatidylinositol 4,5-bisphosphate diC8 (Echelon, #P-4508) was reconstituted in 25 mM TBS for a final concentration of 2 mM. The

carrier lipid dioleoylphosphatidilserine (1,2-dioleoyl-sn-glycero-3-phospho-L-serine sodium salt, Sigma #P-1060) was reconstituted in an organic solvent mixture (9:1, $CHCl_3$/MeOH) for a final concentration of 10 mM. After use, lipid stock solutions were flash frozen in liquid nitrogen and kept at -20°C. The Malachite Green Reaction Buffer contained 100 mM sodium acetate, 50 mM bis-tris, 50 mM Tris (pH 5-8), 2 mM DTT, and was freshly prepared from stock solutions. Usually, 1 ml of Malachite Green Reaction Buffer was sufficient for up to 50 reactions. Equal amounts of lipid stock solutions (1 µl each per sample) were combined in a test tube and dried under nitrogen. Malachite Green Assay Buffer (18 µl per sample) was added and the lipids were brought in suspension by sonication until the suspension was taking on a uniform, pearlescent shine, indicating complete dispersal. Eighteen microliters of substrate preparation per reaction was transferred to a clean test tube and pre-warmed for 10 min in a dry bath (30°C). The reaction was initiated by adding two microliters of immunoprecipitated SAC9 and incubated for 15 min at 30°C, after which the reaction was terminated by adding an equal volume (20 µl) of 100 mM NEM (n-ethylmaleimide, Sigma #04260-5G-F), followed by centrifugation at 18,000 x g for 10 min at 4°C to sediment lipid aggregates that might interfere with subsequent spectrophotometric measurements. Twenty five microliters of the supernatant was combined with 100 µl Malachite Green Reagent (Echelon, K-1500) and incubated for 15-30 min at RT followed by absorbance readings at 630 nm. The amount of inorganic phosphate released in each lipid sample was calculated based a phosphate standard curve. Under this protocol, the total amount of inorganic phosphate liberated in each sample was 1.6 times that of the calculated value from the standard curve, because the total sample volume after termination of the reaction mixture was 40 µl (25 µl x 1.6 = 40 µl).

RESULTS AND DISCUSSION

SAC9 is hypothesized to be a phosphoinositide phosphatase (Williams et al. 2005). This assumption is solely based on sequence homology of SAC9 to other phosphoinositide phosphatases and elevated levels of $PI(4,5)P_2$ and IP_3 in *sac9* mutant roots, but lacks biochemical proof. Preliminary experiments by Elizabeth Drake suggest a phosphatase function towards $PI(4,5)P_2$. However, the tested SAC9 protein was immunoprecipitated with polyclonal anti-SAC9-antibodies, which showed non-specific cross-reactivity (personal communication with Dr. Mary Williams). To remedy this shortcoming, I attempted to obtain functional SAC9 protein by two different approaches. I first expressed the protein from pYES-DEST52+SAC9 in yeast using the *S. cerevisiae* strain INV*Sc*1 (Invitrogen), a fast-growing diploid strain ideal for recombinant protein expression. I purified the recombinant protein by immobilized metal affinity chromatography (IMAC). The other approach consisted of generating similar-to-monoclonal anti-SAC9-antibodies and to use these antibodies for immunoprecipitation of SAC9 from *A. thaliana* plant extracts. Immunoprecipitated protein was tested with the Malachite Green Assay for the quantification of inorganic phosphate release.

Time-course of induction

In order to determine the time of maximum induction for the SAC9 protein from pYES-DEST52+SAC9, a time course was performed. At certain time intervals (t = 0, 4, 8, 12, 24, 48 h), induced cells were collected, lysed, and the soluble protein extracts were analyzed by 10% SDS-PAGE. After transfer to a PVDF membrane, proteins were probed with two different antibodies to detect recombinant SAC9. Contrary to theoretical predictions, several bands showed signs of induction-related expression. As can be seen in Figure 4-2A (arrow), a prominent band around 140 kDa was getting stronger over time. Although this band was not of the predicted size for the

SAC9 protein (180 kDa), I thought it was a good candidate. Two other polypeptides with an apparent size of 55 and 65 kDa, respectively, were also detected in increasing amounts with anti-V5-antibodies (Fig. 4.2A, grey arrowheads). These could represent proteolytic breakdown products of the antigen. It should be noted that the presence of several bands is not necessarily the result of suboptimal experimental conditions or cross-reactivity since many proteins have several isoforms, and an antibody may detect more than one of them.

Since the plasmid contained a sequence not only for the V5 epitope, but also for a polyhistidine tag at the far C-terminus, anti-His(C-term)-antibodies were used to probe the same samples obtained from the time course of induction as seen in Figure 4-2A.

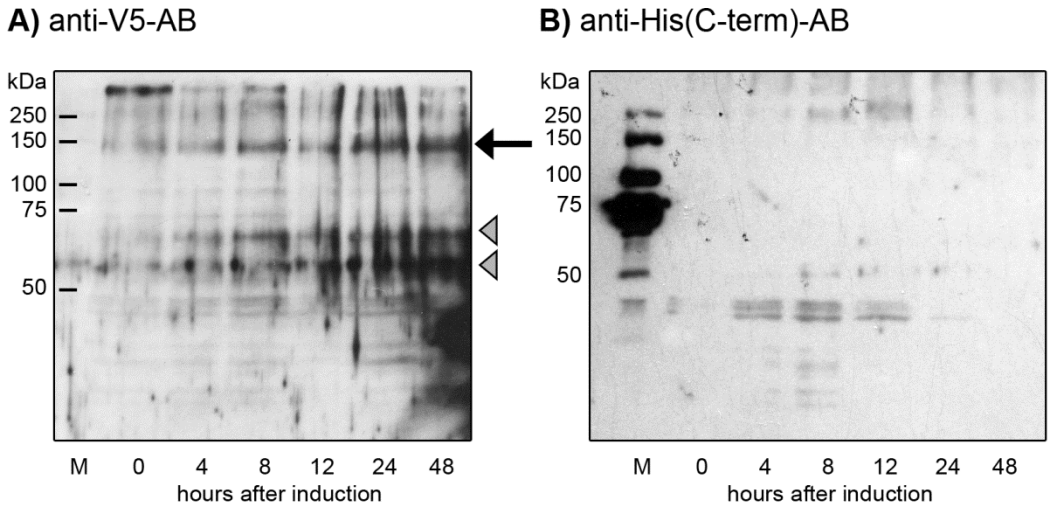

Fig. 4-2 Time course of recombinant SAC9 induction in yeast.
A Soluble proteins were extracted from *S. cerevisiae* carrying the plasmid pYES-DEST52+SAC9 and separated by 10% SDS-PAGE, electro-transferred to a PVDF membrane, and probed with anti-V5-antibodies.
B The same samples as in (**A**) but probed with anti-His(C-term)-antibodies
M, molecular weight markers. Note that a band of ~ 140 kDa (arrow) was detected with prolonged induction with the highest concentration seen after 24-48 h. Two other bands with an apparent molecular weight of ~ 55 and 65 kDa were also induced (arrowheads). None of these bands were detected with the anti-His(C-term)-antibodies

Although not necessary, Western blotting with anti-His(C-term)-antibodies was a good check for the presence of the C-terminal 6xHis tag, since this tag was essential for the following purification procedure with nickel-chelated agarose. The results were somewhat discouraging. None of the higher molecular weight proteins were detected with the anti-His(C-term)-antibodies (Fig. 4-2B).

Assuming that there was no SAC9 expressed by yeast host cells before the switch to galactose/raffinose in the medium, I did not include protein extracts from non-induced yeast cells in the analysis. The first aliquot collected at t = 0 in Figure 4-2A, however, already showed some signs of low concentrations of SAC9 (the 140 kDa band, arrow), which might be attributed to a slightly leaky promoter region on the plasmid. Therefore I repeated the experiment and grew yeast cells in induction or non-induction medium for 24 h, a time period which previously yielded good expression. The results are shown in Figure 4-3.

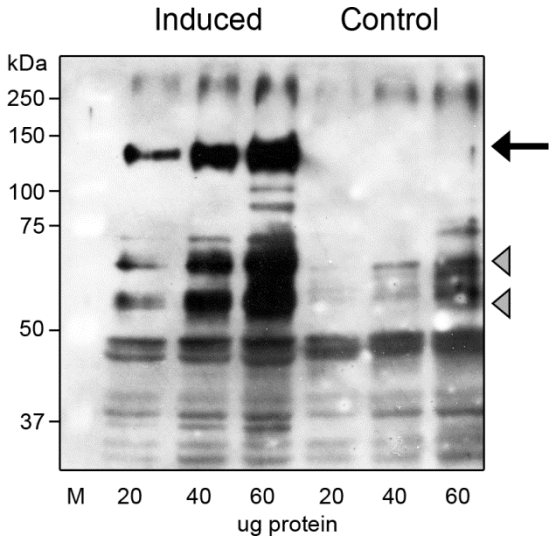

Fig. 4-3 Recombinant SAC9 expression after 24 h growth in induction or control medium. Western blot analysis with anti-V5-antibodies. M, molecular weight markers. Note a strong band around 140 kDa was present in the induced cell lysate, but not in the non-induced control (arrow). Two other bands ~ 55 and 65 kDa, respectively, seemed increased upon induction (arrowheads). However, they were also detected in the control, albeit to a lesser degree

Figure 4-3 demonstrates that the 140 kDa polypeptide was strongly detected in induced cells but not at all in non-induced (control) cells (Fig. 4-3, arrow). Hence it could be concluded that the 140 kDa polypeptide indeed was recombinant SAC9 protein. The other two polypeptides recognized by anti-V5-antibodies in Figures 4-3 (grey arrowheads) were present in the control but to a lesser degree. These smaller polypeptides might indicate degradation products of SAC9 that still had the 6xHis tag intact and accessible. However, it is more likely that they were SAC9-unrelated proteins that were non-specifically bound by the antibody. The almost identical banding pattern below 50 kDa in all lanes also indicated a certain amount of cross-reactivity or non-specific binding.

In conclusion, recombinant SAC9 protein was strongly detected with anti-V5-antibodies in soluble yeast protein extracts, particularly after an induction period of 24 hours. Therefore, I proceeded with metal affinity chromatography to purify the recombinant protein using a nickel column.

Purification of recombinant SAC9 by IMAC

The fusion protein collected after 24 h induction was purified by immobilized metal affinity chromatography (IMAC) using mini columns pre-packed with Ni^{2+}-chelated agarose. The 6xHis tag at the C-terminus of the recombinant SAC9 protein was utilized for the separation of the recombinant protein from other non-specific proteins, since the string of histidine residues binds to several types of immobilized metal ions, including nickel. Nickel provides good binding efficiency to His-tagged proteins but also tends to bind nonspecifically to endogenous proteins that contain histidine clusters. Samples from each fraction (one flow through, four wash steps, two elutions) were collected for later analysis by 10% SDS-PAGE and visualized by silver staining (Fig. 4-4). This purification procedure resulted in one small polypeptide with an estimated

molecular weight of less than 40 kDa (Fig.4-4, arrow). A white band (aka ghost band) was visible in the non-purified protein extract, in the flow through, and in the first wash fraction (Fig. 4-4, lanes 1, 3 and 4, grey arrowhead). This band seemed to correlate with the 140 kDa polypeptide seen in Figures 4-2 and 4-3. It was barely visible in the non-induced (control) cell lysate mirroring the findings in Figure 4-2 (t = 0). Conspicuous ghost bands of the same size were also visible in the flow through and the first wash fraction. Ghost bands typically appear as a halo with no signal in the middle of the band, or the entire band appears white in a dark background. Ghost bands are commonly caused by overloading the gel with excess protein. In Western blots, they are sometimes seen as a result of antibodies cross-reacting with component(s) of the blocking

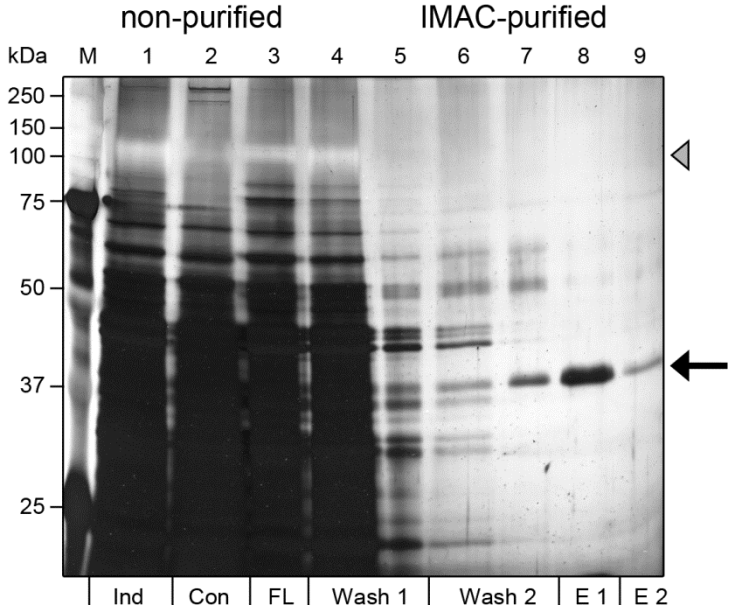

Fig. 4-4 Purification of histidine-tagged recombinant SAC9 protein from *S. cerevisiae* (I): Silver-stained SDS gel. Fractions were analyzed by 10% SDS-PAGE followed by Silver staining.
Lane 1 : crude lysate extracted from *S. cerevisiae* grown under inducing (Ind)
Lane 2 : crude lysate extracted from *S. cerevisiae* grown under non-inducing conditions (Con)
Lane 3 : flow through (FL) of the lysate after loading onto a Ni^{2+}-chelated column
Lanes 4-5 : two washes with 6xHis Wash Buffer 1 (Wash 1)
Lanes 6-7 : two washes with 6xHis Wash Buffer 2 (Wash 2)
Lanes 8-9 : 6xHis-tagged protein eluted from column with 6xHis Elution Buffer (E1 and E2)
Lane M : molecular weight markers

solution. Whatever the identity of the 140 kDa ghost band was, it apparently did not contain a histidine patch sufficient for binding to the nickel-chelated agarose beads and was therefore most likely lost in the wash fraction.

The same samples as in Figure 4-4 were separated by 10% SDS-PAGE, and a Western blot was performed with anti-His(C-term)-antibodies (Fig. 4-5). The results shown here confirmed that the ghost band seen in Figure 4-4 contained a 6xHis tag and was therefore most likely recombinant SAC9 protein (Fig. 4-5, arrowhead). Western blotting also confirmed that it was in the wash fraction and therefore did not bind to the Ni-column and was subsequently lost (Fig. 4-5, arrow).

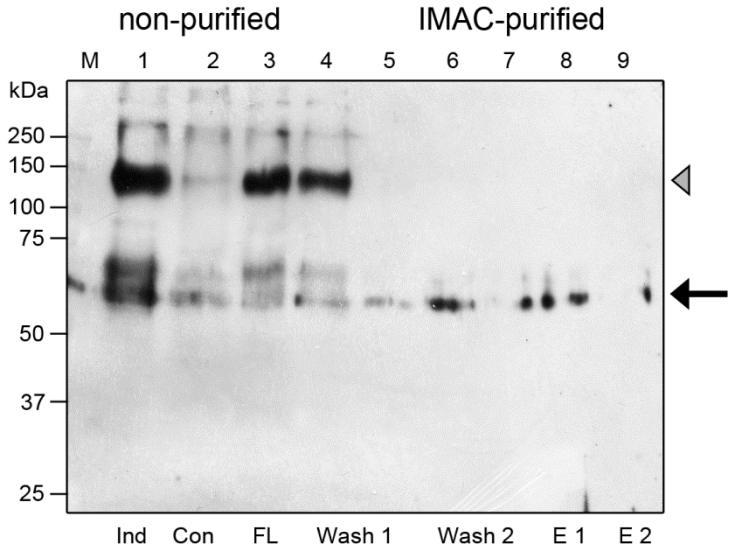

Fig. 4-5 Purification of histidine-tagged recombinant SAC9 protein from *S. cerevisiae* (II): Western blot with anti-His(C-term)-antibodies. The same samples as in Figure 4-4 were analyzed by 10% SDS-PAGE followed by electro-transfer and Western blotting.
Lane 1 : crude lysate extracted from *S. cerevisiae* grown under inducing conditions (Ind)
Lane 2 : crude lysate extracted from *S. cerevisiae* grown under non-inducing conditions (Con)
Lane 3 : flow through (FL) of the lysate after loading onto a Ni-chelated column
Lanes 4-5 : two washes with 6xHis Wash Buffer 1 (Wash 1)
Lanes 6-7 : two washes with 6xHis Wash Buffer 2 (Wash 2)
Lanes 8-9 : 6xHis-tagged protein eluted from column with 6xHis Elution Buffer (E1 and E2)
Lane M : molecular weight markers

The stark difference between induction and control demonstrated the activation of the galactose-stimulated *GAL1* promoter and subsequent expression of SAC9. As expected though, there was some base level of recombinant SAC9 protein visible even in the non-induced sample, which was attributed to a slightly leaky promoter region. The anti-6xHis(C-term)-antibody detected a polypeptide in the wash and elution fractions above the 50 kDa marker – not as seen in the SDS-gel from Figure 4-4 below the 50 kDa marker. This might reflect a different migration pattern of the proteins through the gel.

At this point of time, I was uncertain about the validity of the results obtained from the purification procedure, particularly because the 6xHis tag was not recognized in the Western blot of the time course of induction experiment (Fig. 4-2B), but it was essential for purification. Therefore I decided to sequence the plasmid from the promoter region through the insert, the V5-epitope, and the 6xHis tag. Plasmid DNA isolated directly from yeast was not sufficiently pure and not concentrated enough for successful sequencing runs. Therefore, plasmids were transformed into *E. coli* for large scale replication of DNA. Plasmids were then isolated and purified from *E. coli* in large quantities. DNA sequencing showed two differences between the sequence obtained from the plasmid and the cDNA posted by Zhong and Ye (2003) at the National Center for Biotechnology Information (NCBI, US. National Library of Medicine, Bethesda, MD) with the GenBank accession number AAP49842.1. The first difference was a G-to-A change at position 544 of the construct (data not shown). This was a silent mutation and did not affect the codon (CTA vs. CTG, both encoding for leucine). The second difference, however, seemed to have enormous consequences for the open reading frame (ORF). The plasmid contained an additional adenine at position 4022. This was predicted to cause a frameshift and to dislocate the sequence for two stop codons to 1/3 upstream. Consequently, the recombinant protein should be shorter by one third as demonstrated by Figure 4-6. The SAC

domain, however, was not affected by this frame shift as it is present from amino acids 147-543 (Zhong and Ye 2003) and 146-640 (Williams et al. 2005), respectively.

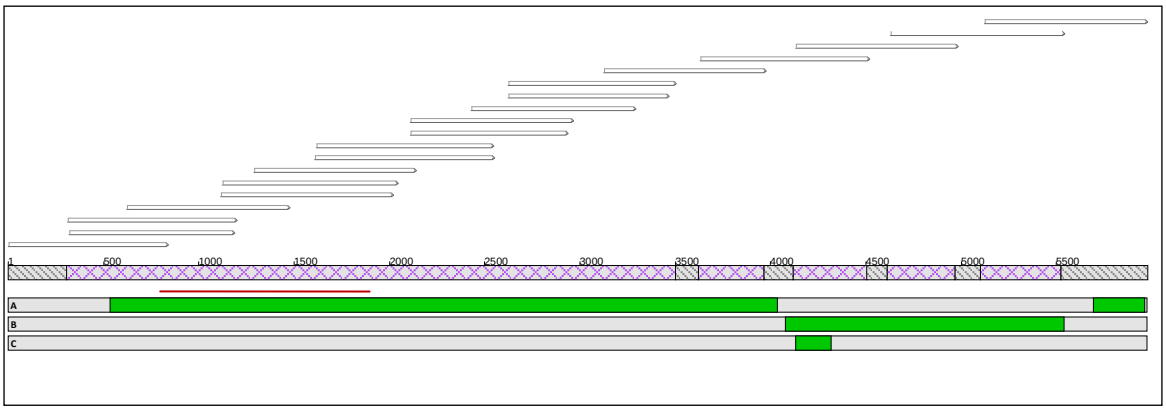

Fig. 4-6 Prediction of open reading frames (ORFs) translated from the *SAC9* gene in pYES-DEST52+SAC9. The whole insert, including the promoter region on the plasmid and the C-terminal V5 epitope and 6xHis tag, was sequenced with 14 different sequencing primers to obtain overlapping fragments (contigs, open arrows) from this 6 kb region. Contigs were aligned and the consensus sequence was used to predict ORFs (green bars). Three possible reading frames on each strand are given (A-C). The insertion of a single nucleotide was predicted to cause a frame shift and the introduction of two stop codons with the result of a shorter reading frame (A). The relative position of the SAC domain is marked by the red bar. Sequence coverage was up to 5x as indicated by the purple cross-hatched boxes below the contigs; hatched black boxes indicated 1x coverage. Sequence alignment and ORF prediction was performed in Vector NTI (Invitrogen)

To test for the presence of the mutation in other plasmids, seven more *E. coli* clones were picked randomly for plasmid isolation and checked for the exact sequence around the mutation site with three overlapping primers. All seven clones contained the additional adenine as marked by the turquoise A in the alignment of plasmid DNA with the cDNA of SAC9 (Fig. 4-7).

To evaluate whether the original yeast colonies, provided by Dr. Mary Williams, were possibly a mixed population with some yeast colonies carrying the mutation and others mutation-free, more than twenty colonies were randomly picked and used for starter cultures in liquid SC-U. Unfortunately, not a single colony from the original plate was viable.

Fig. 4-7 Alignment of plasmid DNA (pYES-DEST52+SAC9) with the cDNA for SAC9.
DNA was sequenced from seven different *E. coli* clones and aligned with the cDNA sequence for SAC9 downloaded from NCBI (GenBank accession number AAP49842.1).The alignment shows only a fraction of the gene from3978 bp – 4163 bp, but with a far-reaching difference in the sequence obtained from all *E. coli* clones at position 4022 (additional adenine in turquoise)

However, colonies used from subcultured SC-U plates were successfully grown in liquid media. DNA was extracted and the region around the mutation was PCR-amplified. Nested PCR fragments were sequenced, which demonstrated, unfortunately again, that none of the tested yeast colonies harbored a mutation-free plasmid (data not shown).

Repair of the point mutation and sequence verification

Given the puzzling nature of the results, I consulted with Dr. Dennis Welker (Utah State University, Logan, UT) who generously volunteered to repair the point mutation of the construct through restriction digest of DNA around the site of the mutation, followed by ligation of a PCR-amplified corrected fragment back into the plasmid. Dr. Welker provided me with several *E. coli* clones of the repaired construct on LB plates, referred to SAC9_76A-F.

To verify the sequence of the plasmid and to check for any other potentially introduced new mutations, the *E. coli* plasmids were isolated and sequencing cocktails were prepared with plasmid DNA from clone SAC9_76F to provide overlapping sequencing coverage of the full insert and bordering plasmid regions. Sixteen fragments were obtained and contigs were assembled as previously. Sequence alignments showed a 100% sequence similarity with the cDNA of AtSAC9 posted at the NCBI (GenBank accession number AAP49842.1) except for one minor silent mismatch at position 9 bp of the insert. The V5-epitope and 6xHis tag were at the correct

position (in-frame), followed by two stop codons after the C-terminal 6xHis tag (data not shown). The repaired construct was transformed into the yeast expression strain INV*Sc*1. Transformation efficiency was high for the transformation of the plasmid + insert and vector only, as several hundred colonies were detected each. As expected, no colonies were observed for the transformation of the yeast strain only (data not shown).

In order to verify the sequence of the new insert in the positive transformants, yeast DNA was extracted, concentrations were estimated and nested PCRs were performed to amplify first a 700 bp, and then a 500 bp region around the site of the mutation. These PCR fragments were used for sequence analysis at the University of Utah. DNA sequencing confirmed that the yeast transformants harbored the repaired construct without the additional adenine.

Recombinant expression of SAC9 with the repaired construct

Recombinant expression studies with the new construct (pYES-DEST52+SAC9_76F) were performed as previously described for the original construct. Surprisingly, the new construct without the point mutation did not lead to expression of a 180 kDa protein (data not shown). A faint band was detected around 140 kDa in protein extracts from induced and in non-induced yeast cells, similar to the 140 kDa band found in lysates from yeast cells carrying the original construct. A comparable banding pattern obtained with both, the original and the fixed construct, indicated that the expression from both constructs did not lead to the synthesis of different recombinant proteins. Banding pattern intensity seemed to differ though, which might reflect differences in expression levels. It is possible that slight differences in cell growth, lysis, and extraction procedures, could also have contributed to these observed differences. Since Ni-purification resulted in only one exceedingly small band of ~ 40 kDa, which was assumed not to be the target, I looked into different ways of obtaining SAC9 protein for functional assays.

Development and testing of anti-SAC9-antibodies

Any protein can be isolated from a complex mixture of proteins by means of IP provided that a specific antibody for the target protein exists. Anti-SAC9-antibodies are not commercially available until today, thus we decided to raise antibodies against SAC9. A third party (Open Biosystems, Thermo Fisher Scientific) was selected for the task. The company recommended using recombinant protein, when possible, to develop monoclonal antibodies, particularly, considering the very large size of the protein. Since I did not have any recombinant protein at this point and due to cost restraints, we decided to go the peptide route to generate so-called "similar-to-monoclonal" antibodies (sAB). Instead of the complete protein as the immunogen, peptides from SAC9 were synthesized and conjugated to a carrier protein. Antibodies generated against a synthetic peptide by direct injection into animals are technically not monoclonal antibodies. Although antisera from animals immunized with peptide-conjugated antigen are generated in the same way as polyclonal antibodies, they are specific to only one epitope, the synthetic peptide, and therefore they are referred to as sAB (similar-to-monoclonal antibodies).

Selected synthetic peptides conjugated to a carrier protein were injected repeatedly into four rabbits (two rabbits received immunizations with peptide 1, and the other two animals received injections with peptide 2). Serum was collected two weeks after each immunization. I tested the crude sera collected after the final immunization for binding affinity towards the synthetic peptides in a modified ELISA (immunodot blot). Basically, a two-fold dilution series of the peptides was spotted on a nitrocellulose membrane and probed with crude serum at different concentrations. HRP-linked secondary antibodies were used, and the signal was visualized by chemiluminescence. Results obtained from immunodot blots indicated that the antisera recognized the synthetic peptides, as predicted, in a peptide-concentration and antibody-dilution-dependent manner with no cross-reactivity in the pre-immune serum (data

not shown). The response from the two animals per antibody was similar enough to allow for pooling of the antisera before further affinity purification by the company.

I then tested the binding affinity of the ammonium-sulfate-precipitated anti-SAC9-antibodies towards the synthetic peptides in immunodot blots as described above for crude sera. Results are presented in Figure 4-8. Both purified antisera showed similar concentration-dependent responses to the synthetic peptides as already seen for the crude sera. Purified antibodies raised against the second peptide (anti-SAC9-AB_940) consistently showed a stronger affinity towards the target than purified antibodies raised against the first peptide (anti-SAC9-AB_515). The minimum concentration recognized by the second antibody was 2-4 µg, whereas the detection limit for the first antibody was around 16 µg of peptide (Fig. 4-8). The immunodot blots and immune response was repeated one year later with the same antibodies kept at 4°C, and the results were very similar (data not shown).

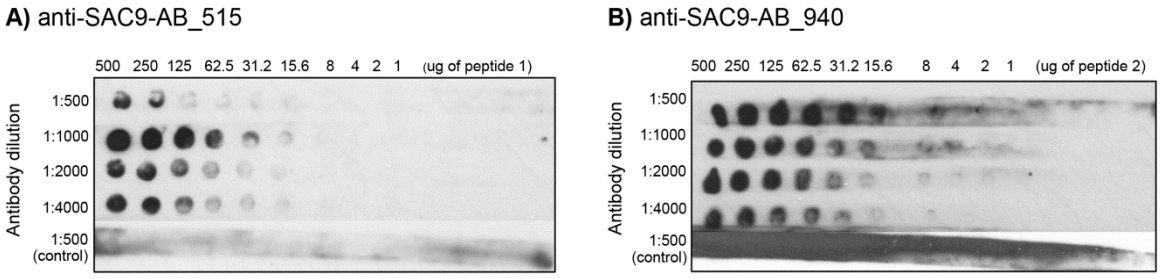

Fig. 4-8 Affinity tests with anti-SAC9-antibodies.
A Immunodot blot with anti-SAC9-AB_515 and peptide 1 (aa 915-933)
B Immunodot blot with anti-SAC9-AB_940 and peptide 2 (aa 940-961)

Detection of SAC9 in plant extracts with anti-SAC9-antibodies

Strong antibody binding and recognition of micromolar quantities of the synthetic peptide did not guarantee that the developed antibodies could also recognize the SAC9 protein from *A. thaliana* WT plants. Therefore, soluble proteins from plants were extracted, separated

by SDS-PAGE, transferred to a PVDF membrane and probed for the target protein with either antibody. Results are presented in Figures 4-9 and 4-10. Anti-SAC9-AB_515 recognized four proteins of increasing size: 45, 48, 80, and 140 kDa. However, the first two were almost too faint to see. Anti-SAC9-AB_940 also recognized several proteins. Size estimation was difficult, as one slightly smeared band was visible (Fig. 4-9C). A second Western blot (Fig. 4-10) led to better results, and the proteins were estimated to be around 140, and 180 kDa. There was no cross-reactivity apparent in the control.

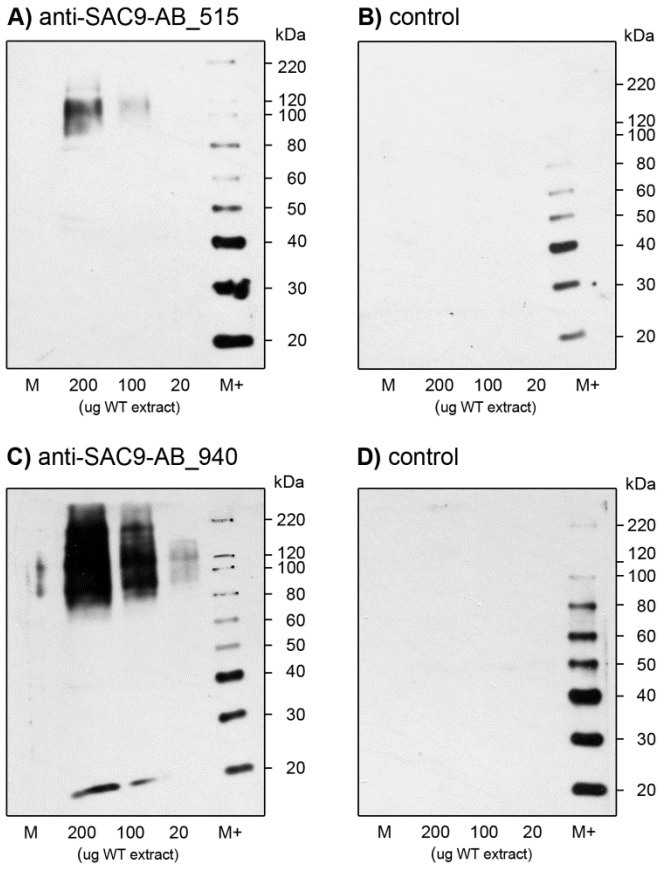

Fig. 4-9 Western blots with anti-SAC9-antibodies (I).
A Protein extracts from *A. thaliana* WT probed with anti-SAC9-AB_515
B Protein extracts from *A. thaliana* WT probed with preimmune serum (control)
C Protein extracts from *A. thaliana* WT probed with anti-SAC9-AB_940
D Protein extracts from *A. thaliana* WT probed with preimmune serum (control)
M and M+, different molecular weight markers

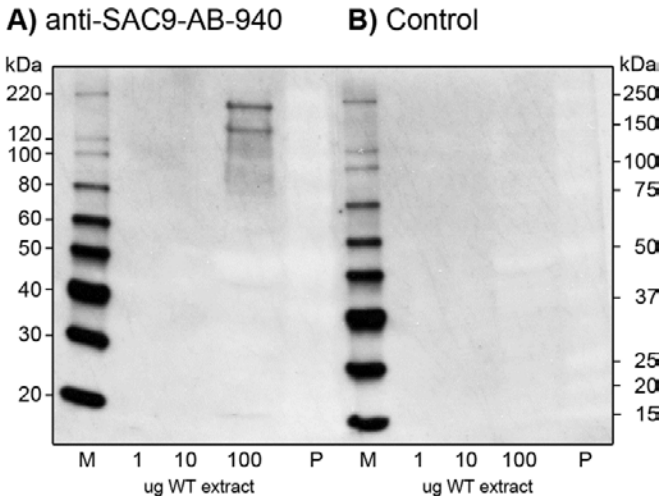

Fig. 4-10 Western blot with anti-SAC9-antibodies (II).
A Protein extracts from *A. thaliana* WT probed with anti-SAC9-AB_940
B Protein extracts from *A. thaliana* WT probed with preimmune serum (control)
M and P, different molecular weight markers. Proteins were extracted the same way as for Figure 4-9, but from a different batch of *A. thaliana* WT seedlings

Immunoprecipitation with anti-SAC9-antibodies

In order to isolate SAC9 protein from the complex mixture of extracted proteins from seedlings and plants, both anti-SAC9-antibodies were used in pull down experiments with Invitrogen's Immunoprecipitation Kit – Dynabeads® Protein A (or G). The results of a typical immunoprecipitation (IP) procedure can be seen in Figure 4-11. Wild-type extracts were used as a positive control to show the presence of the predicted 180 kDa large SAC9 protein. Different antibodies for the IP led to slightly different eluted proteins, despite the fact that both antibodies were raised against synthetic peptides from the same protein, namely SAC9. The 180 kDa band of the predicted SAC9 protein was clearly visible with anti-SAC9-AB_940 (Fig. 4-11, Lane 6) but very faint with the other antibody, anti-SAC9-AB_515. The 180 kDa band was not present in either preserum. Other smaller proteins were detected with preimmune serum, with a prominent band showing up around 50 kDa.

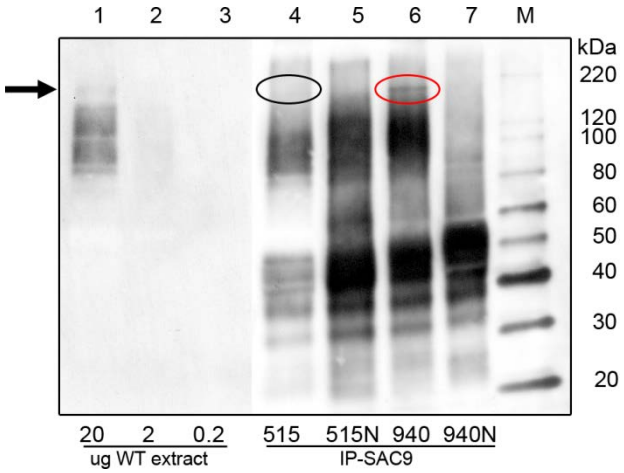

Fig. 4-11 Western blot of proteins immunoprecipitated with anti-SAC9-antibodies.
Lanes 1-3 : 20, 2, and 0.2 µg *A. thaliana* WT extract
Lane 4 : Immunoprecipitated sample with anti-SAC9-AB_515
Lane 5 : Immunoprecipitated sample with anti-SAC9-AB_515-preserum
Lane 6 : Immunoprecipitated sample with anti-SAC9-AB_940
Lane 7 : Immunoprecipitated sample with anti-SAC9-AB_940-preserum
Lane M : Molecular weight markers
Protein extracts from *A. thaliana* plants were prepared as previously described, and immunoprecipitated (IP) with either anti-SAC9-AB_515 (515) or anti-SAC9-AB_940 (940) and the respective preserum (515N, 940N). Various amounts of WT extracts and immunoprecipitated samples were separated by 10% SDS-PAGE, transferred to a PVDF membrane and incubated with anti-SAC9-AB_940 (3 mg/ml stock diluted 1:500, overnight at 4°C). Note that WT extract showed a faint band of 180 kDa (arrow) similar to the one seen in Figure 4-10. This band was still visible on x-ray when both antibodies were used for IP, but the faint band in Lane 4 did not scan well and is therefore hardly noticeable here. The same band was much stronger for the IP with anti-SAC9-AB_940 (Lane 6, red oval). Note that several other smaller proteins were detected in samples immunoprecipitated with preserum

Functional assay of immunoprecipitated SAC9 with the Malachite Green Assay for inorganic phosphate release

To test the activity of the putative phosphoinositide phosphatase SAC9, immunoprecipitated protein was used in a reaction with its putative substrate, PI(4,5)P_2. The reaction product, inorganic phosphate, was measured colorimetrically with the Malachite Green Assay. Any free orthophosphate released during the enzymatic reaction binds to malachite green molybdate and forms a green molybdophosphoric acid complex (D'Angelo et al. 2001).

The color formation can be measured at 620-640 nm and is directly related to the free inorganic phosphate concentration. The Malachite Green Assay was used because it is well suited to detect and quantify minimal amounts of inorganic free phosphate in aqueous solutions under acidic environments.

Micelles with PI(4,5)P_2 and a five-fold molar excess of a carrier lipid (dioleoylphosphatidilserine) were prepared and brought into suspension in the reaction buffer by sonication. The enzyme obtained through immunoprecipitation from wild-type extracts was added and incubated for 15 min at 30°C, after which the reaction was terminated by addition of an alkylating agent. It should be noted here that immunoprecipitated proteins were eluted from the Dynabeads under two different elution conditions: denaturing conditions for SDS-PAGE and Western blots, and gentle, non-denaturing conditions for activity tests. To test the effect of antibody concentration on the quantity of the final elution product, IP reactions were performed with either low (10 µl at ~ 3 mg/ml) or high (100 µl at ~ 3 mg/ml) amount of anti-SAC9-antibodies. After termination of the reaction, the complete mix was centrifuged to sediment the lipids. A fraction of the supernatant was combined with the Malachite Green Reagent and incubated again until color saturation. Absorbance at 630 nm was measured and used for quantification of released inorganic phosphate. The assay was repeated three times with the same samples over a period of five days.

Results are presented in Figures 4-12 and 4-13 (absolute and net amount of recorded Pi, respectively) and indicate that phosphate measurements were slightly variable but did not correlate with time. Therefore, it can be concluded that frozen protein samples did not degrade appreciably over time, at least not within five days. Wild-type extracts had the highest amount of recorded free inorganic phosphate (Pi) with or without the addition of the substrate. This was not surprising as the extract likely contained many different phosphatases, as well as possibly

some hydrolysis products in the form of free inorganic phosphates. Yet, the release of almost 1000 pmol of orthophosphate indicated that the assay had worked and that the lipids were provided in a functional way. Both antibodies used for immunoprecipitation seemed to have resulted in the isolation of protein(s) that could liberate phosphate, although some differences existed in the absolute amount of released phosphate, i.e. immunoprecipitation with anti-SAC9-AB_940 led to the isolation of polypeptides that caused a higher absolute amount of liberated Pi than polypeptides immunoprecipitated with anti-SAC9-AB_515 (Fig. 4-12). However, this difference was negligible for the net release of phosphate (Fig. 4-13). Also, the amount of antibodies used for immunoprecipitation of SAC9 (low vs. high) seemed not to have an influence on the net release of phosphate.

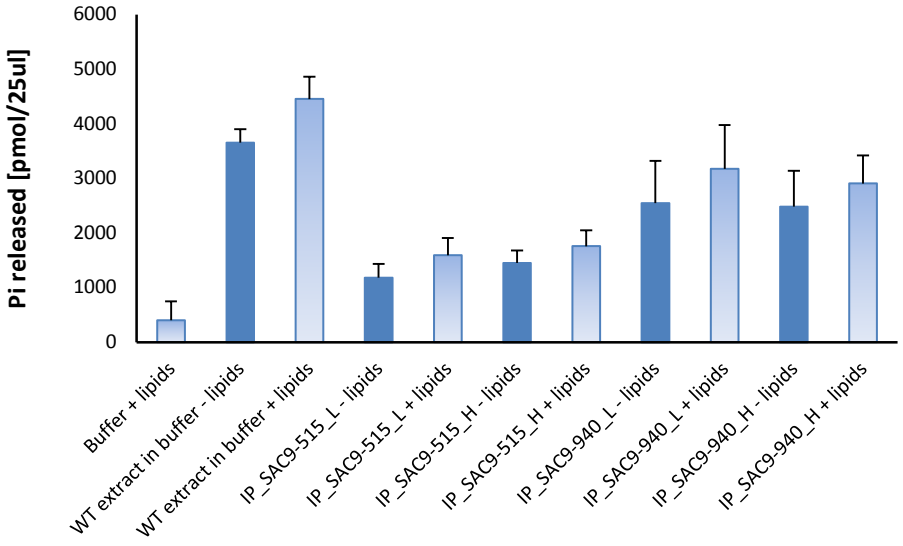

Fig. 4-12 Absolute release of inorganic phosphate (Pi) from wild-type extracts and extracts immunoprecipitated (IP) with anti-SAC9-antibodies. Two different anti-SAC9-antibodies (515 and 940) and two different antibody concentrations (L and H, low and high, respectively) were used for IP. The same samples were assayed with the Malachite Green Assay in three independent runs on consecutive days. Samples were kept frozen at -20°C between runs. Bars with gradient fill represent samples with substrate addition (lipids in buffer), whereas solid bars represent samples without substrate addition. Error bars show positive SD

All components of the Malachite Green Assay were tested and found essentially phosphate free (Appendix C). Minor phosphate amounts were detected in samples of reconstituted substrate in assay buffer (Fig. 4-12 and Appendix C) most likely reflecting some hydrolysis of the substrate, $PI(4,5)P_2$. Raw data for all performed experiments are listed in Appendix C.

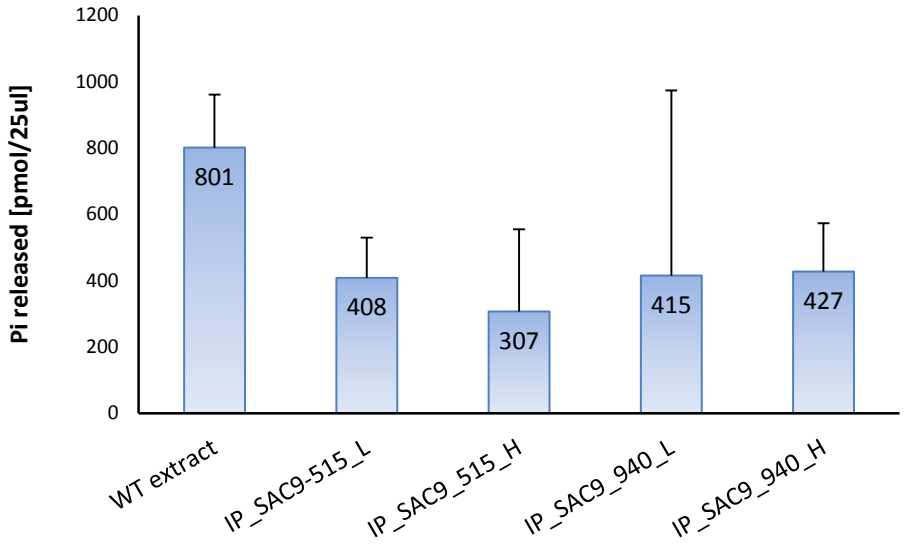

Fig. 4-13 Net release of inorganic phosphate (Pi) from wild-type extracts and extracts immunoprecipitated (IP) with anti-SAC9-antibodies. Two different anti-SAC9-antibodies (515 and 940) and two different antibody concentrations (L and H, low and high, respectively) were used for IP. The same samples were assayed with the Malachite Green Assay in three independent runs on consecutive days. Samples were kept frozen at -20°C between runs. Error bars show positive SD

In conclusion, there was no difference in Pi release due to antibody type used for IP (AB_515 vs. AB_940) or antibody amount used for target capture (high vs. low), i.e. higher absolute amounts of released Pi for samples immunoprecipitated with anti-SAC9-AB_940 did not translate into higher net phosphate release from the same samples.

Although these experiments were the first corroborative evidence for the hypothesis that the SAC9 protein was most likely a phosphatase with at least one specific substrate, $PI(4,5)P_2$, I was not completely sure of the identity of the immunoprecipitated proteins, nor did I know which of the detected bands in Figure 4-11 caused the phosphate release. I conducted a repeat of the Malachite Green Assay with another negative control, namely immunoprecipitates from the preserum in addition to the anti-SAC9-antibodies. I further tested the effect of an additional purification step by utilizing a 30 kDa protein filter (Centricon 30, # 4208, Amicon Inc.) after immunoprecipitation, based on the idea that any smaller proteins were either inactive SAC9 fragments or other non-specific proteins. I also changed the acidic environment of the assay to near neutral to test the effect of pH on phosphatase activity, since it was shown in an earlier report to affect the release of phosphate (D'Angelo et al. 2001).

The results of the repeated Malachite Green Assays are presented as described previously in two bar diagrams (Figs. 4-14 and 4-15, absolute and net release of Pi). Again, the highest quantity of liberated phosphate was measured for wild-type extracts. Phosphate release was slightly greater for wild-type extracts than in Figure 4-12, reflecting different batches of plant material. Also, the absolute amount of liberated Pi was higher in all samples when the assay was run under slightly acidic conditions (pH 5 vs. pH 7). As reported by D'Angelo et al. (2001), the pH of the reaction solution had to be slightly acidic for optimal phosphate release. The data in Figure 4-14 supported this statement. The use of a 30 kDa filter after immunoprecipitation led to a minor decrease of measured phosphate release.

The addition of the substrate to the protein immunoprecipitated with anti-SAC9-AB_940 led to a sizable release of measured orthophosphate (Fig. 4-15), which was corroborative evidence for a phosphoinositide phosphatase function of SAC9. This conclusion cannot be drawn, however, without acknowledging the fact that measured phosphate released from

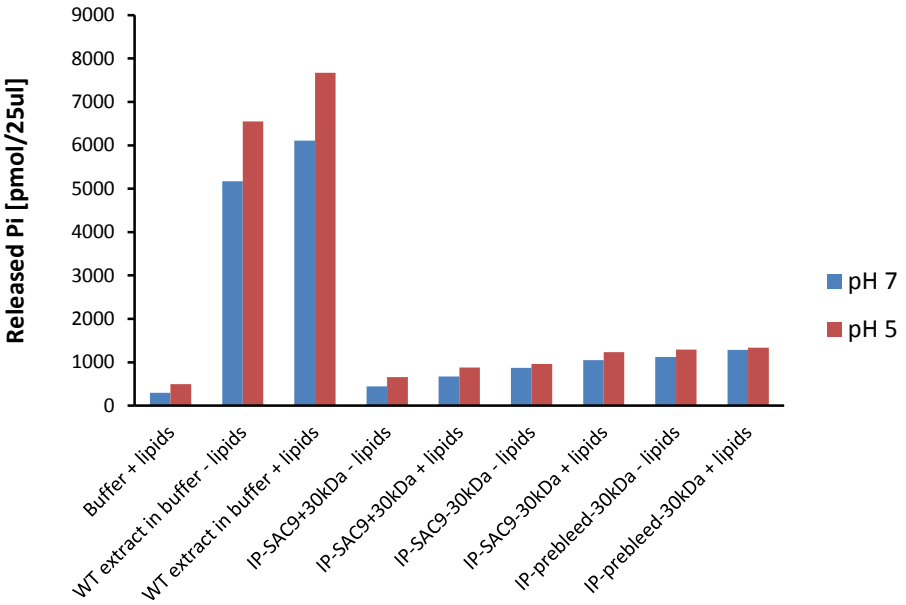

Fig. 4-14 The effect of pH and an additional purification step on the absolute release of inorganic phosphate (Pi) from WT extracts and extracts immunoprecipitated with anti-SAC9-antibodies (940). The Malachite Green Assay was performed with samples obtained from the same IP procedure under slightly acidic (pH 5) or neutral (pH 7) conditions. The additional purification step included the application of a 30 kDa separation filter after the IP procedure. The experiment was performed without biological replicates

samples immunoprecipitated with the preserum was higher than expected for a negative control. However, and as already pointed out, running the assay under slightly acidic conditions was beneficial; not only was the absolute amount of released Pi higher than for the same samples run under neutral conditions, but it also seemed to have suppressed the non-specific release of Pi from control samples (IP-prebleed). The very similar net amount of released Pi from protein samples with and without the additional purification step suggested that the filter did not have an effect. The generally low levels of free phosphate in all but wild-type extracts might indicate that either the Malachite Green Assay was susceptible to unobserved minor changes in the experimental conditions, or immunoprecipitations varied significantly from one batch to another.

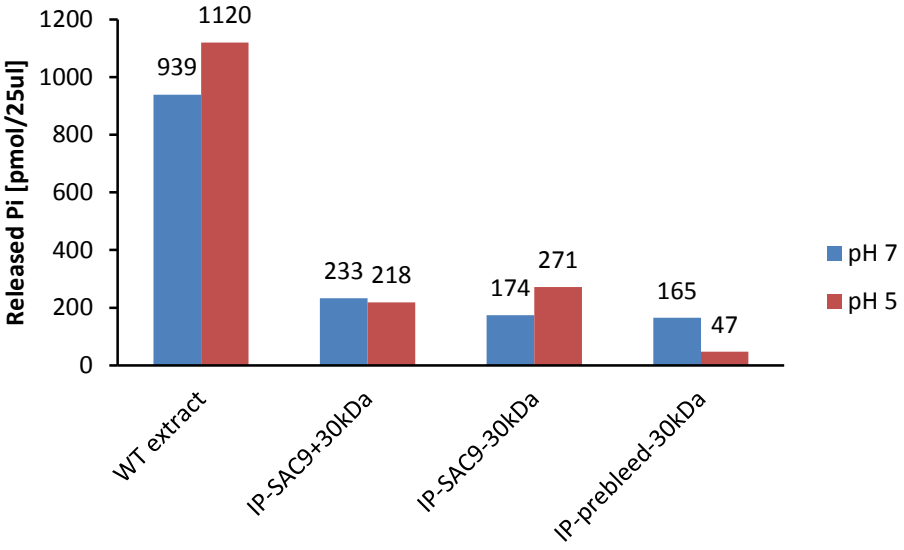

Fig. 4-15 The effect of pH and an additional purification step on the net release of inorganic phosphate (Pi) from WT extracts and extracts immunoprecipitated with anti-SAC9-antibodies (940) and the respective preserum. The Malachite Green Assay was performed with samples obtained from the same IP procedure under slightly acidic (pH 5) or neutral (pH 7) conditions. The additional purification step included the application of a 30 kDa separation filter after the IP procedure. The experiment was performed without biological replicates

Optimization of Immunoprecipitation

Since the basis for the Malachite Green Assay is the protein obtained through immunoprecipitation (IP), several parameters, such as affinity and concentration of the antibody, incubation time of the antibody-antigen complex, number and times of wash steps, and elution conditions, can affect the elution product in quantity as well as quality.

I assumed at that time, that either the 140 or the 180 kDa band represented SAC9 as seen in Figure 4-10, because the molecular weight for SAC9 was estimated to be around 180 kDa. Ideally, IP procedures should lead to only one eluted antigen, yet I also knew that detection of multiple bands was not uncommon, which could be proteolysis products, isoforms, splice variants, or possible binding partners. I therefore tried to optimize conditions by testing

different antibody concentrations, incubation times, cross-linking, preclearing, and extensive washing.

First, I tested different concentrations of antibody used for antigen binding and subsequent IP. The recommended amount of antibody added to the Dynabeads ranged from 1-10 µg. I applied anti-SAC9-AB_940 in three different amounts (3, 30, 300 µg) with no apparent effect (Fig. 4-13 and other data). Thus for routine immunoprecipitation, I used the lowest concentration of antibody tested.

I further tested the effect of incubation time of antibody-antigen complex, keeping in mind that the standard protocol suggested a ten-minute incubation period for the formation of antibody-antigen complex. Increasing incubation times for optimal binding to one or four hours, respectively (at RT or 4°C), did not lead to the elution of a stronger 140 or 180 kDa band when visualized on a Western blot (data not shown).

Next, I tested the effect of cross-linking the antibody to the beads. In the standard protocol, the antibody is added to the Dynabeads and forms an antibody-Dynabeads complex. The target antigen binds then to the antibody. After binding, the beads are washed extensively to get rid of non-bound sample components and the antigen is eluted from the support using an appropriate elution buffer. Depending on elution buffer, dissociation of the complex does not only lead to elution of the target antigen, but also to co-elution of the antibody since the antibody is not permanently bound to the beads. Co-elution of antibody fragments and their co-migration with the antigen in SDS-PAGE can pose a significant obstacle in analysis. Downstream processes such as the Malachite Green Assay might also be negatively affected. Using the cross-linking reagent BS^3 (Bis[sulfosuccinimidyl] suberate), Thermo Scientific, Pierce Protein Products #21585), before adding the protein extract should covalently link adjacent amines of the antibody and Protein A (or G). Cross-linking with BS^3 should therefore allow for target antigen

elution without antibody contamination. Cross-linking with BS^3, however, can potentially decrease antibody binding efficiency by modifying too many of the amine groups in the antibody binding site.

Figure 4-16 shows the results of immunoprecipitations performed with cross-linked anti-SAC9-antibodies. The effect of two other parameters on the quality of the elution was also tested. These were preclearing of the beads and additional wash steps before elution. Preclearing included incubation of WT extract with a volume of beads followed by magnetic separation of beads and extract. The beads were discarded and the supernatant (now without proteins that non-specifically bind to Protein G) was used with new beads for the IP. Generally, the same results were obtained for all different treatments with neither the 140 nor the 180 kDa band in the elute. Instead a very prominent polypeptide of 50 kDa was detected as already seen in Figure 4-11. No proteins were found in the last wash regardless of the number of washes. The 140 and 180 kDa bands visible in the wild-type extracts were also detected in the flow through fraction; this indicated that the proteins did not bind to the Dynabeads-antibody-complex.

Optimization of extraction conditions

The previous results demonstrated that immunoprecipitation with anti-SAC9-antibodies was surprisingly insensitive to varying conditions. Therefore I turned my attention to the protein extraction procedure and consulted with Dr. Joanie Hevel (Utah State University, Logan, UT) for additional optimization approaches. I tested the effect of two recommended additives on the extraction of soluble proteins from plant material. NaCl was used to disrupt non-specific protein interactions, and NP-40 was included to reduce background. Both components were made up as 2X strength in extraction buffer, and separately added to previously made wild-type extracts in a 1:1 ratio. After complete mixing, extracts were allowed to sit for 15 min on ice, with occasional

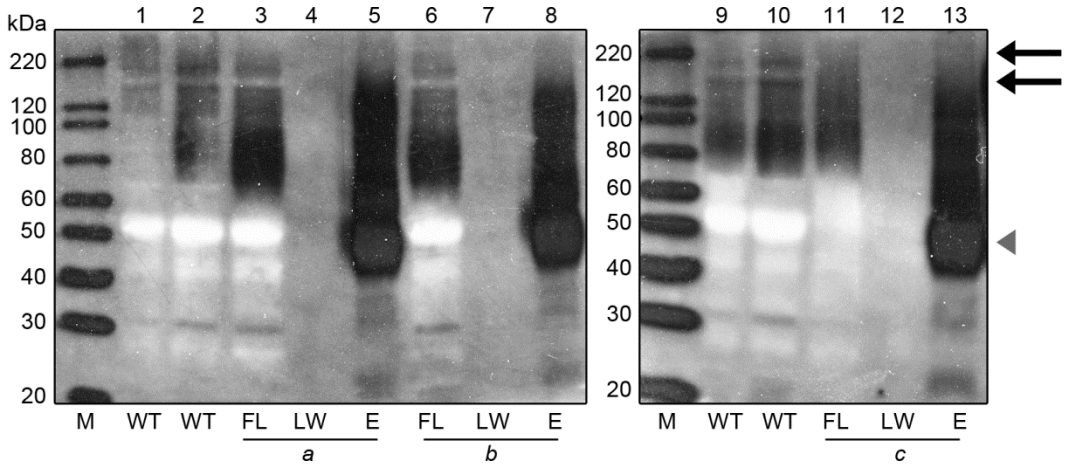

Fig. 4-16 Optimization strategy I: The effect of BS^3 conjugation, preclearing, and extra washes on the immunoprecipitation of SAC9. Protein extracts and fractions from the IP procedure were analyzed by 10% SDS-PAGE followed by Western blotting with anti-SAC9-AB_940.
a IP procedure with BS^3-conjugated beads, preclearing and three wash steps
b IP procedure with BS^3-conjugated beads, preclearing and six wash steps
c IP procedure with BS^3-conjugated beads, no preclearing and three wash steps
Lanes 1 and **9** : 100 µg *A. thaliana* wild-type (WT) extract
Lanes 2 and **10**: 200 µg WT extract
Lanes 3, 6, 11 : Flow through (FL)
Lanes 4, 7, 12 : Last wash (LW)
Lanes 5, 8, 13 : Elution (E)
Lane M : Molecular weight markers
Note that the three different treatments did not lead to elution of higher molecular weight proteins. The 140 and 180 kDa bands, respectively (arrows), were detected in WT extracts and in the flow through fraction collected from the supernatant after antigen binding. The last wash was always free of any measurable proteins. The eluted fraction still contained a highly concentrated polypeptide of approx. 50 kDa (arrowhead) as already seen in Figure 4-11

agitation by inverting the tube, before proceeding with standard IP. NaCl concentrations ranged from 0-1000 mM and NP-40 concentrations ranged from 0-2%. Fractions from the flow through and first elution were visualized by Western blotting. WT extracts served as control. Since aliquots of WT extracts showed some cloudiness after thawing, they were centrifuged in the cold for 10 min at maximum speed (13,500 rpm) in a table top centrifuge. The cleared supernatant was loaded in two different concentrations. Results presented in Figure 4-17 show that neither additive led to the elution of the 140 kDa or the 180 kDa band.

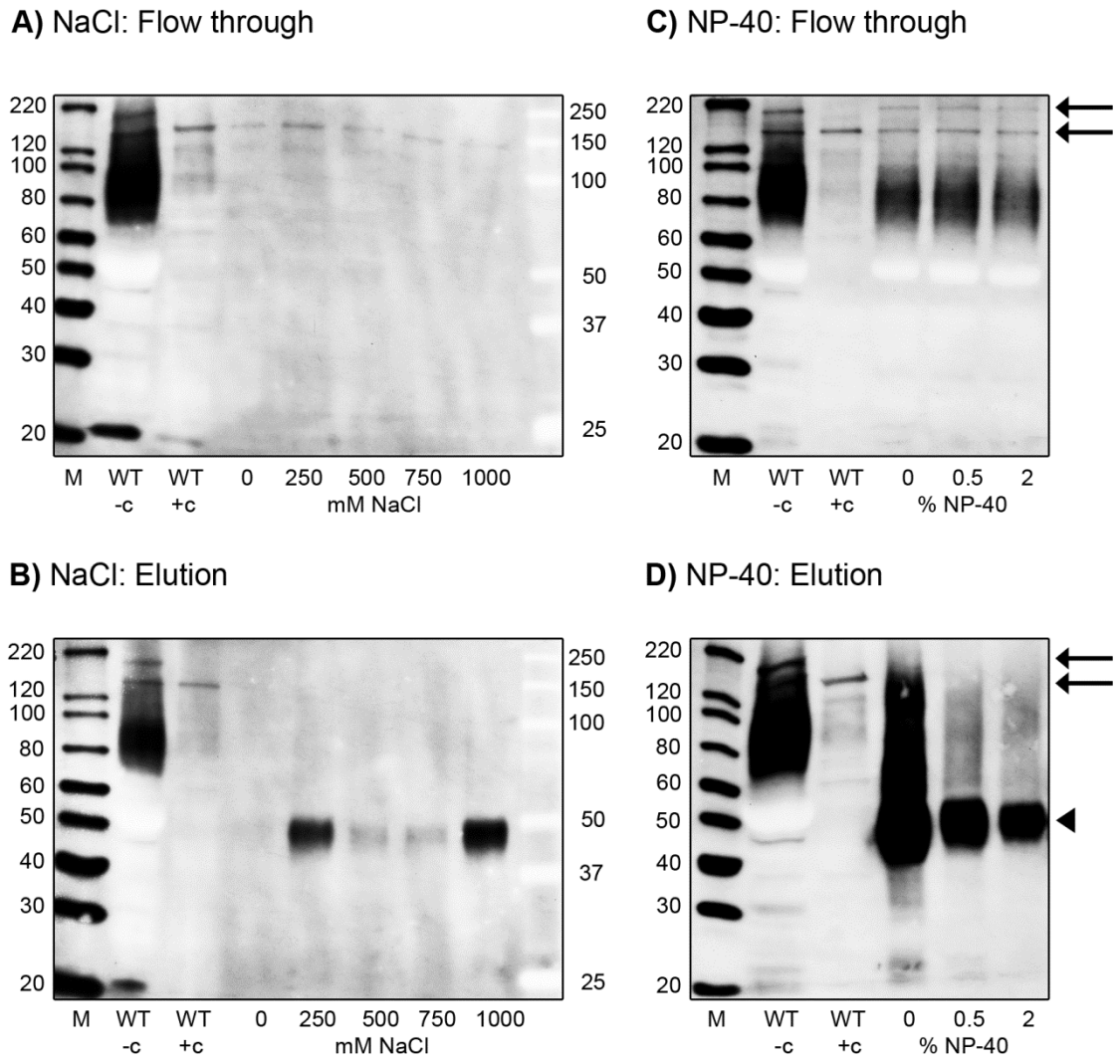

Fig. 4-17 Optimization strategy II: The effect of extraction buffer additives on the immunoprecipitation of SAC9. Protein extracts and fractions from the immunoprecipitation (IP) procedure were analyzed by 10% SDS-PAGE and Western blotting with anti-SAC9-AB_940.
A Flow through fraction from the IP procedure performed with NaCl in the extraction buffer
B Flow through fraction from the IP procedure performed with NP-40 in the extraction buffer
C Eluted fraction from the IP procedure performed with NaCl in the extraction buffer
D Eluted fraction from the IP procedure performed with NP-40 in the extraction buffer
Note that none of the buffer additives led to the elution of the target protein (arrows). Instead a prominent 50 kDa polypeptide was strongly detected (arrowhead) as previously seen, albeit with less background. M, molecular weight markers in kDa; WT -c, *A. thaliana* wild-type extract - not centrifuged after thawing; WT +c, *A. thaliana* wild-type extract - cleared supernatant after centrifugation

On the contrary, a 50 kDa band was the only band detected in the elution. Again, both bands (140 and 180 kDa) were only visible in the wild-type extracts and in the flow through, and therefore were not recognized by the antibody. Centrifugation of the lysate after thawing led to a much reduced background. However, the 180 kDa band was also lost to the pellet. If this was SAC9, then it was barely soluble and centrifugation led to its precipitation and sedimentation into the non-soluble fraction.

GenScript project

Since both anti-SAC9-antibodies seemed not to be that efficient in the reported IP experiments regardless of extraction parameters, I revisited my recombinant protein strategies, and Dr. DeWald, my former major professor, suggested to have this part of the project outsourced to a third party (GenScript USA Inc, Piscataway, NJ). GenScript was contracted to synthesize the complete *SAC9* gene with optimized codons for expression in yeast and to add a TEV cleavage site for later proteolytic tag removal. After synthesis, the gene was planned to be subcloned into a proprietary yeast expression vector containing two different tags: a Flag tag as well as a 6xHis tag at the C-terminus. Expression evaluation and 1L yeast expression was expected, followed by a two-step affinity purification process, tag removal, and quality control by MALDI-TOF. Unfortunately, GenScript failed over several months to synthesize the gene. Since I had constructs with the cDNA sequence for the complete SAC9 protein in an expression vector (pYES-DEST52+SAC9 and pYES-DEST52+SAC9_76F), I decided to have GenScript use these constructs for expression studies. According to GenScript, they grew yeast cells harboring either construct under comparable conditions and induced expression with galactose for 48 h. Soluble proteins were extracted with acid-washed glass beads, and recombinant SAC9 was purified with Ni-NTA columns. Collected fractions were analyzed by SDS-PAGE and Western blotting with anti-

His(C-term)-antibodies. Results are presented in Appendix D. The company's purification procedure ended with the isolation of several proteins with two prominent bands around 40 and 95 kDa, respectively, but none above 100 kDa, as seen by my expression and immunoprecipitation experiments. Anti-His(C-term)-antibodies recognized two bands in Western blots of slightly lower apparent molecular weight (40 and 70 kDa for pYES-DEST52+SAC9 and 60 and 90 kDa for pYES-DEST52+SAC9_76F). Only protein bands visualized by Coomassie Brilliant Blue staining were abundant enough for identification through mass spectrometry. The prominent 40 and 95 kDa bands were excised from an SDS gel. Isolated proteins were identified by mass spectrometry using enzymatic digestion patterns based on the primary sequence. They confirmed that neither band was the target protein SAC9 or a fragment of SAC9. Based on these results, the project with GenScript was terminated.

CONCLUDING REMARKS

SAC9 is a unique protein in *Arabidopsis thaliana*. Its precise function is not known but the identification of a mostly conserved Sac1p homology domain (SAC) at the C-terminus of SAC9 strongly suggested a phosphoinositide phosphatases function. Further evidence came from the fact that *sac9* roots accumulated PI(4,5)P_2 and its hydrolysis product IP_3. Combining these two pieces of information, Williams et al. (2005) hypothesized that SAC9 most likely was a phosphoinositide phosphatase involved in lipid signaling, particularly under stress conditions. The study presented in this chapter was designed to test this hypothesis.

Recombinant expression of SAC9

The goal of this study was to provide evidence for the *in vitro* function of AtSAC9. To achieve this, I initially expressed recombinant SAC9 from yeast and purified the 6xHis tag fusion

protein with immobilized metal affinity chromatography. This procedure was complicated by the fact that the construct contained a point mutation, which was predicted to result in a shortened open reading frame. The point mutation was repaired with site-directed mutagenesis (courtesy of Dr. Dennis Welker) and then used for SAC9 expression. Surprisingly, induction with galactose did not lead to the expression of a 180 kDa protein. On the contrary, the expression pattern was similar to that of the old construct with the additional nucleotide, but expression was generally lower. This unexpected result opens up a new line of future investigations, beginning with amino acid sequencing of various bands to determine what polypeptides exactly were expressed under this particular expression system.

Immunoprecipitation of SAC9

In an alternative approach, I planned to obtain SAC9 protein from *A. thaliana* WT seedlings through IP. Since no antibodies against SAC9 were commercially available, we had to raise anti-peptide-antibodies against sequences specific to SAC9. Crude sera from the immunization were tested for affinity towards the synthetic peptides, further affinity-purified, and then re-tested for affinity. Immunodot blots indicated similarly strong responses of both antibodies towards the respective peptide. Western blots demonstrated slightly different specificities of the antibodies with extracted proteins from wild-type plants. Anti-SAC9-AB_940 consistently showed a stronger affinity than anti-SAC9-AB_515 and detected two polypeptides with apparent molecular weight of 140 and 180 kDa, respectively. The predicted molecular weight of AtSAC9 is around 180 kDa. The smaller second polypeptide was thought to be a possible splice variant or isoform and not a cleaved protein fragment, since the extraction buffer contained sufficient concentrations of various protease inhibitors. A thorough online re-investigation on the *SAC9* gene led to the discovery of a splice variant with a predicted

molecular mass of 155 kDa (Fig. 4-18) explaining the detection of two bands instead of only the expected one. A 15-kDa difference between the 140 kDa polypeptide detected with anti-SAC9-AB_940 and the 155 kDa splice variant was hard to separate by SDS-PAGE. It was interesting that the splice variant was deposited only at TAIR (The Arabidopsis Information Resource) and not at GenBank at NCBI (National Center for Biotechnology Information). GenBank generally has more deposited sequences than TAIR, but it appeared that TAIR was curated with more detail. The presence of a putative splice variant of SAC9 greatly emphasizes the importance of regular literature search and the utilization of a variety of online resources.

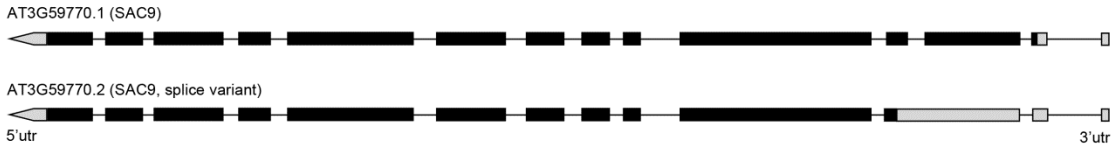

Fig. 4-18 Gene model of *AtSAC9* with the exon-intron structure of the SAC9 transcript. Exons are represented by black boxes, introns by a black line. Grey arrows symbolize the 5'untranslated region (5'utr), whereas grey boxes denote the 3'untranslated region (3'utr). The *SAC9* gene is located on locus AT3G59770 of chromosome three of *A. thaliana* and encodes a 1630 aa protein with an estimated molecular weight of 180 kDa. One splice variant is additionally predicted with 1405 aa and a molecular weight of 155 kDa. Adopted from TAIR (http://www.arabidopsis.org/servlets/TairObject?type=locus&id=36642)

Activity of SAC9

Both antibodies were used for immunoprecipitation with magnetic beads, and the resultant immunoprecipitated proteins were tested for the presumed activity towards PI(4,5)P_2 with the Malachite Green Assay. Preliminary results were encouraging and indicated that AtSAC9 immunoprecipitated with either antibody hydrolyzed PI(4,5)P_2. In repeated experiments, including negative controls with preimmune serum, however, negative controls had higher than anticipated phosphate release. Upon closer inspection, most of the phosphate release was non-

specific, as measured phosphate levels were almost identical regardless of substrate addition. I ascribe the differences in measured amounts of phosphate release from different immunoprecipitates partially to minute and unnoticeable variations in the extraction method, as well as to differences in SAC9 expression from plants depending on age, organ, and possibly other fluctuating environmental parameters. Similar conflicting results on SAC9 expression have been reported in the literature. Microarray and RT-PCR data suggested that AtSAC9 was expressed throughout the whole plant body with higher expression levels in the root (Zhong and Ye 2003; Schmid et al. 2005; Williams et al. 2005). Contrary to this, Gong et al. (2006) found AtSAC9 transcript levels to be highest in leaves and reduced in roots.

Gene expression studies performed by GenScript

GenScript was contracted to codon-optimize and completely synthesize the *SAC9* gene for improved expression in heterologous systems, to subsequently subclone the gene into an appropriate expression vector and perform expression studies with this new construct. Codon optimization was desirable for genes that originate from plants but are expressed in lower eukaryotes. The insertion of a TEV site for proteolytic cleavage of the C-terminal FLAG and 6xHis tag was also thought to be highly advantageous. Unfortunately, the company was not successful in synthesizing the gene. Thus, I decided instead to use their resources to conduct recombinant expression of SAC9 from both of our constructs. The original and the newly repaired vector pYES-DEST52+SAC9 were sent to GenScript for recombinant expression and purification. Fractions obtained from the nickel purification procedure and analyzed by SDS-PAGE showed nearly identical banding patterns between the two constructs. It was difficult to see if the cell lysate contained any bands around 140 kDa since the company did only include size markers below 94 kDa. This was surprising and disappointing since the company was informed that the

full length SAC9 protein was predicted to have a molecular weight of 180 kDa and that a prominent band of approximately 140 kDa was visible in some of my Ni-purified fractions (Figs. 4-4 and 4-5). Two proteins of slightly different size were recognized with the anti-His(C-term)-antibodies in Western blots in the final elute. Corresponding bands were excised from the SDS gel and both bands (40 and 95 kDa, respectively) were subjected to trypsin digestion and peptide fragments were identified with mass spectrometry. MS results confirmed that neither band was the target protein. These results led us to terminate the project with GenScript.

Two different expression constructs and one protein?

The similar banding pattern in SDS gels and Western blots observed in samples from both constructs expressed by GenScript, as well as my results, point to the possibility that the mutation in the original construct had no effect on the expression of recombinant SAC9. If that was the case, it would be very surprising, since one additional adenine at position 4022 in the sequence of the original construct was predicted to cause a frame shift followed by the insertion of two stop codons. Since I did not have sequence confirmation of the original construct and due to the problem with the detection of the 6xHis tag, I believed that the sequence for this tag was possibly incorrect, or that the tag was either not functional or accessible. Sequencing showed the 6xHis tag to be complete. A truncated protein around position 4022 would not contain the C-terminal V5 epitope and 6xHis tag. The truncation therefore would preclude it from being detected with either antibody. The fact that I detected induced SAC9 protein with the anti-V5 antibody but not the anti-His antibody was confusing. Possible mechanisms for the suppression of the first and subsequently the second stop codon to generate a 180 or a 155 kDa SAC9 protein include readthrough (McCaughan et al. 1995), alternative splicing (Szabo et al. 1994), or RNA editing (Sommer et al. 1991). In view of the reported splice variant of AtSAC9 at TAIR,

which is smaller protein but still with the N-terminus and the SAC domain intact, it seems likely that the original inducible vector might lead to the expression of the target protein.

Co-factors for activity

Some phosphoinositide phosphatases are metal-dependent. Rudge et al. (2004) demonstrated the absolute requirement for magnesium in the activation of the yeast phosphoinositide phosphatase Fig4. His-tagged recombinant Fig4 phosphatase activity was observed only when 1 mM magnesium was included in the assay mixture. It is conceivable, that SAC9 also needs a metal for activity, although the results from the Malachite Green Assay indicated that this requirement most likely is not absolute. However, I cannot exclude the possibility that metal ions would act as activity enhancers.

WW domain

Several authors have noted on the WW domain inserted in motif seven of the SAC domain in AtSAC9 (Zhong and Ye 2003; Williams et al. 2005; Gong et al. 2006). The WW domain, also known as the WWP or rsp5 domain, is a stretch of around 40 amino acids with two conserved tryptophans spaced 20-22 amino acids apart. It is thought of as an interaction module that binds specific proline-rich sequences and thus functions in a diverse set of signaling proteins. With only 40 amino acids, it is the smallest domain known (Ilsley et al. 2002). The precise function of this domain in SAC9 at such an interesting location begs the question of possible binding partners. It is tempting to speculate about the nature of this hypothetical binding and the downstream consequences. What if the putative binding partner conferred phosphatase activity? It is equally likely though that a binding partner would not contain any enzyme activity but rather specify subcellular location. A third possibility for the function of a binding partner might lie in the regulation of the phosphatase activity of SAC9 by either

competitive binding or potentially changing the confirmation of SAC9. One of the anti-SAC9-antibodies (anti-SAC9-AB_515) that we generated was raised against a synthetic peptide from the seventh motif of the SAC domain and included part of the WW motif. When used to immunoprecipitate SAC9 from wild-type extracts, this antibody routinely performed not as well as the other anti-SAC9-antibody (anti-SAC9-AB_940), which was raised against a peptide closer to the C-terminus. I contributed this to the fact that the epitope in anti-SAC9-AB_515 was too close to the active site, and antigen binding therefore was most likely negatively affected by impaired physical accessibility. It is conceivable though that with this antibody a possible binding partner was isolated and not SAC9, an interesting avenue which leads the way for new experiments.

SUMMARY

Results from several Malachite Green Assays for the quantification of inorganic phosphate release neither support nor refute the hypothesis that SAC9 is a phosphoinositide phosphatase. Phosphatase activity was detected in protein samples immunoprecipitated with specific anti-SAC9-antibodies. However, immunoprecipitation (IP) experiments led to the isolation of more than one polypeptide. It is conceivable that other co-isolated polypeptides caused the measured release of free inorganic phosphate. At this point, it is not known which of the polypeptides in the IP mixture caused the activity. Optimization strategies of protein extraction and IP techniques did also not lead to the isolation of only the target protein SAC9. Further IP experiments with other anti-SAC9-antibodies are therefore needed for clarification.

Although all reagents and glassware used for the Malachite Green Assays were phosphate-free, the minor amount of phosphate detected in reconstituted PI(4,5)P_2 might have skewed the data to some degree. To rule this out, a complimentary way of testing the enzyme

for phosphatase activity could be employed, namely the utilization of fluorescent phosphoinositide substrates in combination with thin-layer chromatography (Tayler and Dixon 2004). With this method, phosphoinositide reaction products are detected instead of the release of inorganic phosphate. This would not only confirm the enzyme activity but also assess phosphatase specificity more effectively.

REFERENCES

Berridge MJ (1984) Inositol trisphosphate and diacylglycerol as second messengers. Biochem J 220 (2):345-360

Berridge MJ (2009) Inositol trisphosphate and calcium signalling mechanisms. Biochim Biophys Acta 1793 (6):933-940

D'Angelo E, Crutchfield J, Vandiviere M (2001) Rapid, sensitive, microscale determination of phosphate in water and soil. J Environ Qual 30 (6):2206-2209

Despres B, Bouissonnie F, Wu HJ, Gomord V, Guilleminot J, Grellet F, Berger F, Delseny M, Devic M (2003) Three *SAC1*-like genes show overlapping patterns of expression in *Arabidopsis* but are remarkably silent during embryo development. Plant J 34 (3):293-306

Di Paolo G, De Camilli P (2006) Phosphoinositides in cell regulation and membrane dynamics. Nature 443 (7112):651-657

Erdman S, Lin L, Malczynski M, Snyder M (1998) Pheromone-regulated genes required for yeast mating differentiation. J Cell Biol 140 (3):461-483

Foti M, Audhya A, Emr SD (2001) Sac1 lipid phosphatase and Stt4 phosphatidylinositol 4-kinase regulate a pool of phosphatidylinositol 4-phosphate that functions in the control of the actin cytoskeleton and vacuole morphology. Mol Biol Cell 12 (8):2396-2411

Gong P, Wu G, Ort DR (2006) Slow dark deactivation of Arabidopsis chloroplast ATP synthase caused by a mutation in a nonplastidic SAC domain protein. Photosynth Res 88 (2):133-142

Guo S, Stolz LE, Lemrow SM, York JD (1999) *SAC1*-like domains of yeast *SAC1*, *INP52*, and *INP53* and of human synaptojanin encode polyphosphoinositide phosphatases. J Biol Chem 274 (19):12990-12995

Harris DM, Myrick TL, Rundle SJ (1999) The Arabidopsis homolog of yeast TAP42 and mammalian alpha4 binds to the catalytic subunit of protein phosphatase 2A and is induced by chilling. Plant Physiol 121 (2):609-617

Hughes WE (2001) The Sac phosphatase domain. Curr Biol 11 (7):R249

Hughes WE, Cooke FT, Parker PJ (2000a) Sac phosphatase domain proteins. Biochem J 350 Pt 2:337-352

Hughes WE, Woscholski R, Cooke FT, Patrick RS, Dove SK, McDonald NQ, Parker PJ (2000b) *SAC1* encodes a regulated lipid phosphoinositide phosphatase, defects in which can be suppressed by the homologous Inp52p and Inp53p phosphatases. J Biol Chem 275 (2):801-808

Ilsley JL, Sudol M, Winder SJ (2002) The WW domain: linking cell signalling to the membrane cytoskeleton. Cell Signal 14 (3):183-189

Maehama T, Taylor GS, Slama JT, Dixon JE (2000) A sensitive assay for phosphoinositide phosphatases. Anal Biochem 279 (2):248-250

Manford A, Xia T, Saxena AK, Stefan C, Hu F, Emr SD, Mao Y (2010) Crystal structure of the yeast Sac1: implications for its phosphoinositide phosphatase function. Embo J 29 (9):1489-1498

McCaughan KK, Brown CM, Dalphin ME, Berry MJ, Tate WP (1995) Translational termination efficiency in mammals is influenced by the base following the stop codon. Proc Natl Acad Sci USA 92 (12):5431-5435

McPherson PS, Garcia EP, Slepnev VI, David C, Zhang X, Grabs D, Sossin WS, Bauerfeind R, Nemoto Y, De Camilli P (1996) A presynaptic inositol-5-phosphatase. Nature 379 (6563):353-357

Minagawa T, Ijuin T, Mochizuki Y, Takenawa T (2001) Identification and characterization of a sac domain-containing phosphoinositide 5-phosphatase. J Biol Chem 276 (25):22011-22015

Munnik T, Nielsen E (2011) Green light for polyphosphoinositide signals in plants. Curr Opin Plant Biol 14 (5):489-497

Munnik T, Testerink C (2009) Plant phospholipid signaling: "in a nutshell". J Lipid Res 50 Suppl:S260-265

Nemoto Y, Kearns BG, Wenk MR, Chen H, Mori K, Alb JG, Jr., De Camilli P, Bankaitis VA (2000) Functional characterization of a mammalian Sac1 and mutants exhibiting substrate-specific defects in phosphoinositide phosphatase activity. J Biol Chem 275 (44):34293-34305

Novick P, Osmond BC, Botstein D (1989) Suppressors of yeast actin mutations. Genetics 121 (4):659-674

Odorizzi G, Babst M, Emr SD (2000) Phosphoinositide signaling and the regulation of membrane trafficking in yeast. Trends Biochem Sci 25 (5):229-235

Rudge SA, Anderson DM, Emr SD (2004) Vacuole size control: regulation of PtdIns(3,5)P_2 levels by the vacuole-associated Vac14-Fig4 complex, a PtdIns(3,5)P_2-specific phosphatase. Mol Biol Cell 15 (1):24-36

Schmid M, Davison TS, Henz SR, Pape UJ, Demar M, Vingron M, Scholkopf B, Weigel D, Lohmann JU (2005) A gene expression map of *Arabidopsis thaliana* development. Nat Genet 37 (5):501-506

Sommer B, Koehler M, Sprengel R, Seeburg PH (1991) RNA editing in brain controls a determinant of ion flow in glutamate-gated channels. Cell 67 (1):11-19

Srinivasan S, Seaman M, Nemoto Y, Daniell L, Suchy SF, Emr S, De Camilli P, Nussbaum R (1997) Disruption of three phosphatidylinositol-polyphosphate 5-phosphatase genes from *Saccharomyces cerevisiae* results in pleiotropic abnormalities of vacuole morphology, cell shape, and osmohomeostasis. Eur J Cell Biol 74 (4):350-360

Stefan CJ, Audhya A, Emr SD (2002) The yeast synaptojanin-like proteins control the cellular distribution of phosphatidylinositol (4,5)-bisphosphate. Mol Biol Cell 13 (2):542-557

Stolz LE, Huynh CV, Thorner J, York JD (1998a) Identification and characterization of an essential family of inositol polyphosphate 5-phosphatases (*INP51*, *INP52* and *INP53* gene products) in the yeast *Saccharomyces cerevisiae*. Genetics 148 (4):1715-1729

Stolz LE, Kuo WJ, Longchamps J, Sekhon MK, York JD (1998b) INP51, a yeast inositol polyphosphate 5-phosphatase required for phosphatidylinositol 4,5-bisphosphate homeostasis and whose absence confers a cold-resistant phenotype. J Biol Chem 273 (19):11852-11861

Szabo G, Katarova Z, Greenspan R (1994) Distinct protein forms are produced from alternatively spliced bicistronic glutamic acid decarboxylase mRNAs during development. Mol Cell Biol 14 (11):7535-7545

Takenawa T, Itoh T (2001) Phosphoinositides, key molecules for regulation of actin cytoskeletal organization and membrane traffic from the plasma membrane. Biochim Biophys Acta 1533 (3):190-206

Taylor GS, Dixon JE (2004) Assaying phosphoinositide phosphatases. Methods Mol Biol 284:217-227

Testerink C, Munnik T (2011) Molecular, cellular, and physiological responses to phosphatidic acid formation in plants. J Exp Bot 62 (7):2349-2361

Thole JM, Vermeer JE, Zhang Y, Gadella TW, Jr., Nielsen E (2008) *ROOT HAIR DEFECTIVE4* encodes a phosphatidylinositol-4-phosphate phosphatase required for proper root hair development in *Arabidopsis thaliana*. Plant Cell 20 (2):381-395

Williams ME, Torabinejad J, Cohick E, Parker K, Drake EJ, Thompson JE, Hortter M, DeWald DB (2005) Mutations in the Arabidopsis phosphoinositide phosphatase gene *SAC9* lead to overaccumulation of PtdIns(4,5)P_2 and constitutive expression of the stress-response pathway. Plant Physiol 138 (2):686-700

Yuan Y, Gao X, Guo N, Zhang H, Xie Z, Jin M, Li B, Yu L, Jing N (2007) rSac3, a novel Sac domain phosphoinositide phosphatase, promotes neurite outgrowth in PC12 cells. Cell Res 17 (11):919-932

Zhong R, Burk DH, Nairn CJ, Wood-Jones A, Morrison WH, 3rd, Ye ZH (2005) Mutation of SAC1, an Arabidopsis SAC domain phosphoinositide phosphatase, causes alterations in cell morphogenesis, cell wall synthesis, and actin organization. Plant Cell 17 (5):1449-1466

Zhong R, Ye ZH (2003) The SAC domain-containing protein gene family in Arabidopsis. Plant Physiol 132 (2):544-555

CHAPTER 5

CONCLUSIONS

Phospholipid signaling has been an area of intensive research in the last three decades reflective of its involvement in a multitude of diverse cellular processes in yeast, animal, and plant cells. Much progress has been made in mammalian systems fueled largely by medical implications of dysfunctional phospholipid signaling leading to devastating diseases, such as cancer. Plant phospholipid signaling on the other hand, has seen less attention. Much of the knowledge is only starting to emerge, leaving us with an incomplete understanding of how plants translate extracellular information into intracellular signaling molecules. Our comprehension of how plants interpret these signaling molecules and respond in a biologically relevant manner is equally patchy. This seems surprising in the light of fundamental cellular processes that are regulated in animals by phosphorylated derivatives of phosphoinositol.

Normal plant development, but also responses to changes in the environment, are dependent on signal transduction processes. Salinity and drought are major environmental stresses which adversely affect plant growth and productivity. New and more salt tolerant crop cultivars are needed to cope with progressive salinization of arable land. Genetic engineering applied to agricultural breeding techniques holds great promise and has already been successful in some herbicide and insect resistance. Such tactics are also being applied to counter salinity. However, a deeper understanding of how plants respond to salinity and other stress factors is required for further manipulation. Basic research in elucidating stress signal perception, transduction and response, is an imperative and the cornerstone for the development of stress tolerant crops. Particularly, characterizing the changes in phospholipid signaling and the specific

effects they mediate as plants mature and respond to environmental conditions is important and will lead to a better understanding of the nature of these physiological responses.

In my dissertation research, I studied phosphoinositide functions indirectly by phenotypic mutant analysis of *sac9* and functional characterization of the affected protein in *A. thaliana* with the hope that this research will contribute to the development of stress-resistant plants and ultimately increased crop yields.

In Chapter 2 of my dissertation, I used phenotypic mutant analysis to examine the cellular effects of *SAC9* gene disruption. In-depth ultrastructural investigations revealed unique cell wall aberrations in some cells of the root meristem that were hypothesized to contribute to the stuntedness of the root. Excess membrane material was associated with these abnormalities, an indication of unregulated membrane trafficking in *sac9* mutants.

The possibility that a defective cytoskeleton was involved in the generation of the above mentioned cell wall aberrations was investigated in Chapter 3 where I visualized microtubules in the developing root of *A. thaliana*. Quantitative analysis by Discrete Fourier Transform of confocal images led to the conclusion that the orientation of cortical microtubules was not different in elongating but in differentiated root cells. This might have implications for the mechanical strength of the mutant shoot. The analysis of cortical microtubule distribution in the meristematic area was complicated by resolution limits imposed by light microscopy techniques. The cell wall aberrations seen in this area with transmission electron microscopy might be caused in part by disorganized microtubules, but at this point I cannot prove this hypothesis. Immunolocalization experiments for the actin cytoskeleton did not reveal any gross morphological differences (Appendix B). However, this statement is only based on qualitative analysis of confocal images. Quantitative analysis with morphometric software might lead to a

more differentiated conclusion as seen for the analysis of microtubule arrays. Unfortunately, appropriate commercial software for computational pattern recognition was not available.

Phenotypic mutant analysis is a powerful tool to investigate gene function. However, it does not come without its drawbacks. One of the limitations in this study is the fact that the mutation in the *SAC9* gene is constitutive, and the visible effects of the mutation are building up over time. For example, wild-type and *sac9* seedlings are impossible to distinguish before day five post germination. This makes it difficult to decipher what the primary effect is and what possible downstream effects are. Compounding to this is the nature of the affected protein, i.e. SAC9 is not a structural protein but an enzyme involved in signaling. It is hardly surprising then that *sac9* mutants display a pleiotropic phenotype affecting the shoot and root but to different degrees and at different developmental stages. Because signal transduction pathways are intertwined and more resemble networks than top-to-bottom cascades, the effects seen in a plant with defects in a phospholipid-modifying enzyme are equally diverse. The redundancy and overlapping functions of many genes involved in signaling provides a certain buffer capacity to the system. This makes it very challenging to establish cause-and-effect-relationships.

As a complimentary approach, I analyzed the size and biochemical function of the putative phosphoinositide phosphatase SAC9 in Chapter 4. I showed that the soluble protein has an apparent molecular mass of 180 kDa, which is in agreement with its predicted mass. Functional assays revealed that a protein mixture immunoprecipitated with anti-SAC9-antibodies can hydrolyze PI(4,5)P_2 *in vitro*. Thus, SAC9 is most likely a phosphoinositide phosphatase and able to catalyze the hydrolysis of phosphate from its substrate, PI(4,5)P_2. However, a disclaimer to this statement is warranted based on data presented in Chapter 4 and Appendix C. Therefore, further experiments are strongly recommended.

In this dissertation I have presented molecular and biochemical data proposing the biochemical function of SAC9, a unique protein in *Arabidopsis thaliana*. Detailed morphological investigations of cellular defects in the mutant helped to further understand the downstream functions of PI(4,5)P_2, the *in vivo* lipid substrate of SAC9. These functions include involvement in membrane dynamics, cell wall deposition, and possibly the arrangement of cortical microtubules in differentiated root cells. More functions are envisioned but are beyond the scope of this dissertation.

APPENDICES

APPENDIX A

PERMISSION TO REPRINT CHAPTER 2

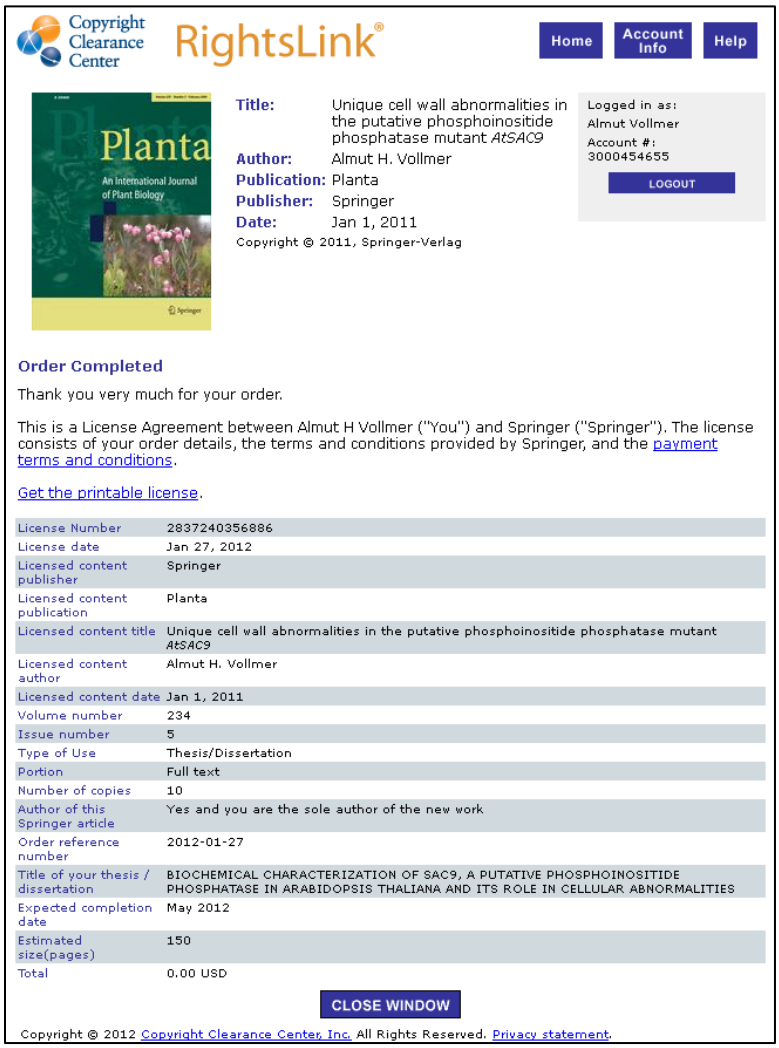

Copyright Clearance Center RightsLink®

Home | Account Info | Help

Title: Unique cell wall abnormalities in the putative phosphoinositide phosphatase mutant *AtSAC9*
Author: Almut H. Vollmer
Publication: Planta
Publisher: Springer
Date: Jan 1, 2011
Copyright © 2011, Springer-Verlag

Logged in as:
Almut Vollmer
Account #:
3000454655
LOGOUT

Order Completed

Thank you very much for your order.

This is a License Agreement between Almut H Vollmer ("You") and Springer ("Springer"). The license consists of your order details, the terms and conditions provided by Springer, and the payment terms and conditions.

Get the printable license.

License Number	2837240356886
License date	Jan 27, 2012
Licensed content publisher	Springer
Licensed content publication	Planta
Licensed content title	Unique cell wall abnormalities in the putative phosphoinositide phosphatase mutant *AtSAC9*
Licensed content author	Almut H. Vollmer
Licensed content date	Jan 1, 2011
Volume number	234
Issue number	5
Type of Use	Thesis/Dissertation
Portion	Full text
Number of copies	10
Author of this Springer article	Yes and you are the sole author of the new work
Order reference number	2012-01-27
Title of your thesis / dissertation	BIOCHEMICAL CHARACTERIZATION OF SAC9, A PUTATIVE PHOSPHOINOSITIDE PHOSPHATASE IN ARABIDOPSIS THALIANA AND ITS ROLE IN CELLULAR ABNORMALITIES
Expected completion date	May 2012
Estimated size(pages)	150
Total	0.00 USD

CLOSE WINDOW

Copyright © 2012 Copyright Clearance Center, Inc. All Rights Reserved. Privacy statement.

file:///U:/Manuscripts/AppDispatchServlet.htm

Terms and Conditions

The following are Copyright Clearance Center's terms and conditions for use of the RightsLink service. Each publisher has a set of terms and conditions as well, available during the order process from the Order Confirmation page.

THIS DIGITAL LICENSING AND REPRINT SERVICE IS ADMINISTERED BY COPYRIGHT CLEARANCE CENTER, INC. ("CCC" or "Us").

General Payment Terms: You may pay by credit card or through an account with us payable at the end of the month. If you and we agree that you may establish a standing account with CCC, then the following terms apply:
Remit Payment to: Copyright Clearance Center, Inc., P.O. Box 9135, Boston, MA 02205-9135.

Payments Due: Invoices are payable upon their delivery to you (or upon our notice to you that they are available to you for downloading). After 30 days, outstanding amounts will be subject to a service charge of 1-1/2% per month or, if less, the maximum rate allowed by applicable law.
Please note that, while you may exercise the rights licensed immediately, the license will be automatically void (as if it never existed) in the event that we do not receive payment for the license on a timely basis. Also please note that you are responsible for any transactions that use your user name and password; please protect the secrecy of those pieces of information.

THE FOLLOWING TERMS AND CONDITIONS APPLY TO ALL TRANSACTIONS THAT YOU ENTER INTO THROUGH THIS DIGITAL LICENSING AND REPRINT SERVICE, REGARDLESS OF THE WEBSITE FROM WHICH YOU ENTER IT. BECAUSE YOU ARE IN THE PROCESS OF OPENING A NEW ACCOUNT WITH US, YOU MUST INDICATE YOUR CONSENT TO THESE TERMS AND CONDITIONS AT THIS TIME. IN THE FUTURE, YOU MAY ALSO SEE THESE TERMS AND CONDITIONS AT ANY TIME OR IN CONNECTION WITH ANY TRANSACTION AT *myaccount.copyright.com*.

ANY LICENSE CREATED IS SUBJECT TO THE TERMS AND CONDITIONS THAT FOLLOW AS WELL AS ANY TERMS AND CONDITIONS ESTABLISHED BY THE RIGHTSHOLDER ON WHOSE WEBSITE YOU FIND THE MATERIAL YOU SEEK TO LICENSE, AND USE OF ANY MATERIALS CONSTITUTES ACCEPTANCE OF ALL SUCH TERMS AND CONDITIONS.

Terms and Conditions That Apply to All Transactions:

1. This digital licensing and reprint service enables you, the "User", to obtain licenses to make certain uses of the online content of many copyright holders (each a "Rightsholder"). Licenses granted through this service are granted by the Rightsholder in the content for which you are seeking a license and from whose Website (containing the content) you reached this service. This service is administered by Copyright Clearance Center, Inc. ("CCC") and your use of the content is governed by these terms and conditions, BUT your use will ALSO be governed by the terms and conditions which are set individually by the Rightsholder whose material you seek to use; the Rightsholder's terms and conditions will be made available to you in the course of the licensing process for each transaction. You, as User, will be deemed to have accepted and agreed to all of those terms and conditions, as well as these terms and conditions, if you use the Rightsholder's copyrighted material in any fashion. CCC reserves the right to send electronic mail to you for the purpose of informing you of changes or additions to this service.

2. User hereby acknowledges and agrees that User is responsible for any transaction entered into through this digital licensing and reprint service and identified with User's user name and password (if on account) or User's credit card information (if by credit card). It is User's responsibility to maintain the secrecy of such information, to notify CCC immediately upon learning of any transaction entered into through this service that was done so without User's authorization, and to use the appropriate automated services within this digital licensing and reprint service to alter passwords and standing payment information whenever necessary to preserve secrecy. User represents and warrants that User is at least 18 years old if User is a person (as opposed to a company or other organization); that in any event User is legally capable in User's place of residence or business of entering into the agreement created by these terms and conditions and Rightsholder's terms and conditions; and that the individual opening an account or seeking transactions under this digital licensing and reprint service on behalf of any User that is a business, corporate entity or other organization is duly authorized by User to do so.

3. Use of User-related information collected by this licensing service is governed by CCC's privacy policy. CCC's privacy policy is accessible through CCC's website www.copyright.com and from numerous locations throughout the webpages comprising this licensing service.

4. As among User, CCC and the Rightsholder, all materials available for licensing, as well as all rights therein, including copyright rights, remain the sole and exclusive property of the Rightsholder. All trademarks not belonging to the Rightsholder, as well as all software and other elements that you encounter in the course of using this digital licensing and reprint service, as well as all intellectual property rights therein, remain the sole and exclusive property of CCC and are not licensed to User in any way. While User may exercise the rights licensed immediately upon issuance of the license at the end of the licensing process for the transaction, the license is automatically revoked, and is null and void as if it had never been issued, if complete payment for the license is not received on a timely basis either from User directly or through a payment agent, such as a credit card company. All rights not expressly granted are reserved; any license granted may be further limited (on a Work-by-Work basis) as set forth in any restrictions included in the Rightsholder's terms and conditions applicable to the transaction (which will be provided at the end of the licensing process, at User's option, on paper or electronically).

5. User hereby indemnifies and agrees to defend CCC and its employees, agents, representatives, officers and directors, against all claims, liability, damages, costs and expenses, including legal fees and expenses, arising out of any use of licensed material beyond the scope of the rights granted, or any use of any licensed material which has been altered in any way by User, including claims for defamation or infringement of or damage to rights of copyright, publicity, privacy or other tangible or intangible property.

6. **LIMITATION OF LIABILITY OF CCC.** UNDER NO CIRCUMSTANCES WILL CCC BE LIABLE FOR ANY DIRECT, INDIRECT, CONSEQUENTIAL OR INCIDENTAL DAMAGES (INCLUDING WITHOUT LIMITATION DAMAGES FOR LOSS OF BUSINESS PROFITS OR INFORMATION, OR FOR BUSINESS INTERRUPTION) ARISING OUT OF (i) THE USE OR INABILITY TO USE ANY LICENSED MATERIAL OR (ii) THE INABILITY TO OBTAIN ADDITIONAL RIGHTS TO LICENSED MATERIALS, EVEN IF CCC HAS BEEN ADVISED OF THE POSSIBILITY OF SUCH DAMAGES. In any event, the total liability of CCC (including its employees, agents, representatives, officers and directors) shall not exceed the total amount actually paid by User for the applicable license. User assumes full liability for the actions and omissions of its principals, employees, agents, affiliates, successors and assigns.

7. **NO WARRANTIES FROM CCC.** CCC DISCLAIMS ALL WARRANTIES RELATING TO THE COPYRIGHTED MATERIALS OF RIGHTSHOLDER, EITHER EXPRESS OR IMPLIED, INCLUDING WITHOUT LIMITATION IMPLIED WARRANTIES OF MERCHANTABILITY OR FITNESS FOR A PARTICULAR PURPOSE. IN ADDITION, THIS LICENSING SERVICE AND ALL SOFTWARE USED IN CONNECTION THEREWITH ARE DISTRIBUTED ON AN "AS IS" BASIS WITHOUT WARRANTIES OF ANY KIND, EITHER EXPRESS OR IMPLIED, INCLUDING, WITHOUT LIMITATION, WARRANTIES OF TITLE OR IMPLIED WARRANTIES OF MERCHANTABILITY OR FITNESS FOR A PARTICULAR PURPOSE. USER HEREBY ACKNOWLEDGES THAT USE OF THE SERVICE IS AT USER'S SOLE RISK.

8. (a) The term "License Grant" is used in these terms and conditions to describe (i) the entire set of details (including User's name as licensee, the nature of the use for which User seeks a license, and the price of the license), as well as (ii) the Rightsholder's terms and conditions applicable to that licensing transaction and governing the particular use User may make of that copyrighted material, and (iii) CCC's general terms and conditions relating to billing and payment that are applicable to ALL transactions. All elements of the License Grant are printed out or referred to in the license document that is delivered to User at the conclusion of each transaction under this digital licensing and reprint service, and are generally available within the service's Website at any time.(b) Any failure by User to pay any amount when due, or any use by User of any licensed material beyond the scope of the License Grant, shall be a material breach of the License Grant. Any breach not cured within ten (10) days of notice thereof shall result in immediate termination of such license without further notice. Invoices are due and payable upon their delivery to User (or upon CCC's notice to User that they are available to User for downloading from the Internet); amounts overdue will be subject to a service charge of 1-1/2% per month or, if less, the maximum interest rate allowed by applicable law in User's place of business, such service charge to begin running 30 days after delivery of, or notice of availability of, invoice.

9. CCC hereby objects to any terms contained in any writing prepared by User or its principals, employees, agents or affiliates and purporting to govern or otherwise relate to any licensing transaction, which terms are in any way inconsistent with any of these terms or the Rightsholder's standard terms or with any standard operating procedures of Rightsholder or CCC, whether such writing is prepared prior to, simultaneously with or subsequent to the License Grant, and whether such writing appears on any paper or electronic version of the License Grant or in a separate paper or electronic instrument, unless such writing is countersigned by CCC.

10. User may terminate its account at any time by sending e-mail to: customercare@copyright.com . Upon termination, User will receive a confirmation via e-mail that the request was received, and access to the licensing service from User's account will be suspended within one business day. User is responsible for all charges incurred up to the time the account is deactivated.

11. Unless the Rightsholder's own terms and conditions for the License Grant designate different terms for governing law, venue and jurisdiction and those terms and conditions are determined by a competent court to apply to a particular dispute, (a) the License Grant shall be governed by and construed under the law of the State of New York, USA, without regard to the principles thereof of conflicts of law, (b) any case, controversy, suit, action, or proceeding arising out of, in connection with, or related to the License Grant shall be brought, at CCC's sole discretion, in any federal or state court located in the County of New York, State of New York, USA, or in any U.S. federal or state court whose geographical jurisdiction covers the principal place of business of the Rightsholder, and (c) the parties expressly submit to the personal jurisdiction and venue of each such U.S. federal or state court.

12. User acknowledges and agrees that CCC may alter these terms and conditions in any fashion and at any time, effective immediately, provided that CCC posts notice of any material alteration hereof to the location at which User's monthly invoice is made available by CCC on the Internet and any such material alteration will be effective on the date set forth in the notice (and which effective date will be at least 30 days following CCC's first posting thereof). User also acknowledges and agrees that CCC may, on notice to User at the time of invoicing or at the time of any re-invoicing of a past-due amount, assign accounts and/or amounts due either to the applicable Rightsholder or to a financial institution; and that CCC may at any time assign all its rights, duties and responsibilities hereunder or under any License Grant to any other person who shall take responsibility for this licensing facility. Finally, User acknowledges and agrees that CCC may, in its sole discretion, terminate or suspend User's access to all or part of the licensing service for any reason, including without limitation breach of this Agreement or persistent failure to pay license fees on a timely basis.

https://s100.copyright.com/help/customeradminhelp/Payment_Terms_&_Conditions.htm

APPENDIX B

THE ACTIN CYTOSKELETON IN THE DEVELOPING ROOT OF ARABIDOPSIS THALIANA

MATERIAL AND METHODS

Arabidopsis thaliana seedlings (wild type, WT, and *sac9*) were grown on Phytagel-solidified ½ MS plates as described in Chapter 3. Seven-day-old seedlings were used for immunolocalization experiments of plant actin. Whole seedlings were in situ fixed and immunostained for plant actin according to Sugimoto el al. (2000) with slight modifications. Slides with stained and mounted root tips were examined under the confocal microscope at the Fluorescence Microscopy Facility, University of Utah, Salt Lake City, UT. Confocal images were taken with the same settings as outlined in Chapter 3, Material and Methods, Microscopy acquisition.

RESULTS AND CONCLUSIONS

Immunolocalization experiments with anti-plant-actin-antibodies were successful and marked globular (G) and fibrillar (F) actin in both genotypes of *A. thaliana* roots. Examples of immunolocalized actin in different areas of wild-type and *sac9* roots are given in Figure B-1. Actin localization was difficult to visualize in the meristematic zone due to the very small cell size (Fig. B-1, zones Ia, Ib). However, a gradual change along the growth axis was observed from uniform, dense, and mostly globular cytoplasmic actin, with a few short strands of fibrillar actin in the meristematic area, to mostly fibrillar actin in the periphery of elongating cells (Fig. B-1, zones IIb, III).

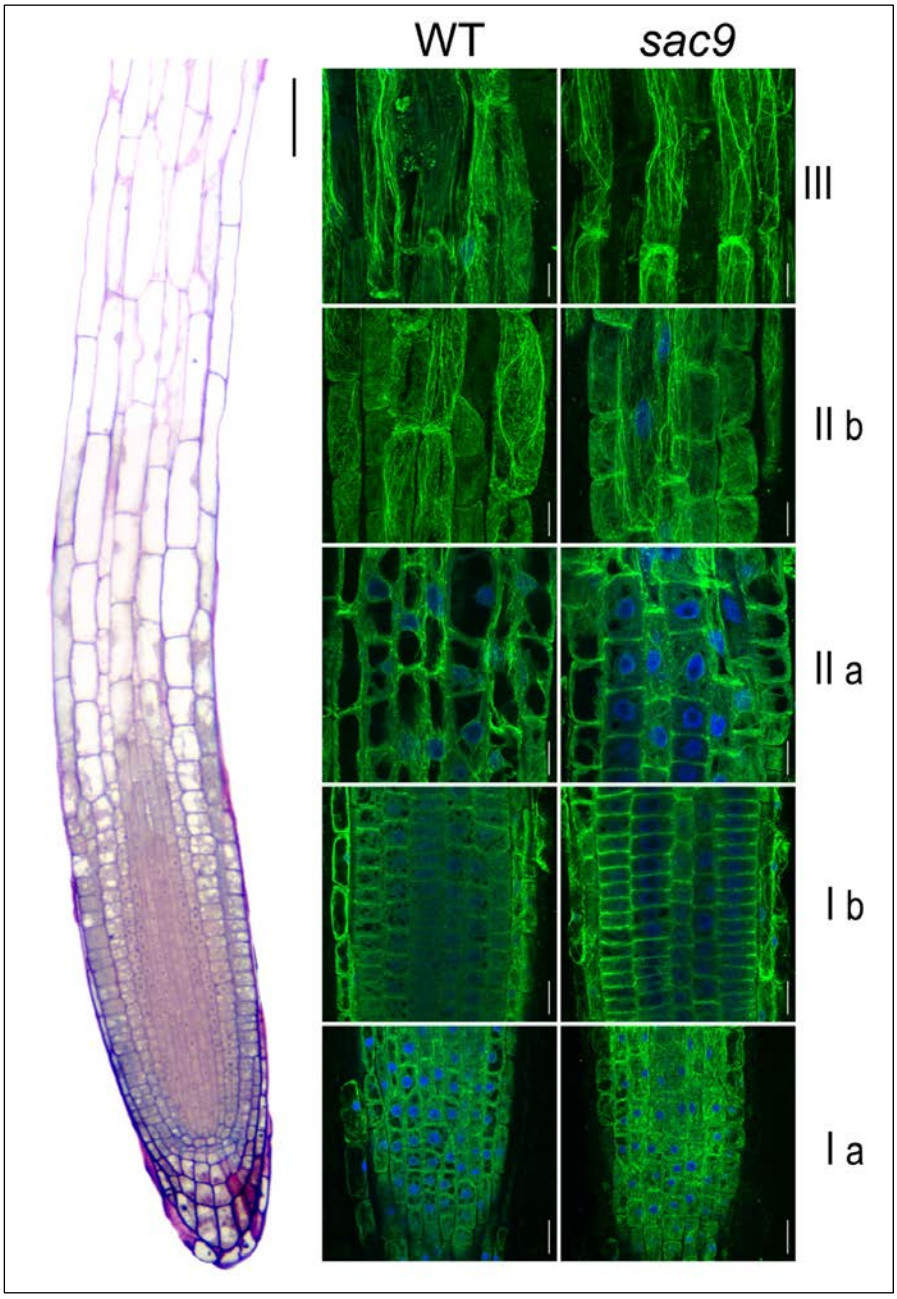

Fig. B-1 Immunolocalization of actin in the developing root of *Arabidopsis thaliana*. Cell differentiation patterns along the growth axis are exemplified with the longitudinal section of a resin-embedded wild-type (WT) root on the left side of the panel. In confocal images, actin was stained with anti-actin-antibodies (green), and nuclei were stained with DAPI (blue). Three different growth zones are presentedS: **Ia**, root cap cells and peripheral epidermis cells from the meristem; **Ib**, cytoplasmic epidermis cells from the meristem; **IIa** cytoplasmic epidermis cells from the zone of rapid cell elongation; **IIb** peripheral epidermis cells from the zone of rapid cell elongation; **III** peripheral epidermis cells from the zone of slow cell elongation. The position of cells from confocal images corresponds roughly with the position of cells in the resin-embedded root. Bar for resin-embedded root, 50 μm; bar for confocal images 20 μm

Visual inspection did not reveal any gross differences in the distribution pattern of actin between WT and *sac9*. However, to come to a significant conclusion, quantitative analysis of the data needed to be performed. This was initiated at the University of Utah, but the tested software did not lead to satisfactory results. This was mainly due to poor computational pattern recognition. It became clear that custom-written software was the key to actin quantification and analysis.

REFERENCES

Sugimoto K, Williamson RE, Wasteneys GO (2000) New techniques enable comparative analysis of microtubule orientation, wall texture, and growth rate in intact roots of Arabidopsis. Plant Physiol 124 (4):1493-1506

APPENDIX C

ADDITIONAL RESULTS FOR CHAPTER 4: MALACHITE GREEN ASSAYS

The Malachite Green Assay (MGA) was repeated with additional controls and performed in triplicates following manufacturer's recommendations.

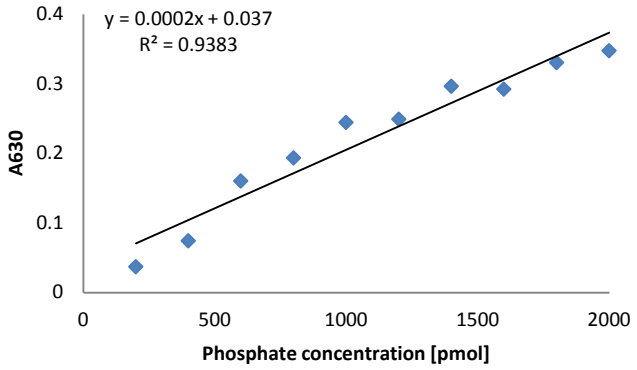

Fig. C-1 Phosphate standard curve. The Malachite Green Assay covered a phosphate range of 200-2000 pmol. The linear regression formula y=0.00002+0.037 was used to calculate the released phosphate amounts from tested samples

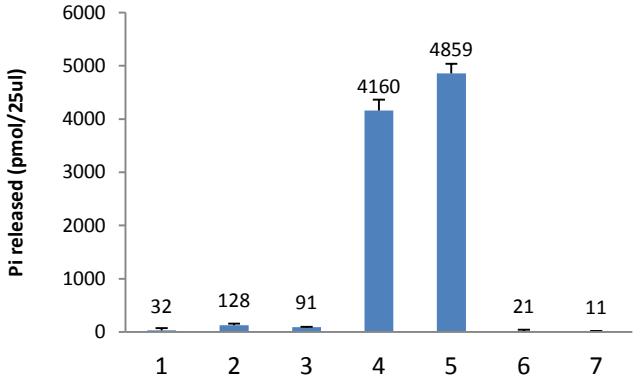

Fig. C-2 Malachite Green Assay results: calculated Pi release. **Sample 1**: Buffer only, **Sample 2**: Buffer + lipids, **Sample 3**: PIP_2 reconstituted in dH_20, **Sample 4**: WT extract 11 in Buffer only, **Sample 5**: WT extract 11 in Buffer + lipids, **Sample 6**: dH_20, **Sample 7**: NEM in dH_20. All samples were run in triplicates. Bars indicate SD

Table C-1 Raw data for Figure C-2. Absorbance (A) readings at 630 nm and calculated release of inorganic phosphate (Pi) from additional Malachite Green Assay

#	Sample	A630 Rep 1	A630 Rep 2	A630 mean	A630 blanked	Pi[*2] blanked	Pi[*3] x1.6	Pi[*4] x2	Pi Mean	Pi Stdev
1	Buffer	0.052	0.047	0.050	0.005	25	40	80	32	42
2	Buffer	0.046	0.046	0.046	0.001	5	8	16		
3	Buffer	0.045	0.045	0.045	0.000	0	0	0		
4	Buffer+lipids	0.059	0.051	0.055	0.010	50	80	160	128	28
5	Buffer+lipids	0.056	0.048	0.052	0.007	35	56	112		
6	Buffer+lipids	0.051	0.053	0.052	0.007	35	56	112		
7	PIP_2	0.051	0.051	0.051	0.006	30	48	96	91	9
8	PIP_2	0.051	0.051	0.051	0.006	30	48	96		
9	PIP_2	0.049	0.050	0.050	0.005	25	40	80		
10	WT11[*1] in Buffer	0.306	0.331	0.319	0.274	1370	2192	4384	4160	204
11	WT11 in Buffer	0.285	0.303	0.294	0.249	1245	1992	3984		
12	WT11 in Buffer	0.314	0.291	0.302	0.257	1285	2056	4112		
13	WT11 in Buffer+lipids	0.344	0.333	0.339	0.294	1470	2352	4704	4859	180
14	WT11 in Buffer+lipids	0.364	0.359	0.361	0.316	1580	2528	5056		
15	WT11 in Buffer+lipids	0.348	0.343	0.346	0.301	1505	2408	4816		
16	dH_20	0.046	0.046	0.046	0.001	5	8	16	21	24
17	dH_20	0.045	0.046	0.045	0.000	0	0	0		
18	dH_20	0.046	0.050	0.048	0.003	15	24	48		
19	NEM in dH_20	0.046	0.046	0.046	0.001	5	8	16	11	9
20	NEM in dH_20	0.045	0.046	0.046	0.001	5	8	16		
21	NEM in dH_20	0.044	0.045	0.045	0.000	0	0	0		

[*1] WT11, WT extract number 11
[*2] Pi blanked, calculated Pi amount based on Pi-standard curve
[*3] Pi x 1.6, calculated Pi amount multiplied by 1.6 due to dilution with NEM as a stopping reagent
[*4] Pi x 2, calculated Pi amount multiplied by 2 due to dilution factor of 2

Table C-2 Raw data for Figures 4-12 and 4-13: Day 1. Absorbance (A) readings at 630 nm and calculated release of inorganic phosphate (Pi) from samples run on Day 1

No	Name	A630 Rep1	A630 Rep2	A630 mean	A630 blanked	Pi blanked	Pi x 1.6	Pi x 2	Net release
1	Lipids in buffer	0.052	n/a	n/a	-0.002	0	0	n/a	-
2	WT extract in buffer	0.377	n/a	n/a	0.323	2368	3789	n/a	-
11	WT extract in buffer + lipids	0.429	n/a	n/a	0.375	2927	4683	n/a	895
3	IP_SAC9-515_L	0.156	n/a	n/a	0.102	626	1001	n/a	-
7	IP_SAC9-515_L + lipids	0.205	n/a	n/a	0.151	923	1477	n/a	476
4	IP_SAC9-515_H	0.177	n/a	n/a	0.123	747	1195	n/a	-
8	IP_SAC9-515_H + lipids	0.220	n/a	n/a	0.166	1024	1639	n/a	444
5	IP_SAC9-940_L	0.261	n/a	n/a	0.207	1325	2120	n/a	-
9	IP_SAC9-940_L + lipids	0.378	n/a	n/a	0.324	2378	3805	n/a	1685
6	IP_SAC9-940_H	0.275	n/a	n/a	0.221	1436	2298	n/a	-
10	IP_SAC9-940_H + lipids	0.311	n/a	n/a	0.257	1740	2784	n/a	486

Table C-3 Raw data for Figures 4-12 and 4-13: Day 2. Absorbance (A) readings at 630 nm and calculated release of inorganic phosphate (Pi) from samples run on Day 2

No	Name	A630 Rep1	A630 Rep2	A630 mean	A630 blanked	Pi blanked	Pi x 1.6	Pi x 2	Net release
1	Lipids in buffer	0.051	0.049	0.050	0.003	200	320	639	-
2	WT extract in buffer	0.258	0.267	0.263	0.216	1189	1902	3804	-
11	WT extract in buffer + lipids	0.299	0.302	0.301	0.254	1468	2348	4696	892
3	IP_SAC9-515_L	0.096	0.099	0.098	0.051	337	539	1078	-
7	IP_SAC9-515_L + lipids	0.119	0.122	0.121	0.074	421	673	1346	268
4	IP_SAC9-515_H	0.133	0.136	0.135	0.088	477	763	1527	-
8	IP_SAC9-515_H + lipids	0.134	0.138	0.136	0.089	483	774	1547	20
5	IP_SAC9-940_L	0.172	0.173	0.173	0.126	652	1043	2086	-
9	IP_SAC9-940_L + lipids	0.183	0.184	0.184	0.137	708	1133	2266	180
6	IP_SAC9-940_H	0.161	0.164	0.163	0.116	603	965	1929	-
10	IP_SAC9-940_H + lipids	0.194	0.196	0.195	0.148	770	1232	2463	534

Table C-4 Raw data for Figures 4-12 and 4-13: Day 5. Absorbance (A) readings at 630 nm and calculated release of inorganic phosphate (Pi) from samples run on Day 5

No	Name	A630 Rep1	A630 Rep2	A630 mean	A630 blanked	Pi blanked	Pi x 1.6	Pi x 2	Net release
1	Lipids in buffer	0.053	0.052	0.053	0.008	175	280	560	-
2	WT extract in buffer	0.221	0.184	0.203	0.158	1051	1682	3365	-
11	WT extract in buffer + lipids	0.254	0.201	0.228	0.183	1244	1990	3981	616
3	IP_SAC9-515_L	0.111	0.111	0.111	0.066	460	736	1472	-
7	IP_SAC9-515_L + lipids	0.138	0.136	0.137	0.092	610	976	1952	480
4	IP_SAC9-515_H	0.127	0.113	0.120	0.075	510	816	1633	-
8	IP_SAC9-515_H + lipids	0.147	0.141	0.144	0.099	653	1044	2089	456
5	IP_SAC9-940_L	0.212	0.199	0.206	0.161	1074	1718	3436	-
9	IP_SAC9-940_L + lipids	0.222	0.19	0.206	0.161	1078	1724	3448	12
6	IP_SAC9-940_H	0.196	0.196	0.196	0.151	1004	1606	3211	-
10	IP_SAC9-940_H + lipids	0.216	0.198	0.207	0.162	1085	1736	3472	261

Table C-5 Raw data for Figures 4-12 and 4-13: Days 1-5. Released inorganic phosphate (Pi) in pmol/25ul from the same samples obtained with the Malachite Green Assay in three independent runs (Day 1, 2, and 5)

No	Name	Run 1 (Day 1)	Run 2 (Day 2)	Run 3 (Day 5)	Mean	SD	Net release
1	Lipid in buffer	0	639	560	400	349	-
2	WT extract in buffer	3789	3804	3365	3652	249	-
3	WT extract in buffer + lipids	4683	4696	3981	4454	409	801
4	IP_ SAC9-515_L	1001	1078	1472	1184	253	-
5	IP_SAC9-515_L + lipid	1477	1346	1952	1592	319	408
6	IP_SAC9-515_H	1195	1527	1633	1452	228	-
7	IP_SAC9-515_H + lipid	1639	1547	2089	1758	290	307
8	IP_SAC9-940_L	2120	2086	3436	2547	770	-
9	IP_SAC9-940_L + lipid	3805	2266	3448	3173	806	626
10	IP_SAC9-940_H	2298	1929	3211	2479	660	-
11	IP_SAC9-940_H + lipid	2784	2463	3472	2907	516	428

Table C-6 Raw data for Figures 4-14 and 4-15: pH 5. Absorbance (A) readings at 630 nm and calculated release of inorganic phosphate (Pi) from samples immunoprecipitated from WT extracts and further separated with a 30-kDa-filter. The Malachite Green Assay was performed under slightly acidic conditions (pH 5)

No	Name	A630 Rep1	A630 Rep2	A630 mean	A630 blanked	Pi blanked	Pi x 1.6	Pi x 2	Pi net
1	Lipids in buffer	0.050	0.054	0.052	0.006	156	249	499	-
2	WT extract in buffer	0.353	0.357	0.355	0.309	2047	3275	6550	-
3	WT extract in buffer + lipids	0.392	0.399	0.396	0.350	2397	3835	7670	1120
4	IP-SAC9-30kDa - lipids	0.065	0.063	0.064	0.018	206	330	661	-
7	IP-SAC9-30kDa + lipids	0.079	0.080	0.080	0.034	275	439	879	218
5	IP-SAC9+30kDa - lipids	0.092	0.078	0.085	0.039	300	479	959	-
8	IP-SAC9+30kDa + lipids	0.104	0.102	0.103	0.057	384	615	1230	271
6	IP-prebleed-30kDa - lipids	0.100	0.114	0.107	0.061	404	646	1292	-
9	IP-prebleed-30kDa + lipids	0.113	0.107	0.110	0.064	419	670	1339	47

Table C-7 Raw data for Figures 4-14 and 4-15: pH 7. Absorbance (A) readings at 630 nm and calculated release of inorganic phosphate (Pi) from samples immunoprecipitated from WT extracts and further separated with a 30-kDa-filter. The Malachite Green Assay was performed under neutral conditions (pH 7)

No	Name	A630 Rep1	A630 Rep2	A630 mean	A630 blanked	Pi blanked	Pi x 1.6	Pi x 2	Pi net
1	Lipids in buffer	0.050	0.050	0.050	0.006	94	150	300	-
2	WT extract in buffer	0.355	0.349	0.352	0.308	1615	2584	5168	-
3	WT extract in buffer + lipids	0.418	0.408	0.413	0.369	1908	3054	6107	939
4	IP-SAC9-30kDa - lipids	0.058	0.059	0.059	0.015	138	221	442	-
7	IP-SAC9-30kDa + lipids	0.072	0.073	0.073	0.029	211	338	675	233
5	IP-SAC9+30kDa - lipids	0.087	0.082	0.085	0.041	273	437	875	-
8	IP-SAC9+30kDa + lipids	0.096	0.094	0.095	0.051	328	524	1049	174
6	IP-prebleed-30kDa - lipids	0.114	0.085	0.100	0.056	351	561	1123	-
9	IP-prebleed-30kDa + lipids	0.112	0.107	0.110	0.066	402	644	1288	165

APPENDIX D

ADDITIONAL RESULTS FOR CHAPTER 4: RECOMBINANT EXPRESSION REPORT FROM GENSCRIPT

GenScript
The Biology CRO

Your Innovation Partner in Drug Discovery!

Order ID: 129306-1 **11/9/2011**

Report: Scale-up expression and purification for yeast

Objective: 129306-1 protein scale-up expression and purification

A:

Description:

Strain	INVSc1, pYES-DEST52+SAC9-76F
Culture medium	SC-U medium
Culture medium volume	500mL
Induction time	48h
Breaking buffer	50 mM Tris-Hcl, pH 8.0;1 mM PMSF
Breaking method	Using acid-washed glass beads

Procedure and figures:

1. Scale-up expression and purification

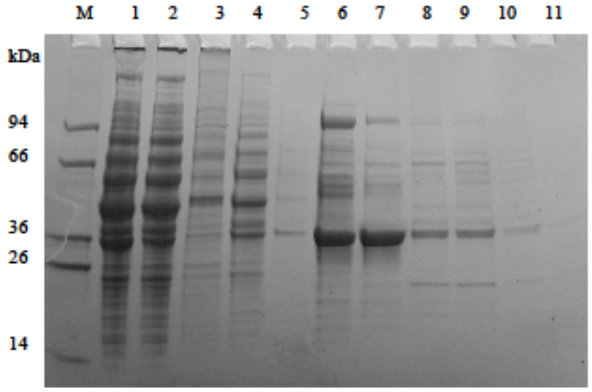

Fig.1 SAC9 protein was purified with Ni-NTA column; fractions were analyzed by SDS-PAGE followed by Coomassie Brilliant Blue staining

Lane M: MW marker

Lane 1: Supernatant after cell lysate centrifugation

Lane 2: Flow through

Lane 3: Pellet after cell lysate centrifugation

Lane 4-5: Washed with 50mM Tris-HCl buffer (pH 8.0)

Lane 6-7: Eluted with 20mM imidazole,150mM NaCl, 50mM Tris-HCl buffer (pH 8.0)

Lane 8-11: Eluted with 250mM imidazole,150mM NaCl, 50mM Tris-HCl buffer (pH 8.0)

120 Centennial Ave., Piscataway, NJ 08854, USA
Tel. 1-732-885-9188 Fax. 1-732-210-0262 Email. info@genscript.com Web. www.genscript.com

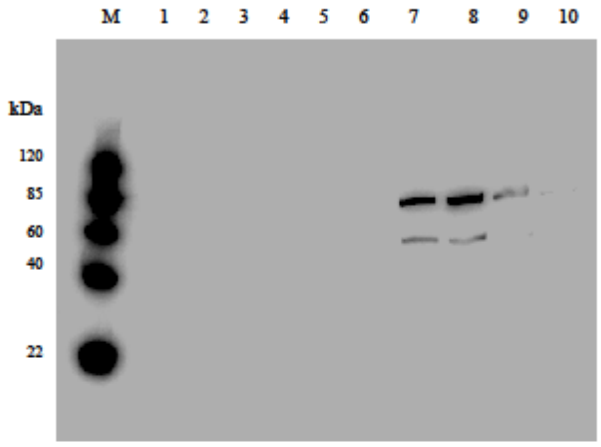

Fig.2 Western Blot analysis of SAC9 protein using anti-His AB

Lane M: Easy western marker

Lane 1: Supernatant after cell lysate centrifugation

Lane 2: Flow through

Lane 3: Pellet after cell lysate centrifugation

Lane 4: Washed with 50mM Tris-HCl buffer (pH 8.0)

Lane 5-6: Eluted with 20mM imidazole,150mM NaCl, 50mM Tris-HCl buffer (pH 8.0)

Lane 7-10: Eluted with 250mM imidazole,150mM NaCl, 50mM Tris-HCl buffer (pH 8.0)

B:

Description:

Strain	INVSc1, pYES-DEST52+SAC9
Culture medium	SC-U medium
Culture medium volume	500mL
Induction time	48h
Breaking buffer	50 mM Tris-Hcl, pH 8.0;1 mM PMSF
Breaking method	Using acid-washed glass beads

Procedure and figures:

1. Scale-up expression and purification

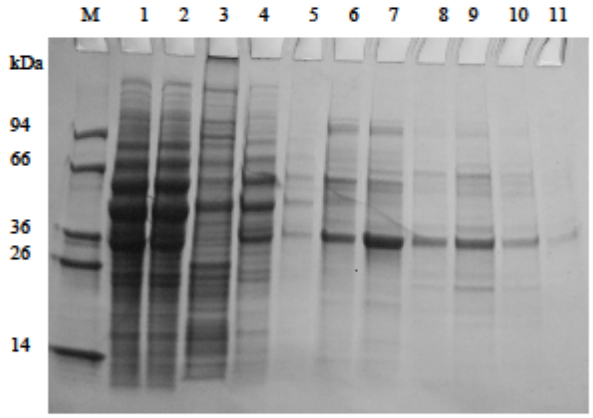

Fig.3 SAC9 protein was purified with Ni-NTA column; fractions were analyzed by SDS-PAGE followed by Coomassie Brilliant Blue staining

Lane M: MW marker

Lane 1: Supernatant after cell lysate centrifugation

Lane 2: Flow through

Lane 3: Pellet after cell lysate centrifugation

Lane 4-5: Washed with 50mM Tris-HCl buffer (pH 8.0)

Lane 6-7: Eluted with 20mM imidazole,150mM NaCl, 50mM Tris-HCl buffer (pH 8.0)

Lane 8-11: Eluted with 250mM imidazole,150mM NaCl, 50mM Tris-HCl buffer (pH 8.0)

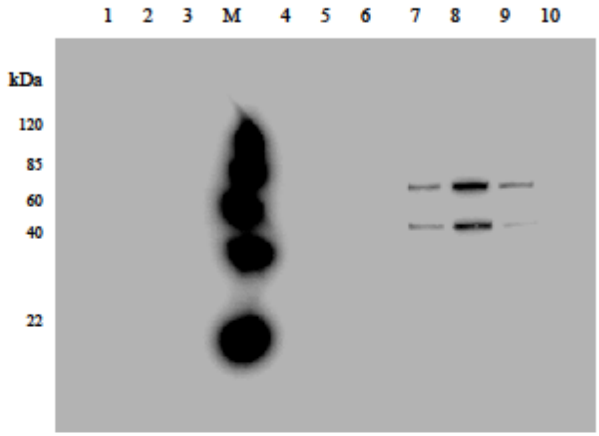

Fig.4 Western Blot analysis of SAC9 protein using anti-His AB

Lane M: Easy western marker

Lane 1: Supernatant after cell lysate centrifugation

Lane 2: Flow through

Lane 3: Pellet after cell lysate centrifugation

Lane 4: Washed with 50mM Tris-HCl buffer (pH 8.0)

Lane 5-6: Eluted with 20mM imidazole,150mM NaCl, 50mM Tris-HCl buffer (pH 8.0)

Lane 7-10: Eluted with 250mM imidazole,150mM NaCl, 50mM Tris-HCl buffer (pH 8.0)

Appendix:

Protein Length-1669 MW-184482.5 Predicted pI-7.01

```
1     MDLHPPGGSK KTSVVVVTLD TGEVYVIASL LSKADTQVIY IDPTTGILRY NGKPGLDNFK
61    SEREALDYIT NGSRGGVRSS VYARAILGYA VLGSPGMLLV ATRLNPSIPD LPGGGCVYTV
121   AESQWVKIPL YNPQPQGKGE TKNIQELTEL DIDGKHYFCD TRDITRPFPS RMPLQSPDDE
181   FVWNRWLSVP FKNIGLPEHC VILLQGFAEY RPFGSSGQLE GIVALMARRS RLHPGTRYLA
241   RGINSCSGTG NEVECEQLVW IPKRNGQSIA FNSYIWRRGT IPIWWGAELK MTAAEAEIYV
301   ADRDPYKGST EYYQRLSKRY DTRNLDAPVG ENQKKAFVP IVCVNLLRSG EGKSECILVQ
361   HFEESMNFIK SSGKLPYTRV HLINYDWHAS VKLKGEQQTI EGLWMYLKSP TMAIGISEGD
421   YLPSRQRLKD CRGEVICIDD IEGAFCLRSH QNGVIRFNCA DSLDRTNAAS FFGGLQVFVE
481   QCRRLGISLD TDLGYGHNSV NNQGGYNAPL PPGWEKRADA VTGKSYYIDH NTKTTTWSHP
541   CPDKPWKRLD MRFEEFKRST ILSPVSELAD LFLQQGDIHA TLYTGSKAMH SQILNIFSEE
601   SGAFKQFSAA QKNMKITLQR RYKNAMVDSS RQKQLEMFLG MRLFKHLPSI PVQPLHVLSR
661   PSGFFLKPVP NMSESSNDGS SLLSIKRKDI TWLCPQAADI VELFIYLSEP CHVCQLLLTI
721   SHGADDLTCP STVDVRTGRH IEDLKLVVEG ASIPRCANGT NLLVPLPGPI SSEDMAVTGA
781   GARLHEKDTS SLSLLYDFEE LEGQLDFLTR VVAVTFYPAG AVRIPMTLGQ IEVLGISLPW
841   KGMFTCERTG GRLAELARKP DEDGSPFSSC SDLNPFAATT SLQAETVSTP VQQKDPFPSN
901   LLDLLTGEDS SSDPFPQPVV ECIASGGNDM LDFLDEAVVE YRGSDTVPDG SVPQNKRPKD
961   SGAHLYLNCL KSLAGPNMAK KLEFVEAMKL EIERLRLNIS AAERDRALLS IGIDPATINP
1021  NSSYDELYIG RLCKIANALA VMGQASLEDK IIASIGLEKL ENNVIDFWNI TRIGEGCDGG
1081  MCQVRAEVNK SPVGSSTKSS RGESGSVFLC FQCMKKACKF CCAGKGALLL SKSYSRDTAN
1141  GGGSLADVSA TSIGSDHYIC KKCCSSIVLE ALIVDYVRVM VSLRRSGRVD NAGREALNEV
1201  FGSNITNHLA VRGQPSPNRE DFNFLRQILG KEESLSEFPF ASFLHKVETA TDSAPFFSLL
1261  TPLNLASSNA YWKAPPSADS VEAAIVLNTL SDVSSVILLV SPCGYSDADA PTVQIWASSD
1321  INKEARTLMG KWDVQSFIRS SPELSGSEKS GRAPRHIKFA FKNPVRCRII WITLRLPRLG
1381  SSSSVSLDKN INLLSLDENP FAPIPRRASF GATIENDPCI HAKHILVTGN TVRDKTLQSV
1441  ESMSVRNWLD RAPRLNRFLI PLETERPMEN DLVLELYLQP ASPLAAGFRL DAFSAIKPRV
1501  THSPSSDVVD IWDPTSVIME DRHVSPAILY IQVSVLQEQY KMVTIAEYRL PEARDGTKLY
1561  FDFPKQIQAQ RVSFKLLGDV AAFTDEPAEA VDLSSRASPF AAGLSLANRI KLYYYADPYE
1621  VGKWTSLSSV YPAFLYKVVR SRGPFEGKPI PNPLLGLDST RTGHHHHHH
```

In grey: GKPIPNPLLGLDST - V5 epitope, HHHHHH - 6xHis tag

CURRICULUM VITAE

Almut H. Vollmer

(February 2012)

Career objectives

Research position in industry that emphasizes plant systems

Professional address

Department of Biology
Utah State University
5305 Old Main Hill
Logan, UT 84322-5305

Post-Secondary Education

Ph.D. in Biology. Utah State University. 2012. Dissertation: Biochemical characterization of SAC9, a putative phosphoinositide phosphatase in *Arabidopsis thaliana*, and its role in cellular abnormalities

Diplom (equivalent to a combined Master and Bachelor of Science) in Biology. University of Bielefeld, Germany. 2004. Thesis: An ultrastructural and biochemical study of paramylon and its synthase in colorless Euglenophyceen algae

Special skills

Plant growth
- Agar based and traditional in greenhouse and growth chamber
- Hydroponics

Microscopy
- Light microscopy
- Confocal microscopy
- Scanning electron microscopy
- Transmission electron microscopy

Molecular Methods
- Growth, harvest, and lysis of bacteria, yeast, and plant material
- Extraction, purification, and amplification of DNA from bacteria, yeast, and plant material
- Primer design and PCR
- Agarose gel electrophoresis
- Recombinant cloning strategies

Biochemical Methods

Recombinant protein expression in *E. coli* and *S. cerevisiae*
Purification of recombinant proteins by chromatography (ion exchange, hydrophobic interaction, affinity, gel filtration, HPLC)
Polyacrylamide gel electrophoresis (SDS-PAGE)
Western blots

Immunological Methods

Antibody production, quality control, affinity and specificity screening
ELISA
Immunohistochemistry (immunofluorescence, immunogold)
Immunoprecipitation

Data Analysis and Management

Statistics (ANOVA, SAS)
Genome sequencing, sequence alignments, phylogenetics (Vector NTI, Blast, Clustal X)
Image processing and analysis (Photoshop, Image J, MatLab)
Endnote Reference Manager

Workshops

Gene Expression and Microarray Analysis, 2006, Center for Integrated Biosciences, Utah State University, Logan, Utah

Microbial Fermentation: Development & Scale-Up, 16-19 October 2007, Center for Integrated Biosciences, Utah State University, Logan, Utah

Downstream Processing of Biotechnology Products, 2008, Center for Integrated Biosciences, Utah State University, Logan, Utah

Teaching Experience

Utah State University, Utah, 2004-2007
General Biology (BIOL 1020), 1 semester
Plant Physiology (BIOL 4400), 2 semesters
Plant Taxonomy (BIOL 4420), 2 semesters
Plant Pathology (BIOL 5410), 2 semesters

University of Bielefeld, Germany, 1999-2004
General Botany, 3 semesters
Advanced Botany, 3 semesters
Plant Identification, 2 semesters
Soil Science, 1 semester
Molecular Biology, 1 semester

Honors and Awards

Teaching Assistant of the Year, 2007, Utah State University, Logan, UT

Deutscher Akademischer Austauschbund (DAAD). Scholarship for field studies performed at the Alberto Manual Brenes Biological Reserve, Costa Rica, 2000, $ 3,000

Professional Affiliations

American Society of Plant Biologists (ASPB), 2009-current

Peer-Reviewed Publications

Vollmer AH, Youssef NN, DeWald DB (2011) Unique cell wall abnormalities in the putative phosphoinositide phosphatase mutant *AtSAC9*. Planta 234(5): 993-1005

Vollmer et al. (in preparation). The cortical microtubule cytoskeleton in the developing root of the putative phosphoinositide phosphatase mutant *AtSAC9*

Abstracts

Vollmer AH, Youssef NN, DeWald DB (2010) Membrane dynamics in *sac9*, a putative phosphoinositide phosphatase mutant of *Arabidopsis thaliana*. Annual Intermountain Graduate Symposium, Utah State University, Logan, Utah. Poster Presentation

Vollmer AH, Youssef NN, DeWald DB (2009) Characterization of *sac9-1*, a phosphoinositide phosphatase mutant of *Arabidopsis thaliana*; early development and ultrastructure of primary roots. Joint Annual Meetings of the American Society of Plant Biologists and the Phycological Society of America, Hawaii Convention Center, Honolulu, Hawaii. Poster Presentation

Vollmer AH, Youssef NN, DeWald DB (2009) NaCl stimulates primary root elongation in the *Arabidopsis* mutant *sac9-1*. 26th Annual Interdisciplinary Plant Group (IPG) Symposium: Root Biology, University of Missouri, Columbia, Missouri. Poster Presentation